N71-13068
NASA CR-111559/24

Vapor Deposited Titanium Dioxide Thin Films: Some Properties As A Function Of Crystalline Phase

By

Eugene T. Fitzgibbons and William H. Hartwig
Department of Electrical Engineering

Technical Report No. 86
April 15, 1970

SOLID STATE ELECTRONICS RESEARCH LABORATORY

ELECTRONICS RESEARCH CENTER
The University of Texas at Austin
Austin, Texas 78712

VAPOR DEPOSITED TITANIUM DIOXIDE THIN FILMS:

SOME PROPERTIES AS A FUNCTION OF CRYSTALLINE PHASE*

By

Eugene T. Fitzgibbons and William H. Hartwig
Department of Electrical Engineering

Technical Report No. 86
April 15, 1970

National Aeronautics and Space Administration
Grant NGL 44-012-043

SOLID STATE ELECTRONICS RESEARCH LABORATORY

ELECTRONICS RESEARCH CENTER

THE UNIVERSITY OF TEXAS AT AUSTIN

Austin, Texas 78712

Abstract

Thin films of TiO_2 are grown in a low temperature (150°C) vapor deposition process by hydrolyzing tetraisopropyl titanate at the substrate. These films can be made uniform over a 1-1/4" substrate to within 100 Å and are found to be amorphous in the "as grown" condition. Films in the amorphous state have an index of refraction of 2.0 and can be etched easily (50 Å/sec) in 0.5% HF. Annealing in air at 350°C converts the film to the anatase tetragonal crystalline form and at 700°C to a mixture of anatase and rutile. Both forms are quite etch resistant, but the anatase can be etched by HF and warm H_2SO_4. At 1000°C, the film is completely rutile with an index of refraction of 2.5. This form is extremely etch resistant even in 120°C H_2SO_4 (1000 Å/hour). The conversion from amorphous to rutile is accompanied by a thickness decrease of 36%.

Electrically, the amorphous material was found to be semiconducting and subject to forming in an electric field. The anatase form showed a mixture of properties depending on the frequency used. The mixed and rutile forms both are insulators with dielectric constants/dissipation factors of 116/.04 and 100/.04, respectively, at 1 kHz. The breakdown field for the rutile form is 7×10^5 V/cm. Surface state density of the rutile films on Si is 3×10^{12} negative states per cm^2. Combinations of TiO_2 and SiO_2 were made in which the sign and density of the surface states could be varied. Conversion from the amorphous to the crystalline forms could

be accomplished selectively in the film by using an electron beam. Lines 2 microns wide were "written" in 3000 $\overset{o}{A}$ of amorphous material. An electron dosage of 0.2 coul/cm^2 with 15 keV electrons was needed to produce sharp lines which remained unetched while the unexposed material was etched away. Similar conversion can be accomplished by exposure to u.v. photons, allowing standard IC and hybrid circuit patterns to be defined in the TiO_2 films without the use of standard photolithographic techniques. Rutile films were tested as a diffusion mask against phosphorous at 1000°C. It was shown that, in that particular case, TiO_2 is a more effective mask than an equal thickness of SiO_2.

TABLE OF CONTENTS

LIST OF ILLUSTRATIONS

LIST OF TABLES

PREVIOUS WORK ON TITANIUM DIOXIDE

INTRODUCTION

An impressive amount of research has been performed in the last 25 years on titanium dioxide (TiO_2). Because of its high index of refraction, it was used as an optical parts coating during World War II. Titanium itself is one of the valve metals, that is, one which is easily anodized, and lends itself to anodized coatings for protection and decoration. TiO_2 - Ti junctions joined other metal oxide/metal rectifiers at the onset of the solid state revolution. Today, TiO_2 has been proposed for a number of uses with hybrid and integrated circuits. It has always been, and will continue to remain, an extremely attractive material because of its high index of refraction, dielectric constant and density. It is certainly beyond the scope and interest of this work to consider all of the research on TiO_2. Rather, the bulk of the work reviewed will involve tests on samples made for electrical measurements and devices. Other data will be included only as needed.

REVIEW OF WORK DONE ON TiO_2

Titanium dioxide has been the object of much research in both the crystalline and thin film form. Single crystals of the material can be found in nature in either the anatase or rutile form and can be grown in the laboratory by a number of methods. Data on both of these crystals has been included in Figure 1. A third phase, Brookite, is primarily found only in nature mixed with metallic ores. The material has also been produced in thin film form by thermal oxidation of bulk or thin film

ANATASE TiO_2

ANATASE TETRAGONAL

ELONGATED CELL. D_{4h}^{19}

a_0 = 3.785 Å

c_0 = 9.514 Å

OCTAHEDRAL COORDINATION

OF O AROUND Ti

SEE REF. 81
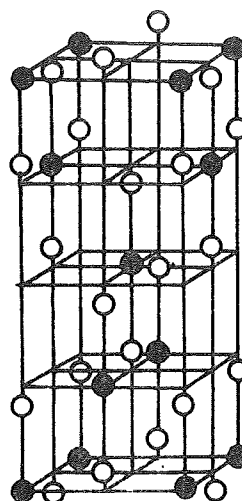
● TITANIUM

○ OXYGEN
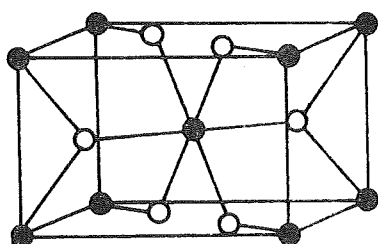
RUTILE TETRAGONAL

CELL. D_{4h}^{14}

a_0 = 2.95 Å

c_0 = 4.58 Å

OCTAHEDRAL COORDINATION

OF O AROUND Ti

SEE REF. 82

RUTILE TiO_2

FIGURE 1. ANATASE AND RUTILE CRYSTAL STRUCTURES

metallic titanium, direct vapor deposition of the oxide, reactive sputter-
ing of the metal, r.f. sputtering of the oxide, anodization and chemical
vapor deposition from a large variety of sources. Material scientists
have, for the most part, concentrated heavily on the properties of the
bulk material, while device and application oriented engineers have sought
to fabricate and test the material in thin film forms. It would be naïve
to assume that all of the above methods of producing the oxide result in
materials with identical properties or, on the other hand, that the mater-
ials bear no relation to one another. Only by considering all of the prop-
erties can one hope to piece together a moderately complete picture of TiO_2
in any form.

During World War II German scientists perfected a chemical vapor
deposition system for coating lenses and other optical parts with thin
films of TiO_2. Its inherent high index of refraction made it ideal for low
reflective coatings on various glasses and the flexibility of the vapor
deposition process for covering odd shaped configurations was recognized
at that time. In 1952 Haas[1] reported a series of comprehensive experiments
on the oxide grown by heating a vacuum evaporated Ti film in air and on an
oxide film grown from a $TiCl_4$ vapor source. The bare evaporated Ti read-
ily formed an oxide at elevated temperatures, especially above 400°C. He
demonstrated that these high density films were of the rutile structure
and had a characteristic index of refraction between 2.5 and 2.7. On the
other hand, films formed from the vapor phase were amorphous for substrate
temperatures below 280°C and anatase if grown over 300°C. Some rutile
lines may have been present for films annealed at 900°C. These films were
generally characterized by a lower density and subsequently a lower index

of refraction (2.3 for films deposited at 300°C). While no electrical data

was taken, this work set the pattern for subsequent work and the trends ob-

served by Haas[1,2] continue to be characteristic of the oxide in thin film

form.

(1)   Single Crystal

Early interest in the electronic properties of TiO_2 was stimu-

lated by reports[3] that the dielectric constant of the crystalline material

along its "c" axis is 170. While Parker[4] found this to be true (ε_c = 167,

ε_a = 89) for rutile crystals subject to long anneals, a number of other re-

searchers found the situation to be far more complex than first expected.

Hollander and Castro[5] reported that what is believed to be a stoichiometric

single crystal of rutile has a maximum resistivity of 10^{12} Ω cm and that

the dielectric constant is not a function of frequency between 10^2 and 10^6

Hz. However, for slightly reduced material the resistivity drops rapidly

and the dielectric constant and dissipation factor became strong functions

of the frequency in the above range. In a later paper[6] they report that

a single crystal of perfectly stoichiometric TiO_2 actually has a resistiv-

ity of 2 x 10^8 Ω cm. The higher resistivities come about by adding oxygen

in interstitial positions while as oxygen vacancies are created in the lat-

tice an impurity band is created, in the c direction and then in the a di-

rection, dramatically reducing the resistivity and producing an extremely

large anisotropy in the resistivity along the c and a axis (ρ_a/ρ_c = 20,000).

van Raalte[7] observed that current flow through high resistivity rutile sin-

gle crystals decreased with time and then rose again and continued to in-

crease to a level orders of magnitude greater than the initial value.

Tests showed that the current was actually reducing the crystal and that

O_2 was evolving at the faces. A loss of oxygen on the order of 1 ppm was accompanied by a resistivity decrease of four orders of magnitude. Similar work on current-reduced rutile crystals was done by Gruner and Whitmore[30]. Work by Kunin, et al.[8] demonstrated that chemically reduced rutile crystals exhibit n-type conduction, whereas, before the reduction, the crystal thought to be stoichiometric exhibited p-type conduction. They observed that this same change in conductivity type could be induced by an electron current and then the crystal could be returned to its original conduction mode by an anneal in oxygen. Evidently, the process of electrical aging by current flow is brought about by the formation of donor defects and is identical with the chemical reduction process. Acket and Volger[9] also observed n-type conductivity in chemically reduced crystals of rutile TiO_2. They postulate that the loss of oxygen results in the creation of two donor levels, one shallow and the second deep. Davis and Granneman[10] studied the conduction in the reduced crystal by forming a point contact diode. Once again the reduced form exhibited n-type conduction with a donor activation energy less than 1 eV.

Because of the semiconducting nature of the crystals a number of the phenomena observed are associated with the contact and the barrier region near the interface[11]. A depolarizing current was found by Condon[12] to flow when the applied voltage across the crystal was removed. This current has a long half life time and is associated with the trapping of electrons at the rectifying contacts. In order to avoid any anomalies provided by the contacts, Cross and Groner[13] measured the dielectric constant ($\varepsilon_c = 167$) and the resistivity ($\rho = 10^6 - 10^7 \ \Omega$ cm) for a flux-grown, single rutile crystal without applying contacting electrodes. Later papers,

such as Bergman, et al.[14], discussed how to best exploit the non-linear electrical and optical properties of a family of metal oxides with unbonded electrons.

(2)   Anodized Thin Films

Titanium is classified as a valve metal, i.e., one which is especially subject to anodization, the formation of an oxide under the influence of an electric field in an electrolyte. Young[15] showed that in the anodization of titanium and tantalum the metal ions were the mobile species and under the electric field, these cations moved through any existing oxide to the oxide-electrolyte interface where they combined with oxygen supplied by the electrolyte. Anodic films of titanium oxide grow at the rate of 22 Å per applied volt, while tantalum oxide films form at a lower rate of 14 Å/volt. Sasaki[16] found that thin anodic Ta_2O_5 films exhibited strong diode characteristics and that it was the oxide itself which formed both the p and the n region of the diode. He reasoned that, due to the nature of the anodic process itself, the oxide near the metallic anode interface was rich with unpaired Ta^{+5} ions while the interface near the electrolyte had an overabundance of oxygen ions drawn into the oxide under the influence of the field. The excess Ta caused donor levels and n-type characteristics in the oxide near the anode while the excess oxygen created acceptor levels and p-type characteristics near the electrolyte. The volume between these regions behaved very much as an intrinsic or compensated semiconductor. Electrical measurements of the capacitance versus voltage of such structure agreed quite well with the semiconductor model. Thin anodic oxides (< 200 Å) demonstrated p-n diode characteristics while thicker ones followed a p-i-n model quite closely. Ta_2O_5 films in the

range of 2000 to 3000 Å have been reported[17,18] to have excellent dielec-
tric properties especially after annealing. The relative dielectric con-
stant is 28 and the breakdown field is in the order of 5 x 10^6V/cm. Hence
it would appear that the semiconducting properties are associated with
fairly thin volumes near the interfaces and can be minimized by annealing.

Similar phenomena have been observed in anodized titanium struc-
tures except perhaps to a greater degree. Huber[19] describes experiments
performed on anodized oxide layers grown on evaporated Ti thin films. The
structures under study were metal/TiO_2/Ti capacitors. When the work func-
tion of the counter electrode was less than that of the TiO_2 (assumed to
be 4.3 eV) the structures acted as capacitors, although their behavior was
later[20] found to be rather complex in that the specific capacitance seemed
to be a function of applied voltage and only a weak function of oxide thick-
ness.

The dielectric constant of these structures was calculated to be
approximately 40. If the work function of the counterelectrode was larger
than that of the TiO_2, the structure had characteristics of a rectifier
with fairly low forward resistance (100 - 1000Ω) and a high front to back
ratio (10^3 - 10^6). The rectification seemed to be taking place in the
bulk of the oxide. The high work function counter electrode (eg Pd, ϕ_W =
5.2 eV) serves only to make ohmic contact to the oxide. Following the
model proposed for Ta_2O_5, it is then assumed that the region nearest the
Ti electrode is effectively n-type while that nearest the counterelectrode
is p-type. Hence the need for a high work function metal to make ohmic
contact. As predicted by the model the diodes were biased in the reverse
direction when the substrate Ti was positive. Thick structures ($\sim$ 1000 Å

or greater) demonstrated poor rectification ratios because of the presence of a large intrinsic region between the p and n volumes. Huber and Rottersman[21] describe the characteristics of these thicker "diodes" by proposing a p-i-n junction model. Magill[22] reviews the phenomena associated with anodized TiO_2 films and concludes that a bulk p-n junction is sufficient, but not necessary to explain the rectification phenomena. Rather, he proposes a model based on Schottky barriers at the electrode interfaces and interprets all of the data in terms of a compound barrier theory. In this case, the TiO_2 bulk need not change conductivity types internally and hence this model can be applied to structures (that exhibit rectifying characerics) formed by processes other than anodization.

Huber[23] uses an array of anodized TiO_2 diodes to demonstrate their feasibility in low-speed switching circuits. These diodes consisted of vacuum evaporated Ti substrates, 300 Å of anodized TiO_2 and Pd counter-electrodes. They demonstrated switching characteristics up to 1 kHz. Hogiwara and Yamashita[24] built electrolytic capacitors using anodized TiO_2. They calculated the dielectric constant to be 107, but admitted the usefulness of such capacitors was limited due to rather high leakage currents. Recently, Kover and Musselin[25] made a comparative study of anodic oxide films. They found that capacitors made with TiO_2 had reasonable dielectric properties ($22 < \varepsilon < 47$ at 1 kHz, depending on the anodizing solution and $\tan \delta \simeq .03$) if they were grown sufficiently thick to minimize the effect of the semiconducting regions near the interfaces, at a low enough rate to allow stoichiometric growth to occur and in an electrolyte containing sufficient oxygen. Bulk resistivity of films grown as above was reported to be on the order of 2×10^9 Ω cm.

(3)   Reactive Sputtering

Even wider ranges in conductivity have been observed in films produced by reactive sputtering of Ti in an oxygen atmosphere. Lakshmanan, et al.[26] performed the sputtering in an oxygen atmosphere at pressures near 10^{-4} torr. They reported producing a good dielectric material with $\varepsilon = 55$ and a dissipation factor of 0.04 at 1 kHz. Resistivity of the films seemed to be near 10^{13} Ω cm. X-ray analysis showed that the films were composed of rutile polycrystals which were shown to be fairly large and with no preferred orientation. Wasa and Hayakawa[27] sputtered the Ti in an atmosphere of N_2 and O_2. When the oxygen partial pressure was below 3 x 10^{-5} torr the films were conductive to various extents and were tested as resistor elements. Above this pressure dielectric films were produced with resistivities on the order of 10^9 - 10^{10} Ω cm with a dielectric constant between 20 and 30 depending on the oxygen content. The films were identified to be in the amorphous form. The authors observed that films with rectifying properties were produced if the oxygen ambient was either rather low or very high during film growth. This agrees with previous observations on single crystals and anodized films that p-type characteristics could be produced by introducing excess oxygen in the lattice while n-type properties were due to an excess of Ti atoms.

A rather thorough study was made by Lakshmanan[28] of sputtered Ti in a reactive atmosphere of oxygen and argon. While the total gas pressure was held at 200 torr during sputtering the gas composition could be varied from 100% Ar to 100% O_2. Corresponding to this variation in the reactive atmosphere is a film resistivity change from 10^{-3} Ω cm to 10^{13} Ω cm. The insulating films were found to be polycrystalline in the rutile phase

with a dielectric constant very near 100 and a tan δ between .0016 and .06 at 1 kHz. Various sputtering conditions alternately produced films with relative dielectric constants between 45 and 350, the higher values corresponding to thicker films. It is felt that dielectric constants on the order of 350 are not associated with the bulk, but rather a barrier or depletion layer which is independent of film thickness. Hence, thicker films would appear to have higher dielectric constants.

Rectifying junctions were also made by forming a layer of very slightly reduced TiO_2 between Ti and Al or Ag electrodes. The operation of the device was strongly dependent on the counterelectrode material, the resistivity of the oxide layer, and that the second electrode be Ti. These diodes operated in the forward direction when the Ti is biased positive. The capacitance vs. voltage curves of such a diode once again suggests strongly a p-n or p-i-n junction or a Schottky barrier.

Films were doped with small amounts of Cr, Fe and Nb by including these impurities in the sputter target. Little effect was seen on the resultant insulating films, all of which had a capacitance per unit area of between 0.6 and 1.1 $\mu f/cm^2$ and a tan δ of .03.

Davidse and Maissel[29] observed many of the same phenomena as above in SiO_2 films sputtered in an r.f. field. Oxygen deficiencies made themselves most apparent in this case, however, in optical measurements.

(4)   Thermally Oxidized Films

Oxides formed by thermal oxidation of bare Ti metal also exhibited a larger spectrum of resistivities due to the stoichiometry problem. Capacitors made by Komolova and Nasledov[31] exhibited forward and reverse currents, current vs. temperature phenomena and capacitance vs. voltage

characteristics all predictable on the basis of a p-n junction model. A gradient of diffusing oxygen atoms could be responsible for such a junction as is the titanium gradient in the case of the anodized films. Schottky barriers at the interface could also explain their data. This second model was proposed by Huber[20] to explain the rectifying effect in thermal oxides. He states that while a bulk p-n junction is responsible for such data in anodic oxides, a surface barrier model must be invoked for thermal oxides. He supports this by observing that ohmic contacts to the oxide only enhance the effect in anodic films while such contacts destroy the effect in thermally grown films.

(5)   Evaporated Films of TiO_2

Maserjian and Mead[32] produced very thin (< 500 Å) films with large ionic space charge by direct evaporation of a TiO_2 source in a vacuum. From current-voltage data on these films they have attempted to measure the density of the space charge. They concluded that the properties of the films were governed by a volume of ionic charge near the contacting electrodes, and the density of this charge remained roughly constant despite large variations in the film preparation parameters. They conclude that the density of this charge is on the order of the saturation density of impurities gettered by the surface of the film. One such source of impurities could be the evaporated Al electrodes used in the structure. This Al can form AlO_2 acceptor centers which have been found to have a strong compensating effect on n-type rutile crystals.

Johansen[33] evaluated vacuum evaporated SiO_2 films and found that they were actually mixtures of SiO, SiO_2 and Si_2O_3. The conductivity of these films was quite high due to a decomposition of the evaporant during

heating and hence the inclusion of a number of unpaired Si atoms in the re-
sulting film. If the evaporation was performed in a slight oxygen atmos-
phere, decomposition was retarded and the conductivity dropped dramatically

Very recently, Shiojiri, et al.[34] vacuum evaporated thin films of
TiO_2 onto rock salt crystals held at room temperature. The films were then
stripped off and placed, unsupported, on a copper grid for analysis with an
electron microscope. The films were found to be amorphous as grown, but
diamond shaped crystals of anatase material began to appear when the film
was heated to $500°C$ or exposed or prolonged radiation from the electron
beam itself. No measurements of the stoichiometry of the films were made
nor were their electrical properties analyzed. More details of the results
are interpretation of this experiment will be presented in later chapters.

(6)   Chemically Vapor Deposited Films

It is interesting to note that the initial work on TiO_2 thin films
for optical purposes done by Haas[1] involved the use of a chemical vapor
deposition approach. More recently, work on TiO_2 thin films is again em-
phasizing the chemical vapor deposition method. Powell, Oxley and
Blocker[35] give an excellent summary of CVD as applied to the vapor deposi-
tion of metals, oxides, borides, carbides, nitrides, silicon and silicides
from both organic and inorganic sources. Thermodynamic conditions for re-
actions along with numerous references for all vapor deposition processes
are included. Vapor phase deposition of metals and their oxides as applied
to microelectronics is reviewed by Buck[36].

TiO_2 films have been formed from both organic[37] and inorganic
sources. Film growth occurs either by vapor reaction with water at a
heated substrate (hydrolysis) or by vapor decomposition at a heated

substrate in the presence of an inert or reactive atmosphere (pyrolysis). Both schemes have been used to deposit films for electrical or optical testing. Feuersanger[38,39] produced TiO_2 films by reacting $TiCl_4$ with steam at a substrate heated to 150°C. While the reaction product is TiO_2, the reaction by-product is HCl gas which tends to limit the usefulness of the process. The films formed were susceptible to etching by HF and were relatively hard. The refractive index at .54 μ is 2.55 indicating a high density. On the basis of the index of refraction compared with the published crystalline values, the author surmises that the film may be a mixture of the anatase and rutile forms. A large variation in dielectric constant was observed depending on the substrate ranging from 25 for polished Al to 82 for Pt. Dissipation factors on the order of .02 and bulk resistivities or 4.5×10^{12} Ω cm were measured. The author also prepared a series of samples using a tetraisopropyl titanate (TPT) organic source in place of the $TiCl_4$. Capacitor dielectrics so formed had a dielectric constant of 178 and a correspondingly high dissipation factor (> 10%) due to a relaxation peak between 50 Hz and 300 kHz. Evidently, research on this film growth method was discontinued because of the high dissipation factor. Harbison[40] reacted TPT with water vapor at substrate temperatures of 900°C. He reported an index of refraction of 2.0 along with moderate mechanical toughness. X-ray analysis gave some evidence that the films so formed were rutile and polycrystalline. The reported dielectric constant, dissipation factor and breakdown strengths are respectively 80, .07, and 5×10^5 V/cm. Lower substrate temperatures during film growth resulted in films with inferior insulating properties, rather high dissipation factors, low breakdown voltages and high leakage currents; however, no semiconducting

properties were reported for these films which were known to be oxygen deficient. Capacitance-voltage data for the 900°C material on Si indicates the presence of negative surface states in the oxide itself near the surface of the Si. No indication was given of the nature of these states.

Utilizing a pyrolytic decomposition of TPT, Peterson, et al.[41] grew TiO_2 films in an O_2 atmosphere at substrate temperatures between 300 and 500°C. These films proved to be electrically unstable in that current flow though the oxide increased with time under moderate electric field stress. Breakdown fields on the order of 3×10^5 V/cm were observed. Similar experiments were conducted by Yokozawa and Iwasa[42] using both oxygen and inert atmospheres. Temperatures ranged as high as 700°C, but most material was grown between 300 and 600°C. Films grown in an O_2 atmosphere were amorphous, porous and easily etched in dilute HF (4 - 60 Å/sec). Oxides grown without an oxygen atmosphere formed in the anatase crystalline phase, were moderately dense and only slowly etched in HF. The etch rate was observed to increase as the deposition temperature was lowered and the fraction of oxygen in the surrounding gas mixture was increased. The specific gravity of the amorphous film is 2.40 to 2.49 and the index of refraction is between 2.00 and 2.05 while these quantities for the anatase film are 2.55 and 2.15, respectively.

Similar trends were observed in other CVD processes. Gannon, et al.[43] produced titanium diboride from a $TiCl_4$ vapor source on graphite substrates heated between 1200 and 1800°C. Not only was the reaction product highly crystalline, but completely oriented with the (110) plane parallel to the surface of the graphite substrate. Sterling and Swann[44] promoted the vapor deposition of Si, SiO and SiO_2 from SiH_4 using an r.f. plasma.

Heating the substrate independently helped order the deposit and greatly increased its adherence. Peterson[45] grew films of alumina silicate from the gas phase. He observed a maximum upper limit on the thickness of the films he could grow in this fashion before the film tore and ruptured. He proposes a surface tension model in which the adherence at the interface and the relative coefficient of expansion of the film and substrate determine the rupture thickness. Film thickness was limited to 6000 $\overset{o}{A}$ on Au film substrates while 20,000 $\overset{o}{A}$ could be grown on polished Al because of the bonding to the natural oxide.

(7)   Films Formed from Solutions

Thin films of TiO_2 and multicomponent oxides have been made by dipping appropriate substrates into solutions containing compounds of titanium or other organometallics. The substrates were then dried at various temperatures in the air. The process could be repeated to obtain thicker films. Krylova and Bagdyk'yants[46] formed TiO_2 films by successive dippings in a solution of orthotitanic acid in ethyl ether. Films dried at 180°C had an index of refraction of 1.95 while those heated at 400°C had n = 2.25. Those heated at 900°C for a prolonged period had n = 2.25 and were thought to be rutile. Samples often cracked and pulled away from the substrate when heated to 500-600°C. Multicomponent films were made by Mitchell[47] by dipping metal plates in alcohol solutions containing titanium isoprypylate, barium methylate and strontium methylate and then drying them at 100°C followed by a 300°C anneal. It is believed that the combined film was amorphous, but some anatase TiO_2 was detected in the material. The dielectric constant of the films was 23 with a moderate dissipation factor.

SIGNIFICANCE OF THE PREVIOUS RESEARCH
AND OF THIS WORK

Several general conclusions can be drawn from the previous work

done on TiO_2 in both single crystal and thin film form.

(1)   Obtaining non-stoichiometric TiO_2 can be accomplished either by

withholding oxygen during formation or by reducing the material

after growth. Such a reduction may take place by heating in a

reducing atmosphere or merely by flowing a current through the

crystal or film.

(2)   Non-stoichiometric material, especially that which is oxygen de-

ficient is a poor insulator and is better classed as a semiconduc-

tor. Resistivity has been shown to be an extremely strong func-

tion of stoichiometry.

(3)   Thin films formed or annealed at elevated temperatures are gen-

erally polycrystalline and show good insulating properties. How-

ever, these polycrystalline forms are dense and notably etch re-

sistant, making their adoption to thin film hybrid or integrated

circuit technology difficult.

(4)   The dielectric constant of the insulating films ranges from 26

to 178 and above. This extreme range is largely due to various

film growth techniques. It may also be due to the series capaci-

tance of various surface layers, such as low dielectric constant

oxides or impurities adsorbed during processing or from the elec-

trodes. Semiconducting material may form diodes, the capacitance

of which and hence the apparent dielectric constant is a function

of conditions at the junction and not of the bulk.

(5)   The large variation in film resistivity has led to a large family of devices based on TiO_2 thin film technology, such as high value capacitors, resistors, diodes and rectifiers. The negative surface charge in some films observed by Masejian and Mead[32] and Harbison[40] has led to speculation about new devices and uses with the already existing Si/SiO_2 technology. These include an n-channel enhancement mode IGFET, passivation layers for various heterojunction configurations and low bias varicaps and surface varactors.

In view of what has already been observed and reported above, a research project was undertaken to extend and unify the TiO_2 thin film technology. It was hoped all or part of the following features would emerge:

(1)   A reliable low temperature chemical vapor deposition process, utilizing tetraisopropyl titanate as the organometallic source for the film growth would be developed. The low temperature process would assure the formation of a film which could be etched and be more compatible with standard thin film processes.

(2)   The measurement of the crystalline phase of the film (as grown) along with other parameters, such as index of refraction, dielectric constant, dissipation factor, optical absorption, and bulk resistivity, would be possible using unambiguous techniques. These same parameters would be measured as a function of anneal treatments of the film between 150°C and 1000°C.

(3)   The exploitation of several unique and novel aspects of TiO_2 thin film technology would lead to its acceptance as an important hybrid and integrated circuit development.

CHAPTER II.

THE CHEMICAL VAPOR DEPOSITION PROCESS

INTRODUCTION

The TiO_2 films used in this work were formed in a chemical vapor deposition arrangement using the organometallic, tetraisopropyl titanate (TPT) as a vapor source. Film formation came about as a result of the hydrolysis of the TPT by water vapor in the immediate vicinity of a heated substrate. Some particular considerations concerning the chemical reaction, the deposition apparatus, and the deposition parameters are now considered in some detail.

CHEMICAL REACTION

In Chapter I, it was shown that there are numerous ways to achieve the chemical vapor deposition of TiO_2 films. The possible choices are:

Source   i) organic

                       ii) inorganic

Type of Re-   i) pyrolysis
action
                       ii) hydrolysis

Atmosphere   i) reactive

                       ii) inert

The major inorganic source used is $TiCl_4$, a chemical which hydrolyzes readily and completely. However, the reaction products of such a process include HCl which, when formed, can attack the substrate or metallic or oxide layers already deposited on a multilayer arrangement. This vulnerability to chemical attack is enhanced by the elevated temperature of the substrate and the surrounding deposition apparatus. While

18

this result may not be bothersome while coating non-reactive materials such as glass or quartz lenses, it is a decided disadvantage for use in electronic applications.

The major organic source is the family of alkyl-titanates. The vapor pressures of these liquids vary over a wide range lending themselves to various vapor transport requirements. The chemicals may be reacted at the substrate by either thermal decomposition or hydrolysis. The reaction product in both cases is usually an alcohol which is unable to react with the substrate or the surroundings. The disadvantages of such a source would be the inclusion of various hydrocarbons in the film in case of incomplete reaction during formation.

Both pyrolysis and hydrolysis have been used to form the TiO_2 at the desired place. The thermal decomposition reaction can be made to occur at the substrate by virtue of its elevated temperature. This process usually involves a moderate substrate temperature, most often between 300 and 500°C and the vapor must not be allowed to hydrolyze by exposure to ambient water while on the way to the thermal decomposition. On the other hand, hydrolysis may occur at room temperature and merely involves the reaction of the vapor with water. The substrate on, or near, which the action occurs is usually heated slightly (150°C) to drive off the reaction products. The disadvantage of this method is the lack of control of where the reaction occurs. TiO_2 may be deposited wherever water can mix with the alkyl titanate.

Hydrolyzing reactions always occur in a reactive atmosphere, i.e., water vapor. However, thermal decomposition may be carried out in an inert atmosphere, such as He or Ar, or a reactive atmosphere such as

O_2 (oxidizing) or H_2 (reducing) and, therefore, several more parameters must be considered when analyzing films formed by this technique.

Because a low temperature process compatible with a variety of substrates is desired, it was decided to choose tetraisopropyl titanate from the organic choices because of its high vapor pressure and have it react with water vapor in the vicinity of the substrate.

Tetraisopropyl titanate is one of a family of alkyl titanates, i.e., a family of compounds in which a Ti atom is bonded to an alkyl group through an O atom. The general formula for these compounds is $Ti(OR)_4$, where R represents the alkyl radical. Included in this group are tetraisopropyl titanate (TPT), tetrabutyl titanate (TBT), polymerized tetrabutyl titanate (PB) and titanium acetyl acetonate (AA).

The process of hydrolysis may be characterized by the following equation for the above group of materials:

$$Ti(OR)_4 + 2H_2O \rightarrow TiO_2 + 4ROH$$
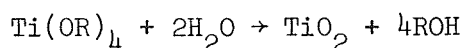
In the specific case of TPT, the process of hydrolysis is carried on in two steps with the formation of an intermediate compound[37]

$$Ti(OC_3H_7)_4 + H_2O \rightarrow Ti(OC_3H_7)_2 O + 2 C_3H_7 OH \rightarrow$$

$$Ti(OC_3H_7)_2 O + H_2O \rightarrow TiO_2 + 2 C_3H_7 OH$$
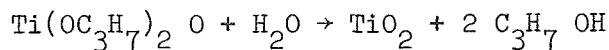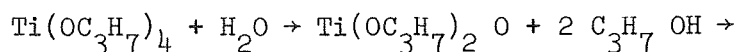
The rate of this reaction is determined by the availability of water vapor. Ideally, the hydrolysis of TPT continues until the oxide is formed and the isopropyl alcohol has been driven off. However, one can anticipate several problems with a thin film growth process based on this reaction:

(1)   Incomplete reaction due to the lack of water at the reaction surface causing inclusions of unreacted TPT.

(2)   Incomplete reaction due to the speed of the film growth, i.e., the TPT reacts partially with water to form the intermediate compound, but due to film growth on top of this form, water is not available to allow the reaction to go to completion.

(3)   The inclusion of alcohol in the film. During the growth process alcohol escaping from the reaction volume must diffuse up through any film being formed on top since there is only one surface from which escape is possible.

It appears then that the deposition parameters should be set while considering the above possible difficulties. It would seem that the following steps should be taken:

(1)   Sufficient water should be supplied to the reaction during growth. This water should be supplied in a method to retard reaction before the vapors reach the substrate.

(2)   The film growth rate should be kept slow enough to allow the reaction to move to completion. Since the surface of the film is simultaneously serving as the site where newly arrived TPT and water react for the first time, the source of water for material already in the process of reaction and the exit point for any alcohol released from completed reactions the growth must be slow and orderly to avoid inhibiting any of the reaction steps.

(3)   The substrate should be held at a high enough temperature to aid any processes which are thermally activated and thus speed the reaction and film growth. It is essential to drive off the

alcohol from the reaction to preclude inclusion. The film coher-
ence, that is the presence of ordering at some range, is also as-
sisted by heating.

DEPOSITION APPARATUS

The deposition apparatus used to grow the films in this work is
shown in Fig. 2. The system is quite simple and operation is straightfor-
ward. Helium carrier gas of a known purity (99.995% pure; 0.2 ppm H_2, 10
ppm Ne, 7 ppm N_2, 0.9 ppm O_2, 0.2 ppm CO_2, no trace of hydrocarbons, anal-
ysis did not include water vapor content) is supplied through a regulator
with a line pressure of 10 psig. This gas is passed through a molecular
seive which serves to extract any water vapor. An LN_2 cold trap was em-
ployed initially at this point to achieve this same purpose, but it was
found that there was little, if any, difference between results with the
molecular seive and the cold trap. A flowmeter is employed to monitor the
flow of gas to the vaporization bottle. Flows between 0.1 1/min. and 2
1/min. can be gauged accurately. The liquid TPT vapor source is kept in a
glass washing bottle which is, in turn, submerged in the water of a constant
temperature bath. The temperature of the source may be kept between room
temperature and 100°C; however, it was found that the best temperature range
for controlled film growth is between 75° and 85°C. The He carrier gas is
passed over the surface of the heated TPT and not bubbled through. It is
felt that this minimizes the possibility of small droplets of TPT travel-
ling with the carrier gas stream and being deposited, unreacted, on the
surface of the substrate. The lines between the vaporizer and the sub-
strate have been kept as short as possible to prevent any condensation of
the TPT out of the carrier stream.

TITANIUM DIOXIDE CHEMICAL VAPOR DEPOSITION SYSTEM .

FIGURE 2

TITANIUM DIOXIDE CHEMICAL VAPOR DEPOSITION SYSTEM .
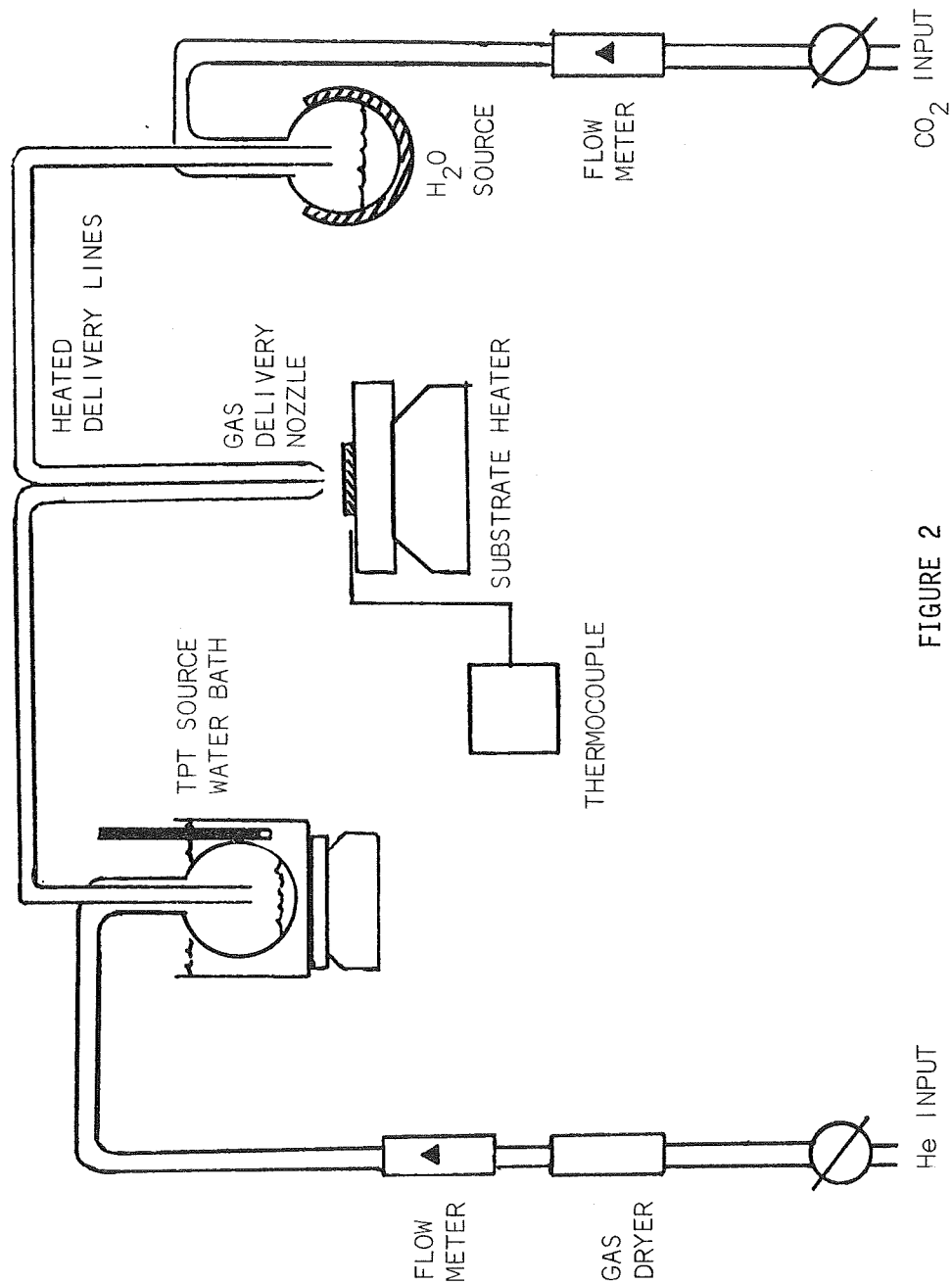
FIGURE 2

The water vapor source is merely a flask containing boiling distilled water. In this case, the carrier gas is CO_2 (99.8% pure; O_2 43 ppm, H_2O 23 ppm, Ar 23 ppm, N_2 12 ppm, H_2 CO, NO < 5 ppm, hydrocarbons ∿ 1 ppm), which is regulated by a flowmeter, but not filtered. Once again the carrier is passed over the surface of the water and not bubbled through it to prevent droplets of water from arriving at the substrate. The lines from the vaporizer to the substrate are heated to 150°C to prevent condensation of the water vapor.

The substrates for the film growth are heated on a hotplate in the open atmosphere. The temperature of the substrate can be caried between room temperature and 350°C and maintained at a temperature of ± 15°.

The delivery lines from the TPT and water sources are brought together and run parallel to about 1 to 2 inches from the substrate. Beyond this point, the gas streams are allowed to run parallel and intermingle until they impinge on the substrate. Fairly good mixing is achieved by the turbulence at impact. The film growth can then be controlled manually by moving the substrate around under the nozzles or by moving the nozzles themselves. Some practice with this method allows the operator to control the thickness of the film within 100-200 Å over a fairly large area (1-1/4" diameter Si wafers) by observing the sharp interference colors of the film during growth.

A number of experiments were run without using the extra water vapor source, relying only on the ambient water vapor in the atmosphere to supply the reaction. The growth dynamics appeared to be almost identical in both cases and later work showed that films grown by both methods have similar crystalline, optical and chemical properties. Later chapters will

show that the only differences observable were in the electrical properties. Hence it appears that the effects of providing an atmosphere saturated with water vapor are fairly subtle and detectable only by electrical measurements. Most of the tests for crystalline, optical or chemical properties were run on samples made without the extra water source. However, this source was always used to make samples for electrical testing.

Typical values for the parameters in a deposition are given below:

He flow rate	- 1 l/min.
TPT temperature	- 75°C
Substrate temperature	- 150°C
CO_2 flow rate	- 0.25 l/min.

With these parameters a 1-1/4" substrate can be covered with 2000 Å of TiO_2 with good uniformity in 10 minutes.

SUBSTRATES

Films were grown on several substrates for a variety of experiments:

(1)   Fused quartz discs were used for optical transmission experiments, X-ray diffraction analysis and adherence measurements.

(2)   Soft glass microscope slides served for experiments in the X-ray diffraction analysis and adherence measurements.

(3)   Fused quartz covered with evaporated Pt films were used with the ellipsometer and interferometer to determine the anneal vs. thickness and index of refraction relationships. Metal-insulator-metal capacitance data was also obtained.

(4)   Polished Si wafers of both p and n type in the resistivity range from 3 Ω cm. to 0.5 Ω cm. were commercially prepared with a

special electromechanical polishing process. Samples on these
substrates were used for X-ray analysis, metal-insulator-semicon-
ductor electrical measurements and interferometric and ellipso-
metric studies of the index of refraction.

The fused quartz and soft glass substrates were cleaned
thoroughly in a low residue detergent and then rinsed for a period of time
in deionized water before film deposition. The Pt films were annealed at
1000°C for 5 minutes in air to stabilize them and no further cleaning was
required or performed. The Si wafers were used as supplied.

DEPOSITION PHENOMENA

A number of observations have been made about the film quality
as a function of the deposition parameters of the system described above:

(1)   TPT bath temperatures between 90 and 100°C for an He flow rate of
        1 l/min without the extra water vapor source produced a film
        which was rather milky in appearance with somewhat diffuse inter-
        ference colors. Microscopic examination revealed that the film
        lacked coherence, but rather was made up of tiny stacked spheres.
        The film had an odor of alcohol or TPT and was soft enough to be
        "smeared" with a cloth. It is felt that the TPT was delivered
        at a rate too fast for complete hydrolysis to occur and that the
        resultant film was actually small droplets of TPT whose surfaces
        alone had reacted with the ambient water.

(2)   He carrier gas flow rates greater than 2 l/min for a TPT tempera-
        ture of 75°C and no extra water vapor produced similar results
        to the above, but less pronounced. Once again the growth rate
        was extremely fast and the film undoubtedly is made up of only
        partially reacted components.

(3)   Bringing the nozzle closer than 1 inch to the substrate also pro-
        duced incomplete reaction since it appears that the TPT has not
        had enough time to mix with water vapor from the extra source or
        the atmosphere before depositing on the substrate.

(4)   Films grown at room temperature or below approximately 100°C have
        a milky cast and are quite soft. These films may be the result
        of incomplete reaction or the inclusion of alcohol in the struc-
        ture.

(5)   Excessive water vapor carrier flow rates (> 0.50 l/min) caused a
        white powdery deposit rather than a film to form on the substrate.
        This powder appeared to be TiO_2 and was the result of premature
        hydrolysis of the TPT over the substrate which then "rained" on
        the area below. Intermediate amounts of water vapor resulted in
        films which had some white powdery inclusions.

(6)   Positioning the nozzle at a distance of approximately 3" or more
        from the substrate caused an extremely low growth rate and was
        always accompanied by the presence of the white powder due to
        premature reaction.

(7)   Argon gas was substituted for He as the TPT carrier. Little dif-
        ference was observed except for an increased growth rate. Lower
        Ar flow rates were used to maintain approximately the same growth
        rate as with the He carrier.

(8)   Some white powdery deposits were observed inside of the TPT va-
        porizer bottles and in the gas lines as the equipment was used
        over a number of runs. The powder was quite like that described
        above and is observed to be due to reaction with water vapor

present either in the carrier gas or leaking into the system be-
tween runs. The system had to be disassembled and cleaned at
regular intervals to keep the powder from becoming air-borne and
being deposited on the substrate.

(9) Any smooth object which could be heated could be coated with a
film of TiO_2.

(10) When film thickness of 4000-5000 $\overset{\circ}{A}$ were reached during a normal
deposition process, cracks would often appear in the film and
propagate over the surface of the deposited layer reducing it to
a field of small triangular pieces of film, separated from the
substrate and slightly convex up. This phenomenon was observed
on all of the substrates mentioned above at approximately the
same thickness. Several experiments were performed to determine
the reason for this behavior. It was observed that films grown
on a fused quartz substrate already coated with several thousand
$\overset{\circ}{A}$ of material grown at 150°C cracked and pulled away from the
quartz when the total thickness of both films fell in the 4000-
5000 $\overset{\circ}{A}$ range. However, if a quartz substrate was covered with
several thousand $\overset{\circ}{A}$ of TiO_2 which was then annealed above 350°C
(to be discussed in the next chapter) a subsequent growth of TiO_2
at 150°C would crack only when it reached 4000-5000 $\overset{\circ}{A}$ leaving the
sub-layer of TiO_2 intact on the substrate. While no explanation
is given for such behavior, it is felt that a combination of sur-
face tension, thermal coefficients of expansion and film adher-
ence are responsible. The phenomenon is quite similar to that
reported by Peterson[45] for chemically vapor deposited alumina

silicate films or for electrodeposited Ni films reported by
Powell, et al.[35]. This cracking of the TiO_2 was not observed
for films grown at $300^\circ C$ or above and deposits thicker than
8000 Å was formed at that temperature.

CHAPTER III.

CRYSTALLINE PHASE, INDEX OF REFRACTION, OPTICAL AND CHEMICAL PROPERTIES AS A FUNCTION OF ANNEAL

INTRODUCTION

In Chapter I, the various techniques for growing thin films of

TiO_2 were reviewed. Some of the methods, such as CVD or thermal oxidation,

involved the direct heating of the substrate from temperatures of 150°C to

over 900°C while other processes, such as reactive sputtering or vacuum

evaporation impart energy to the growing film, not necessarily by heating

the substrate directly, but through the kinetic energy of the impacting

particles. In general, the low temperature processes resulted in films

identified to be amorphous and characterized by a low index of refraction

while the higher temperature films (300-900°) are thought to be polycrys-

talline composed of anatase or anatase-rutile crystals and having a larger

index of refraction (2.2 to 2.65). The samples made by Feuersanger[38]

seemed to be the notable exception in that, although grown from $TiCl_4$ at

150°C, the films possessed a high index of refraction (2.55) quite close

to that of pure rutile reported by Haas[1] (2.65), yet could be etched

in a 10% HF solution, a property reserved mostly for the amorphous or low

anatase form.

Most notably lacking in the work surveyed above is a comprehen-

sive set of experiments correlating the growth or anneal temperature with

various measurable parameters of the resulting films, such as the crystal-

line phase, index of refraction, dimensional changes, chemical activity in

various etches, optical absorption, and others. Not mentioned are the ob-

vious electrical measurements possible, such as the electrical nature of

30

the film (semiconductor or insulator), the dielectric constant and dissipation factor, the critical breakdown field and the nature of the surface states at the TiO_2-Si interface. Discussion of this second group will be deferred until Chapter IV. It will then be the object of this chapter to present the results of a series of experiments which were designed to study the effect of annealing at various temperatures on the films grown by the process described in Chapter II.

X-RAY DIFFRACTION ANALYSIS OF CRYSTALLINE MATERIAL

A number of samples were made to measure the crystalline phase of the TiO_2 thin films on various substrates as a function of anneal temperature after the film growth at 150°C. These samples will be referred to as follows:

1. Powder Samples

2. TiO_2 on Fused Quartz

3. TiO_2 on Soft Glass

4. TiO_2 on Polished Si

All X-ray diffraction analysis were performed on a General Electric XRD-5 powder diffractometer using copper $K_{\alpha1}$ radiation. While only one group of samples is powder, it was found that 3000-4000 Å of the TiO_2 thin films provided sufficient scattering to allow meaningful interpretation. To test for any preferred orientation that might occur in a particular film-substrate configuration, the amplitudes of various diffraction peaks were observed as the sample was rotated in its holder. Large variations did occur when a preferred orientation was present in the polycrystalline material, while little or no variation occurred when no preferred orientation existed.

1. Powder Samples

These samples were made by allowing the standard deposition pro-
cess to continue for several hours until a white powdery deposit had built
up on the microscope slide substrate. This deposit could be scraped off
easily, ground into a fine white powder and divided into groups for test-
ing.

Analysis of the "as grown" 150°C powder showed no signs whatso-
ever of crystallinity and it is assumed to be amorphous. A sample heated
to 350°C to 10 minutes in air revealed the presence of the anatase form of
TiO_2. It is evident that after this short anneal only a portion of the pow-
der has become crystalline since only the 100% and 33% lines were observed
(see Table I). A third sample annealed at 700°C for 2 hours was composed
of a mixture of the anatase and rutile forms. All of the anatase lines
from 100% to 19% along with the three strongest rutile lines were observed.
A longer anneal (8 hours) at the same temperature resulted in the same mix-
ture of phases with all but the weakest rutile peak present. A 20 hour
long anneal at 1000°C completely converted the powder into the rutile form,
no anatase peaks were observed whatsoever.

A portion of the amorphous powder was allowed to remain out in
the air at room temperature for a period of one week. After this time the
material was still amorphous and showed no tendency toward the crystalline
state.

2. TiO_2 on Fused Quartz

A 3000-4000 Å film of TiO_2 was grown on a polished wafer of fused
quartz which had been cleaned in a very mild HF etch, thoroughly rinsed,

ANATASE			RUTILE		
"d" SPACING	CRYSTAL PLANES	INTENSITY %	"d" SPACING	CRYSTAL PLANES	INTENSITY %
3.51	101	100	3.245	110	100
2.435	103	9	2.489	101	41
2.379	004	22	2.297	200	7
2.336	112	9	2.188	111	22
1.891	200	33	2.054	210	9
1.699	105	21	1.687	211	50
1.665	211	19	1.624	200	16

TABLE I.

CRYSTALLINE "d" SPACINGS FOR ANATASE AND RUTILE TiO_2.

and then heated at 1000°C for 10 minutes in air to drive off any surface

contamination. As in the case of the powder, the "as grown" film proved

to be amorphous. After a 350°C anneal for 10 minutes, a few of the

stronger anatase lines were present. These same lines were observed in

a sample identical with the first but grown at 300°C and then tested with-

out benefit of an anneal. Unlike the powder sample, no rutile lines ap-

peared after a 1-hour anneal at 700°C and only the stronger anatase lines

(100% and 33%) were observed. The sample was then heated to 1000°C for 1

hour and tested and then 20 hours and tested. In each case, more anatase

lines were found (down to the 19%), but even after the long anneal only a

trace of the strongest rutile line could be found.

Hence, it appears that the simple transition from amorphous to

anatase to rutile as exhibited by the powder sample does not take place

with the fused quartz substrate. It is evident the substrate and the ana-

tase phase of the film find some type of preferential "match" which causes

this phase to be energetically preferred. While no sharp peaks associated

with the fused quartz could be found, a large, wide peak in the background

noise centered near a d-value of approximately 3 Å was found to be due to

the fused quartz. This may be due to the formation of minute crystallites

at the surface of the quartz during the 1000°C anneal prior to the film

growth or during the film anneal. It may be this surface condition which

causes the TiO_2 to remain in the anatase phase. A similar phenomena may

have been observed by Krylova and Bagdky'yants[46], who reported that optical

coatings made for fused quartz lenses by dipping them into a solution of

orthotitanic acid and subsequently dried at 900°C remained in the anatase

form.

3. TiO_2 on Soft Glass

In order to partially test the validity of the conclusions above, the experiment was repeated using a soft glass microscope slide as the substrate rather than the fused quartz. The surface of the slide was etched very lightly in dilute HF, rinsed and then baked at 350°C in air for 1 hour to drive off surface contaminants. A film 3000-4000 Å thick was then grown at 150°C and tested. As expected, no crystalline peaks were observed. After a 10 minute anneal at 350°C, the stronger anatase lines were observed. Unlike the film on the fused quartz, lines from both the anatase and rutile forms were easily seen after 10 minutes at 700°C. No diffuse scattering peak due to the substrate was observed. Longer anneals at elevated temperatures were not possible because of the softening of the substrate. Hence it appears that the behavior of the film on soft glass is quite similar to that of the powder sample.

4. TiO_2 on Polished Si

A 3500 Å film of TiO_2 was grown at 150°C on a commercially polished (described previously) single crystal Si wafer, 1 Ω cm. n-type. The < 100 > crystal axis was known to be inclined several degrees away from the wafer axis making it possible to orient the Si slice with respect to the impinging X-ray beam to minimize the signal diffracted from the Si at the collector. Even following this procedure the lines due to the Si lattice were extremely strong compared to those from the TiO_2 surface film and a data subtraction technique had to be employed. A complete set of peaks were obtained for the Si crystal itself by running it before the TiO_2 film was deposited. These peaks were then subtracted from any results

obtained for the Si and the annealed TiO_2 film. Any resulting peaks were then candidates for identification.

As with the previous substrates, the 150°C material as grown proved to be amorphous. After annealing at 350°C for 30 minutes only the strongest anatase peaks could be identified, most likely because of the high background scattering. Both anatase and rutile forms were detected after a 1-hour anneal at 700°C and only rutile peaks could be seen after 2 hours at 1000°C. It is evidently the case then that the material on the Si acts quite similar to the powder sample and shows no special surface effects as in the case of the TiO_2 and fused quartz.

Table II summarizes the data for the films on the various substrates. It appears, then, that the transition between the amorphous phase and the anatase occurs near 300°C. This conclusion is substantiated by some of the work reviewed in Chapter I. Mitchell[47] reported anatase crystallites present in an amorphous matrix after heating a compound film to 300°C. Haas[1] observed that films grown from the vapor phase below 280°C were amorphous while those grown at temperatures above 280°C were anatase. Krylova and Bagdyk'yants[46] reported that films cured above 350°C showed the characteristics of anatase while those cured at lower temperatures remained amorphous. Yokozawa and Iwasa[42] showed that films grown by thermal decomposition of TPT in N_2 between 400° and 700° are mostly anatase. Anneals in the range of 400° to approximately 850°C result in a mixture of the anatase and rutile crystalline forms, while heating at 1000°C seems sufficient to produce completely rutile material. Sakurai and Watanabe[48] produced completely rutile films by thermal decomposition of TPT in a vacuum on substrates heated to greater than 900°C. Haas[1] also found that thermally formed oxides on bare Ti metal at 450°C and above were rutile.

CRYSTALLINE PHASE VS. ANNEAL

FOR SEVERAL SUBSTRATES

ANNEAL TEMP.	POWDER	SOFT GLASS	POLISHED Si	FUSED QUARTZ
150°C (as grown)	AMORPHOUS	AMORPHOUS	AMORPHOUS	AMORPHOUS
350°C	ANATASE	ANATASE	ANATASE	ANATASE
700°C	RUTILE +ANATASE	RUTILE +ANATASE	RUTILE +ANATASE	ANATASE
1000°C	RUTILE	_____	RUTILE	ANATASE

SUB-STRATE

ALL ANNEALS CARRIED OUT IN AIR

TABLE II

INDEX OF REFRACTION, THICKNESS CHANGE

Much of the work reported and synopsized above has defined a strong dependence of the index of refraction on density which is, in turn, a function of the degree of crystallization. Index values and densities in the neighborhood of 2.0 and 2.45, respectively, have been reported for the amorphous films while these values for the rutile films are approximately 2.6 and 4.2, respectively.

Experiments were run in order to measure the index of refraction and the thickness of a film as a function of the anneal treatment. While measurements on the absolute specific gravity of the films were not made, it is assumed that any changes in thickness are proportional to changes in the density of the films since their surface area and mass remains constant.

Measurements of both the index of refraction and the thickness were made by a multiple beam interference microscope and an ellipsometer. Excellent discussion of both methods is included in Chapter I of Burger and Donovan[49]. The 5460 Å green line of Hg was used with both methods so all index values will be valid for this wavelength only.

The multiple beam method involves etching a step in the film to be measured, covering the step with a highly reflective vacuum evaporated metal which duplicates the step perfectly and then measuring the displacement in interference patterns set up by a reference plane. In this case, the thickness is then

thickness of film = (displacement of interference fringe)
x (wavelength/2)

Once the thickness is known, the index of refraction may be calculated by

counting the number of Fizeau interference fringes in the uncovered sec-
tion of the etched step under monochromatic light. In order to accomplish
this, the step must actually have some slope to it and be a wedge. The
index, n, can then be calculated as

$$n = (\text{\# of fringes in wedge})\left(\frac{\text{wavelength}}{2}\right)\left(\frac{1}{\text{thickness}}\right)$$

The ellipsometer method measures the index of refraction by mea-
suring the rotation of elliptically polarized light passing through the
film. The thickness can then be calculated from the index. In our labora-
tory, the calculations are made with the help of an ellipsometer computer
program and an XDS 930 research computer.

Data was taken on two sets of samples, thin film TiO_2 on Si and
thin film TiO_2 on evaporated Pt on fused quartz. Interferometer and ellip-
sometric measurements were made on both sets of samples and the results
were averaged. Fig. 3 shows the index of refraction and the thickness as
a function of the anneal temperature. The transition between amorphous
and anatase can be seen quite clearly near 300°C by the sudden increase
in both the density and index of refraction. No clear transition between
the anatase and rutile forms exist since the two crystalline forms co-ex-
ist over a fairly large temperature range. Similar data is portrayed in
Fig. 4, except the absolute values for the specific gravity have been
given based on the value calculated by Yokozawa and Iwasa[42] of 2.5 gm/cm³
for an amorphous film with an index of refraction of 2.0. Data points ex-
tracted from various authors are included in the graph. In general, their
data is clustered near the curves representing the results of this work.
The work of Feuersanger[38] and Harbison[40] are notable exceptions. In the
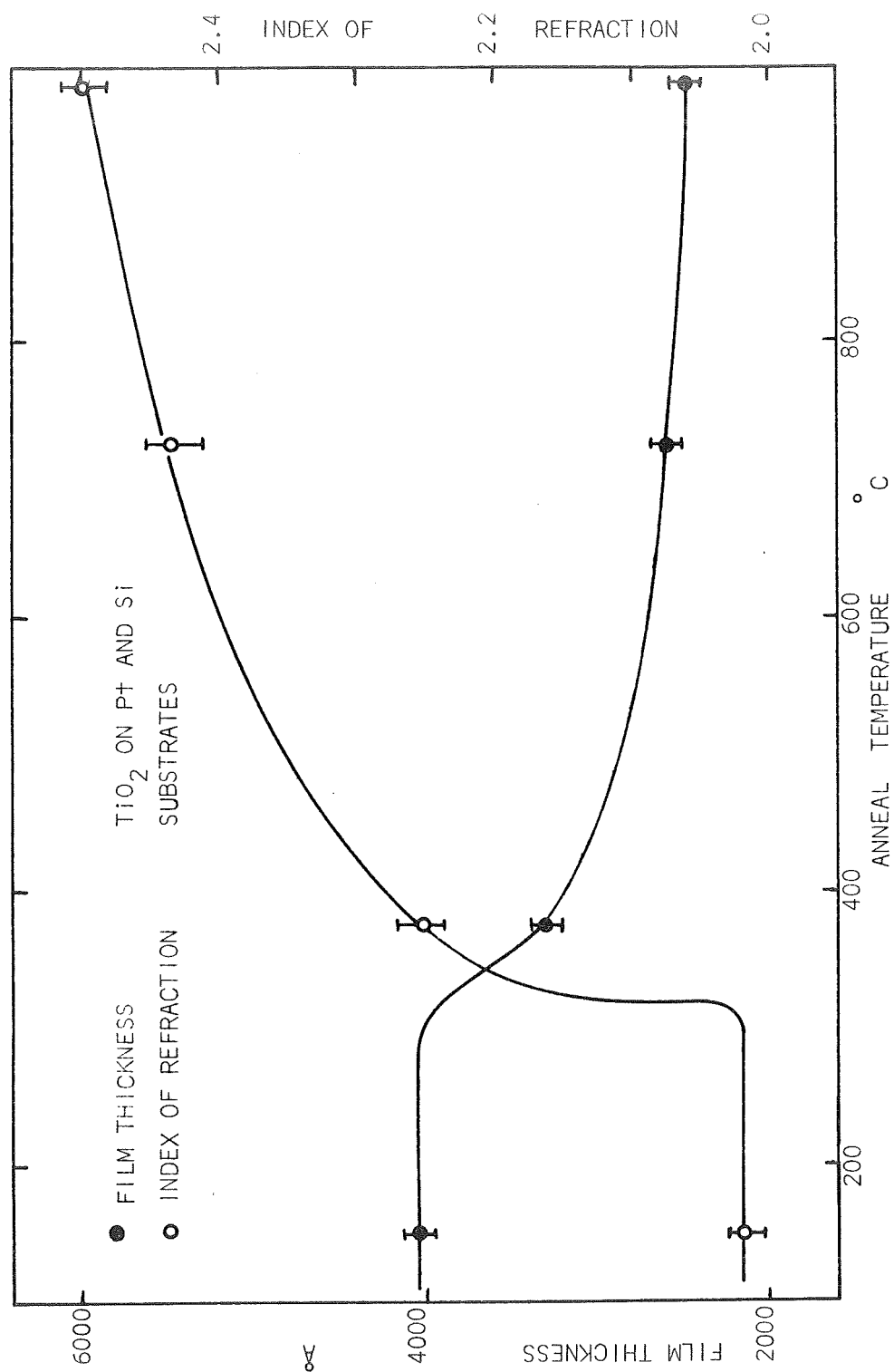
FIGURE 3. FILM THICKNESS AND INDEX OF REFRACTION vs. ANNEAL TEMPERATURE.
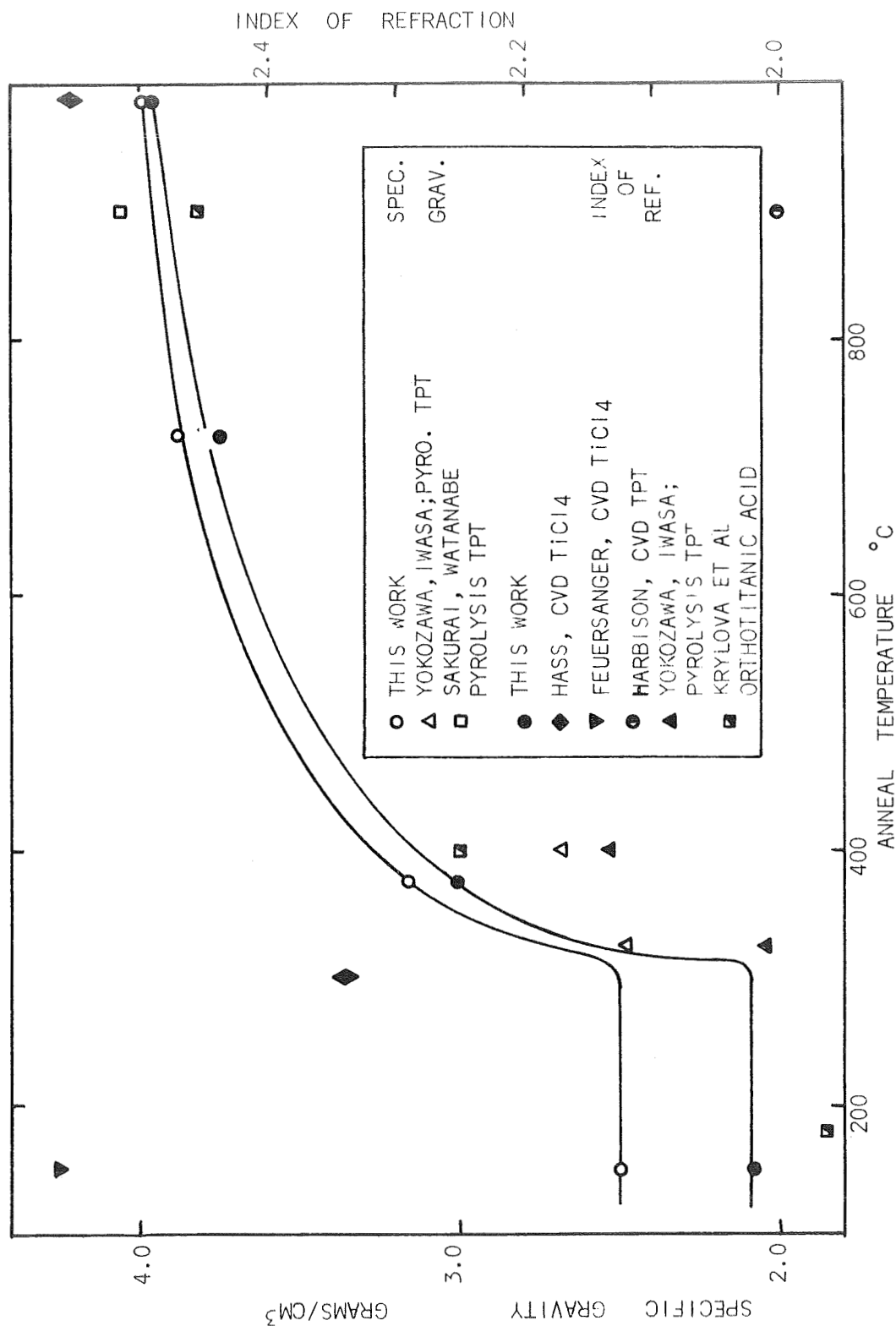
FIGURE 4. SPECIFIC GRAVITY AND INDEX OF REFRACTION vs. ANNEAL TEMPERATURE:
A COMPARISON WITH OTHER WORK.

case of Feuersanger, the TiO_2 films, grown at 150°C, have high indices of

refraction ($\sim$ 2.5) and are quite dense, indicative of the rutile form.

However, the films are easily etched in a 10% HF solution. In the light

of all of the other data, these conclusions seem to be mutually exclusive.

On the other hand, the samples fabricated by Harbison were most likely in

the rutile form. His index of refraction and thickness data was obtained

by using standard ellipsometric techniques. Such techniques when used

with material of a high index of refraction result in index values which

are especially vulnerable to measurement errors (see reference 49, Fig. 2-40).

It is believed that the large discrepancy between the index value deter-

mined by Harbison and the values generally accepted for the rutile form

may be due to such an error.

Some question about the surface quality of the films after a

shrinkage to 62% of the original thickness was entertained. It would ap-

pear that such a violent reduction may set up surface stresses which tear

the film apart in the process. This, however, proved not to be the case.

Electron micrographs taken with a Jeolco SEM2 scanning electron microscope

could resolve no surface detail such as cracks, tears or eruptions at

20,000X after an anneal at 1000°C. An occasional pinhole or dust particle

could be seen breaking the surface of the film. This is to be expected

and is not a result of the annealing process.

A simple model may be postulated for a change in the index of

refraction as a function of any change in the density. The dielectric con-

stant of the material may be written as the sum of its various components,

i.e.,

$$\text{Dielectric Constant} = \text{Contribution of Lattice}$$

$$+ \text{ Contribution of Molecules}$$

$$+ \text{ Contribution of Atomic Electrons}$$

$$+ \text{ Misc. Contributions}$$

An optical frequencies, it is reasonable to expect a contribution from the orbiting electrons alone. Hence

$$K_{OPT} = \frac{N}{V} P$$

where $\frac{N}{V}$ is the number of atoms per unit volume and P is the polarizability per atom. This dielectric constant and the index of refraction are related as

$$n = \sqrt{K_{OPT}}$$

or

$$n = (\frac{N}{V} P)^{1/2} = (\frac{NP}{Ad})^{1/2}$$

where A is the area of the film and d its thickness. If it is then assumed that the number of atoms is the same during the crystallization process and that the polarizability P is a constant, then the only change occurs in the volume or specifically the thickness if the area A remains constant. Hence,

$$\frac{n_1}{n_2} = (\frac{t_2}{t_1})^{1/2}$$

A plot of the index ratio vs. the square root of the thickness ratio is shown in Fig. 5. A fairly good straight line dependence is observed.

SUSCEPTIBILITY TO CHEMICAL ETCH

In Chapter I it was mentioned that one of the major drawbacks to utilizing TiO_2 films as they were being prepared up to that time was a certain difficulty etching the films with standard I.C. techniques. Generally,
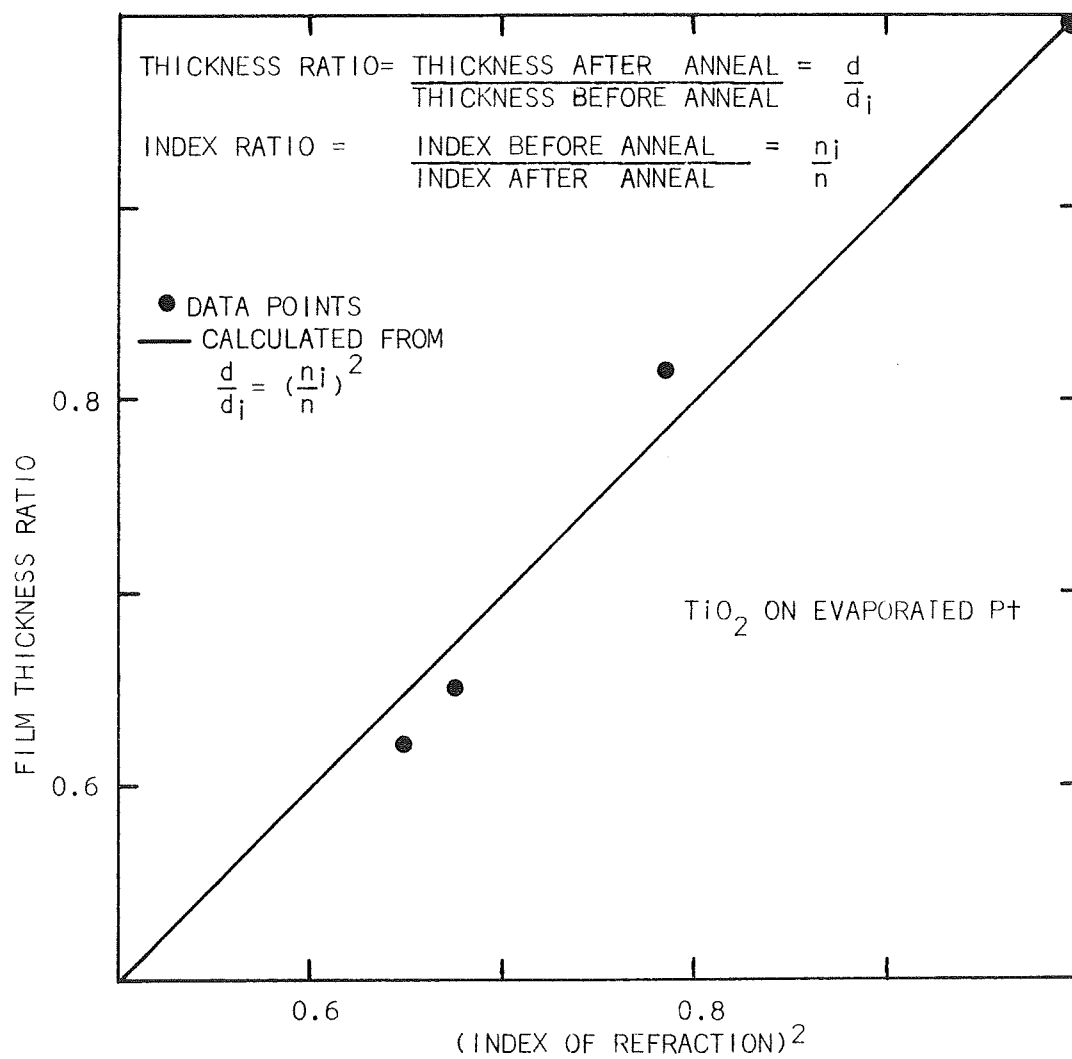
FIGURE 5. FILM THICKNESS RATIO vs. (INDEX OF REFRACTION)^2.

films identified as amorphous have been fairly easy to etch while the anatase form can be etched with some difficulty and the pure rutile forms are quite impervious to chemical attack. In an early book on the subject, Barksdale[50] observes that TiO_2 is known to be somewhat soluble in H_2SO_4, a few strong alkalis and HF. If, however, the TiO_2 is heated near 1000°C the resultant form is almost completely chemically inert.

Determination of the etchability of films after various anneals was done using TiO_2 thin films on polished Si wafers and a solid block of polished Pt.

Amorphous films were found to be quite easily etched in very weak HF solutions. A standard 0.5% aqueous, HF solution gave etch rates on the order of 50 to 75 Å/sec for the amorphous material. These etches were performed at room temperature and proceeded quite uniformly over fairly large areas with no resulting residue. Room temperature concentrated H_2SO_4 etched this material rather slowly, but increasing its temperature to 50°C increased the etch rate to approximately 25-40 Å/sec. Hot H_3PO_4 was also used, but some residue and staining of the film resulted.

Anatase films, i.e., those annealed at 350°C, appeared to be unaffected by the 0.5% HF. Concentrated HF (48%) etched the films on the Pt substrates fairly slowly and, at times, rather non-uniformly. This same etch caused the TiO_2 to be lifted off the surface of the Si wafers, evidently by undercutting them and dissolving a very thin layer of SiO_2 present there. Once again hot (50°C-100°C) H_2SO_4 etched the TiO_2 on both substrates at a relatively slow rate (< 15 Å/sec). Films annealed at 700°C proved even more difficult to etch in the HF and H_2SO_4. As expected, however, the rutile films were almost impervious to chemical attack.

Undercutting of films on Si was again observed with 48% HF. The TiO_2 film floated off and broke up into small triangular patches, some 1 mm on an edge. It seems that while undercutting did occur, the HF did not actually attack the TiO_2 itself. This conclusion was borne out by the TiO_2 on the Pt substrate which was unaffected by the 48% HF. Very hot H_2SO_4 (120° - 200°C) was shown to have some effect, but the etch rates were quite small ($\sim$ 1000 Å/hour).

It seems fairly obvious that the amorphous film alone lends itself readily to the various etching operations necessary to have a compatible thin film technology since it can be removed completely or partially (i.e., the thickness can be reduced) in a uniform and controllable manner with a weak, room temperature etch. While the higher crystalline forms could be completely removed from the surface of Si with HF by undercutting, this would generally be viewed as undesirable. Etching with hot (> 100°C) H_2SO_4 is also extremely undesirable since few, if any, commercial photo resists would hold up under such extreme conditions.

Yokozawa and Iwasa[42] reported that their amorphous material was etched in very dilute HF at rates between 4 and 60 Å/sec., while their anatase films were etched only slowly in more concentrated solutions. Feuersanger's[38] data seems to be contradictory in that he states that his films could be etched easily in a 10% HF solution. This is as expected since they were grown at 150°C and are, most probably, amorphous. However the author states his belief that the films are crystalline, a mixture of anatase and rutile, based on the index of refraction. Harbison[40] reported an etch rate of 700 Å/min. in 48% HF for material grown at 800°C. There seems to be some question about this conclusion in light of the above work.
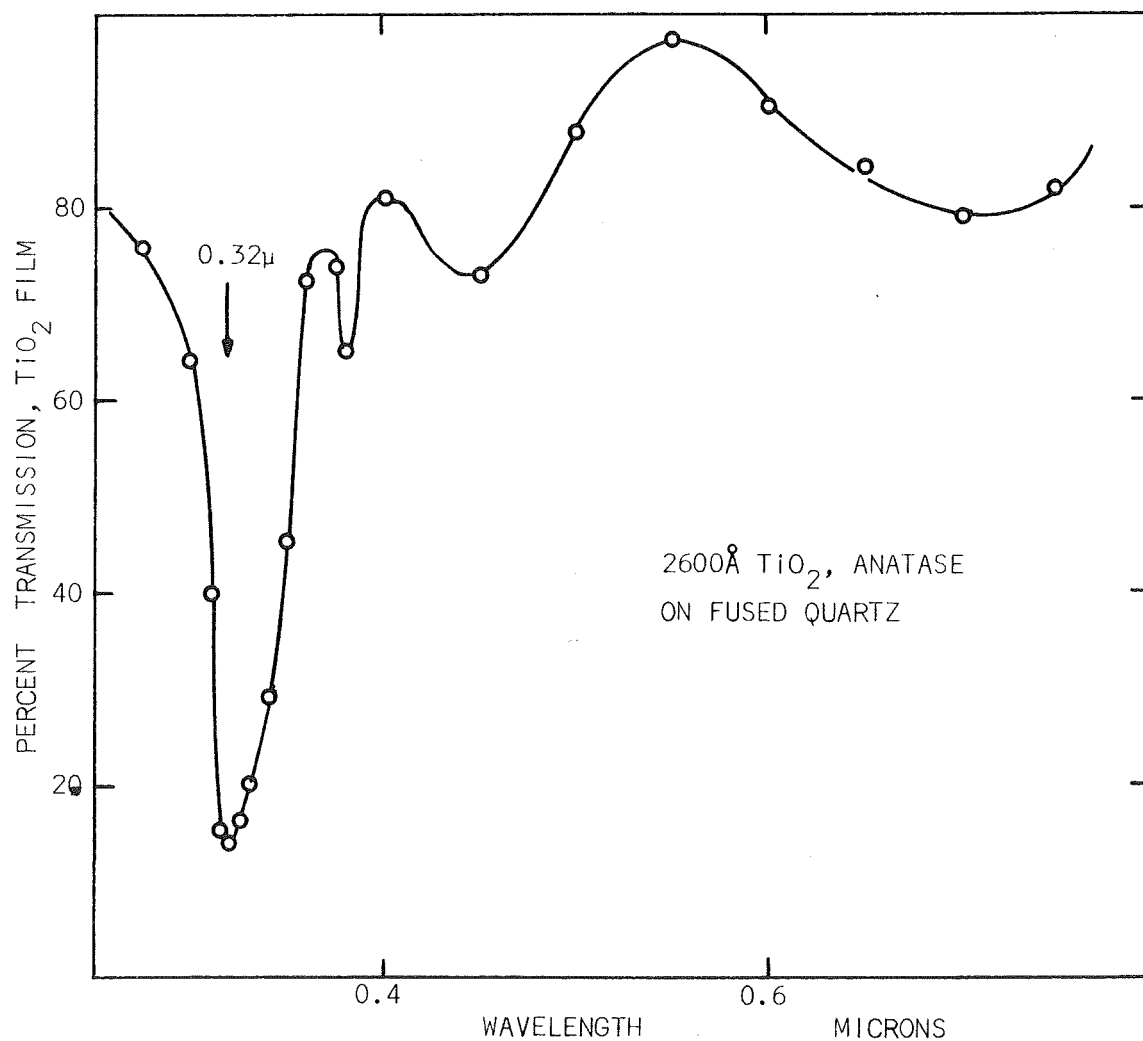
FIGURE 6. OPTICAL TRANSMISSION SPECTRUM OF ANATASE TiO$_2$ FILM.

OPTICAL ABSORPTION

An optical transmission spectrum for a thin layer (2600 $\mathring{A}$) of anatase TiO$_2$ on a fused quartz disc is shown in Fig. 6. It is obvious that there is a strong absorption in the u.v. at .32 μ corresponding to a photon energy of 4 eV. A similar absorption peak centered at .32 μ was observed by Maserjian[51] for a completely rutile thin film. The absorption in an amorphous film was also measured and similar results were noticed, except that the absorption in the u.v. was far less sharp, although centered at the same energy. Van Raalte[7] reports that optical transmission experiments on a single crystal places the 3d conduction band about 3.2 eV above the valence band. Maserjian[51] attempts to reconcile the two pieces of data by suggesting that the bandgap may well indeed be 3.2 eV and that the 4 eV represents a transition between the 0^{-2}(2 p) and the Ti^{+5}(4 p) bands. While this may or may not be the case, it is evident that the 4 eV absorption edge exists in all forms of the film and, if it does not indicate the bandgap limits, it certainly remains the strongest optical absorption mechanism in both the crystalline and amorphous material.

CHAPTER IV.

ELECTRICAL CHARACTERISTICS

INTRODUCTION

As with the properties discussed in Chapter III, some electrical characteristics of thin film TiO_2 have been studied for various film-making techniques and film treatments. This work was reviewed in Chapter I and it was pointed out there that little attempt has been made to correlate the electrical properties measured with the crystalline nature of the film or a series of anneals under known conditions. It is apparent from other work that the resistivity of TiO_2 is a strong function of the stoichiometry of the material along with the defect density and a number of other structural properties.

Keeping the results of previous authors in mind and utilizing a number of facts presented in Chapter III, it is the purpose of the experiments and analysis in this chapter to unify the various electrical parameters, such as resistivity, dielectric constant, dissipation factor, surface state density and electron conduction mechanisms in terms of the anneal history of the thin films.

SAMPLES AND EQUIPMENT

The majority of the data was taken on simple capacitor-like samples of either a metal-insulator-metal (MIM) or metal-insulator-semiconductor (MIS) structures. Figure 7 shows a cross-sectional representation of both of these samples. The MIM samples consist of a polished fused quartz substrate, an evaporated Pt film for the bottom conductor, the TiO_2 thin film deposited at 150°C and annealed and an evaporated Al dot for a counter electrode. A simple "screw-down" pressure contact was used to

METAL-INSULATOR-METAL   METAL-INSULATOR-SEMICONDUCTOR
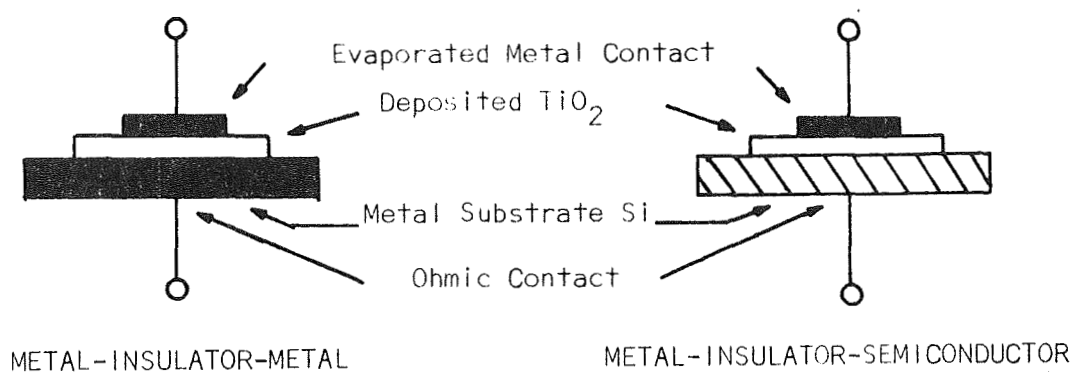
FIGURE 7.   METAL - INSULATOR - METAL AND METAL - INSULATOR -
            SEMICONDUCTOR SAMPLE CONFIGURATIONS.

make contact with the Pt electrode while a spring-loaded probe was used to contact the top Al. The spring tension could be adjusted to exert a pressure on the Al sufficient to make good electrical contact while exerting the minimum force on the TiO_2 layer beneath. In general, care had to be taken only while contacting the low temperature, "as grown" samples since the insulators annealed at elevated temperatures proved to be quite durable.

The majority of MIS samples have p type 1-ohm cm. substrates. Ohmic contact to these substrates is made with a GaIn eutectic paste on the backside of the wafer. The TiO_2 layer and the Al counterelectrode are similar to the MIM samples. In both cases, the Al dot is on the order of .25 mm^2.

Two types of electrical data were taken from these samples:

(a) Current-voltage d.c. measurements (I-V)

(b) A.C. small signal capacitance vs. d.c. bias (C-V)

Figure 8 shows a schematic representation of the electrical test apparatus. In the case of both the I-V and C-V measurements, the d.c. bias is varied manually and the subsequent current or capacitance is measured. It is recognized that due to the inherent lack of speed of taking data with this method any ionic drift present will manifest itself as distortion in the curves. On the few occasions that such drift was observed its magnitude was recorded and its significance mentioned in the analysis. The capacitance data is limited to frequencies between 20 Hz and 100 kHz. No high frequency data above 100 kHz could be obtained and the parameters measured are characteristic of the films between 1 kHz and 100 kHz.
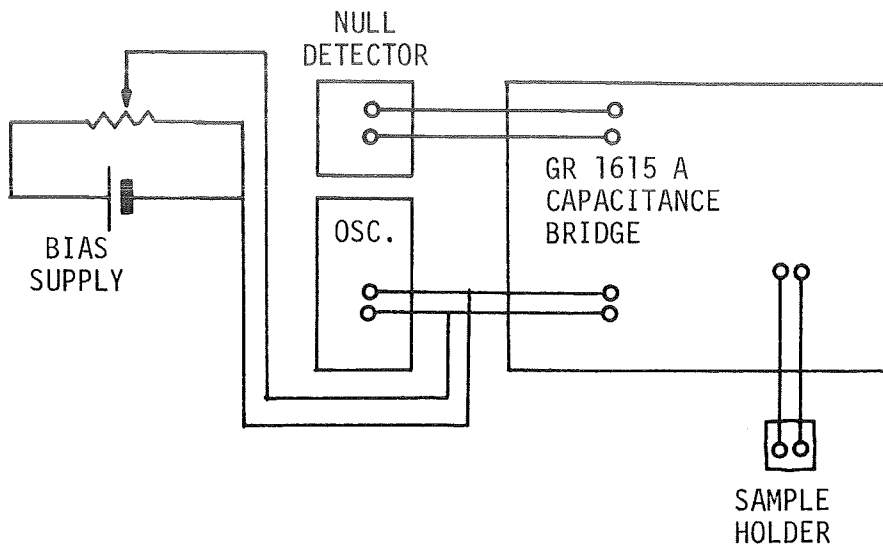
CAPACITANCE MEASURING CIRCUIT
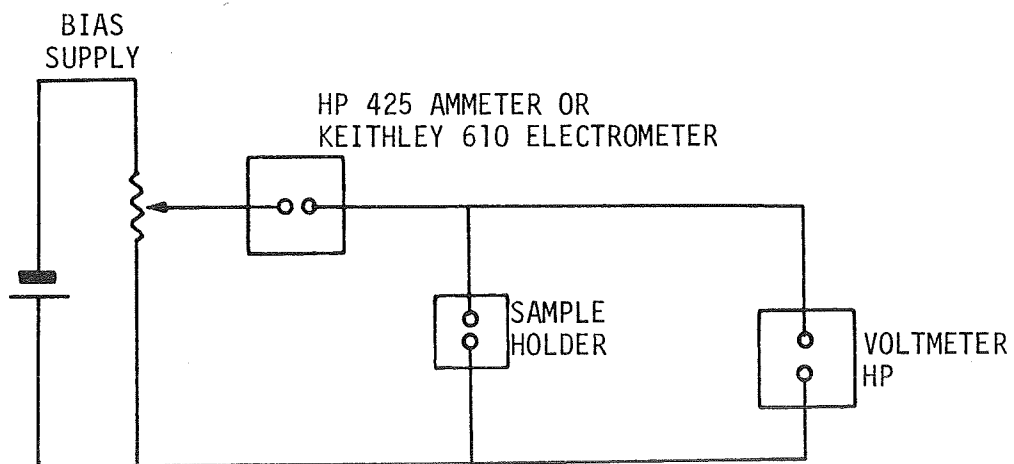
CURRENT VS. VOLTAGE MEASURING CIRCUIT

FIGURE 8.   ELECTRICAL TEST APPARATUS.

‌

ELECTRICAL MEASUREMENTS

(1)   The 150°C "As Grown" Material

From the previous chapter, it was found that this material is

amorphous, of relatively low density and index of refraction. There is

some possibility that pockets of reaction products or unreacted TPT are

incorporated into the film. For this reason and owing to its relatively

low density and unordered amorphous structure, it would not be unreason-

able to anticipate that these films are poor insulators and exhibit a mix-

ture of properties characteristic of insulators and high resistivity semi-

conductors.

Fig. 9 shows the I-V characteristics of a typical MIM structure.

Immediately obvious is the strong asymmetry of the current with bias.

Such a characteristic is suggestive of some type of diode action and re-

sembles the results obtained by Lakshmanan[28], Magill[22], Huber and

Rottersman[21], Komolova and Nasledov[31] and Dorin and Patrokova[52] for sput-

tered and anodized films. All attempt to explain the I-V and C-V charac-

teristics they observe in terms of a graded p-n junction internal to the

TiO_2 itself or in terms of a Schottky barrier at the TiO_2 electrode inter-

face. It is not unreasonable to expect the presence of a graded junction

in an anodized layer of TiO_2 due to the drift of Ti ions in the anodized

field. However, for other methods of film formation, such as CVD, it is

difficult to imagine how such a junction could come about and homogeneous

bulk properties are far more plausable. On the basis of the work reviewed

in Chapter I, it is expected that the bulk properties of the TiO_2 will re-

semble those of a high resistivity n type semiconductor. Huber[19] reports

a work function for TiO_2 of this description of approximately 4.3 eV.
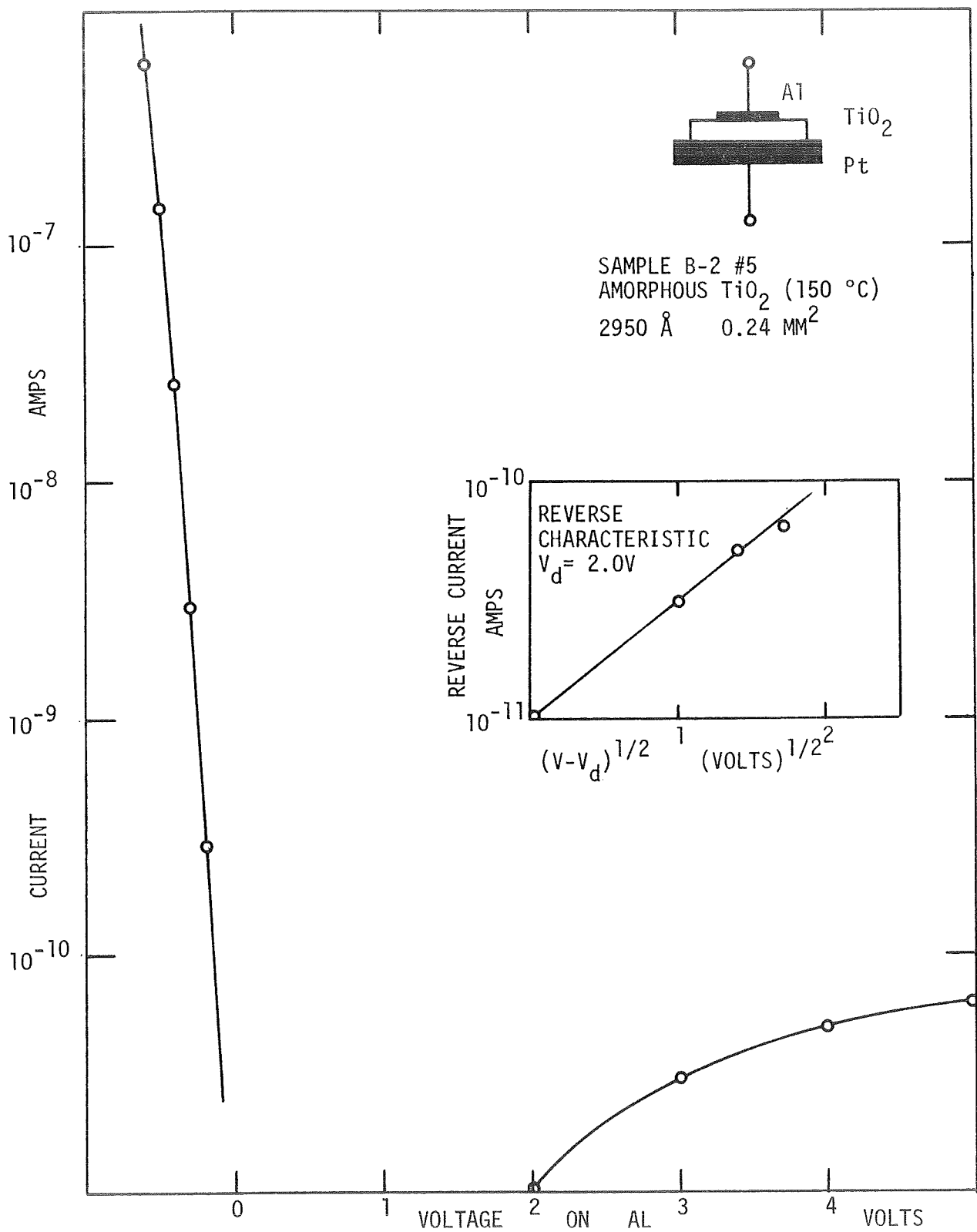
FIGURE 9. CURRENT vs. VOLTAGE FOR AMORPHOUS TiO_2.

By postulating that this low temperature TiO_2 is a high resistivity n type semiconductor with a work function of approximately 4.3 eV, it is possible to explain the I-V characteristics on the basis of a Schottky junction at the TiO_2-Pt interface. The Al electrode, with a work function of 4.2 eV, will form an ohmic contact with n type TiO_2 which has a higher work function. The characteristics will be governed by the barrier at the TiO_2-Pt interface and the bulk properties of the TiO_2.

The nature of such a metal-semiconductor junction is considered by Shockley[53] and Henisch[54] and most recently, quite thoroughly by Sze[55]. He considers three separate approaches to current transport in Schottky barriers: (a) the simple thermionic theory; (b) the isothermal diffusion theory; (c) a general theory which incorporates currents due to both (a) and (b) into a single thermionic-diffusion current. It is this last theory which will be utilized here. Details of the derivation will not be considered.

The complete Schottky I-V characteristic based on the thermionic-diffusion theory can be expressed as:

$$J = J_S(e^{qV/kT} - 1) \qquad [1]$$

where

$$J_S = A^{**}T^2 \exp\left(-\frac{q\phi_{BN}}{kT}\right)$$

and

$$A^{**} = A^* f_p f_q / (1 + f_p f_q v_R / v_D)$$

A^* is the Richardson constant usually associated with metals. The value of this constant is reduced by the factor containing f_p and f_q which are the probabilities of an electron crossing the barrier and then being scattered back by optical or phonon scattering and reflection due to quantum

mechanical scattering respectively. The quantities v_D and v_R are the effective diffusion velocity and the effective recombination velocity, respectively. The value of A** for electrons in a metal-n type Si system is approximately 110 amp/cm^2°K^2, while for holes in a metal-p type Si system the value is approximately 30 amp/cm^2°K^2. The meaning of ϕ_{BN} is best explained by Fig. 10. The rounding of the barrier near the interface is due to the superimposed effects of the electric field associated with ionized donors and the image force correction. The barrier lowering due to these forces is represented in the figures as $\Delta\phi$. Using Eq. [1], the generalized Schottky current is

$$J = A^{**}T^2 \exp\left\{-\frac{q}{kT}\phi_{BN}\right\}\left\{e^{qv/kT} - 1\right\} \qquad [2]$$

$$= A^{**}T^2 \exp\left\{-\frac{q}{kT}\phi_{BO}\right\}\left\{e^{\frac{q}{kT}(V + \Delta\phi)} - 1\right\} \qquad [3]$$

In the forward direction, i.e., with the Pt biased + with respect to the TiO$_2$, the exponential term containing the bias V becomes much larger than 1. Hence, the forward current may be written

$$J_F = A^{**}T^2 \exp\left\{-\frac{q}{kT}\phi_{BO}\right\}\exp\left\{\frac{q}{kT}(V + \Delta\phi)\right\} \qquad [4]$$

Both A** and $\Delta\phi$ are functions of the junction bias. In addition to this dependence some portion of the applied bias, V, is dropped across the TiO$_2$ bulk. This voltage drop may be expected to be exponential rather than linear because of the high resistivity and insulating nature of the bulk. These effects will have a tendency to reduce the junction current for a given applied bias. Correction for the functional dependence of $\Delta\phi$ on V and the bulk voltage drop may be made by altering the argument of the exponent, i.e.,

METAL

VACUUM

TiO_2

ϕ_M

E_F

ϕ_W

χ

E_C

E_F

E_V

$\phi_M - \chi$

E_C

E_F

E_V

$\Delta\phi$

ORIGINAL BAND BENDING

$\phi_{BO} = \phi_M - \chi$

ϕ_{BN}

CORRECTED BY IMAGE FORCE

E_F
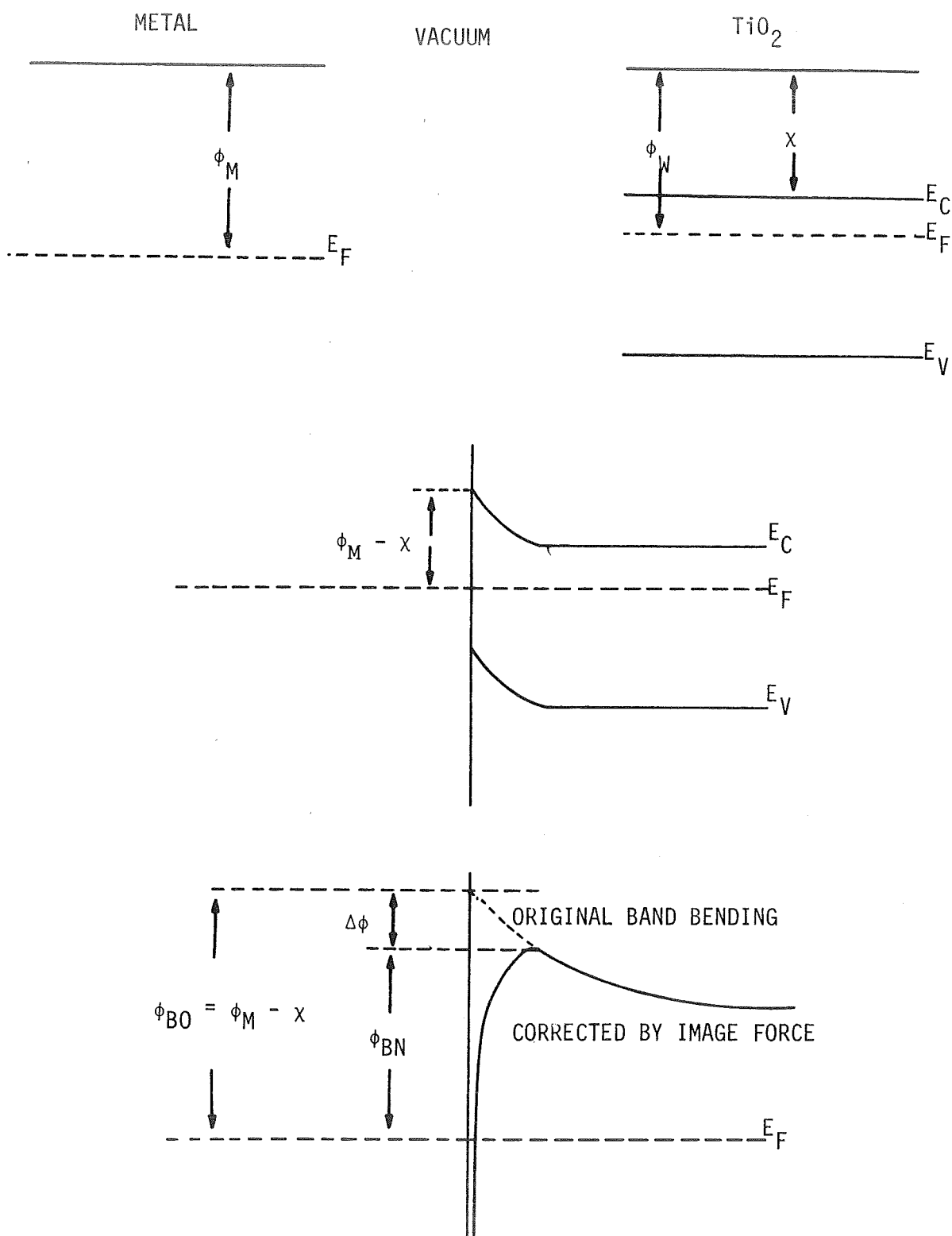
FIGURE 10. ENERGY BAND DIAGRAM FOR METAL- TiO_2 INTERFACE.

$$J_F \propto \exp \{\frac{qV}{nkT}\} \tag{5}$$

where $n \geq 1$ and may be found as

$$n = \frac{q}{kT} \; \partial V/\partial \; (\ln J)$$

From Fig. 9, the slope of the characteristic in the forward direction is 20.7/volt. Equating this with the argument in Eq. [5]

$$\frac{q}{nkT} = 20.7/\text{volt}$$

yields

$$n = 1.86$$

This correction has been found to be 1.02 for a W-Si diode of fairly low bulk resistivity and 1.04 for a W-GaAs diode[56].

By extrapolating the forward characteristic to give the zero bias current $J(0)$, the barrier height can be obtained from the following equation

$$\phi_{BN} = \phi_{BO} - \Delta\phi = \frac{kT}{q} \ln \left[\frac{A^{**}T^2}{J(0)}\right] \tag{6}$$

For an intercept of 9×10^{-10} amp/cm^2 and A^{**} equal to the Richardson constant of 120 amp/cm^2

$$\phi_{BN} = .95 \text{ eV}$$

This barrier height is a function of the surface state density at the interface, the metal-semiconductor work function difference and the barrier lowering term. Assuming that the effect of the surface states are small

$$\phi_{BN} = \phi_m - \chi - \Delta\phi \tag{7}$$

where χ is the electron affinity of the TiO_2 and is related to the work function, ϕ_ω, and the distance of the fermi level from the conduction band edge.

$$\phi_\omega = \chi + (E_C - E_F) \qquad [8]$$

From Eq. [7]

$$\chi = \phi_m - \phi_{BN} - \Delta\phi$$

For Pt ϕ_m = 5.2 eV and, at moderate fields, 0.1 < $\Delta\phi$ < 0.3 eV. Then

$$\chi = 5.2 - .95 - .2 = 3.95 \pm .1 \text{ eV}$$

Using the value of 4.3 for the work function discussed earlier, obtain

$$E_C - E_F = 4.3 - (3.95 \pm .1) \text{ eV} = .35 \pm .1 \text{ eV}$$

This value is quite similar to a value (0.25 eV) reported by Harbison[40] for

the trap depth of sites in insulating TiO_2.

In the reverse direction, the exponential term in V becomes small

compared with 1. From Eq. [3] the reverse current is

$$J_R = A^{**}T^2 \exp\left\{- \frac{q}{kT} \phi_{BO}\right\} \exp\left\{\frac{q}{kT} \Delta\phi\right\} \qquad [9]$$

From this expression, it is evident that the reverse current is controlled

by the barrier lowering term, $\Delta\phi$, which is a function of the electric field.

This functional dependence, developed in the classical Schottky theory is:

$$\Delta\phi = \left\{\frac{q\xi}{4\pi K_o \epsilon_o}\right\}^{1/2} \qquad [10]$$

where ϵ is the electric field at the barrier and K_o is the optical relative

dielectric constant of the material. The electric field at the junction of

a back-biased, one-sided abrupt junction in terms of the applied bias can

be calculated from Poisson's equation to be

$$\xi = \left\{\frac{2qN_D}{K\epsilon_o} (V + V_{bi})\right\}^{1/2}$$

where V_{bi} is the built-in voltage of the junction, N_D is the density of

donor sites in the semiconductor and K is the low frequency relative

dielectric constant of the material. Combining Eqs. [9], [10] and [11]

$$J_R \propto e^{mV^{1/4}} \qquad [12]$$

where m is the slope of the characteristic. This dependence on $V^{1/4}$ is only the case if a portion of the applied bias is used to increase the depletion layer width in the semiconductor. However, if the donor density is very low, i.e., a material is of a high resistivity as is the TiO_2, the depletion layer may easily extend throughout the bulk of the material and reach the counterelectrode at some applied bias V_d. After this has occurred, the electric field across the barrier increases linearly with applied bias. That is, for $V > V_d$

$$\xi = \frac{V - V_d}{d} + \xi_d \qquad [13]$$

where ξ_d is the field corresponding to V_d and d is the thickness of the TiO_2 layer. In this case,

$$J_R \propto \exp[m'(V - V_d)^{1/2}]$$

where m' is the slope of this characteristic.

The inset in Fig. 9 shows I_R as a function of $(V - V_d)^{1/2}$, where V_d has been allowed to be 2 volts. A fair straight line agreement is observed with a tendency to curve slightly down at higher voltages. This curvature could easily be due to the forming process occurring while the data was being taken since the current was observed to decrease slightly with time at a given bias.

A calculation of the resistivity of the bulk material from this I-V data is not possible since the characteristics of the junction are the

controlling factor. Several samples were subjected to higher biases and it was generally found that the forward current saturated in the milliamp range at approximately 2 volts. It is believed that this current saturation is caused by the series resistance of the bulk material.

The C-V data of these low temperature samples is severely complicated by the fact that the material exhibits rather strong forming characteristics. Fig. 11 shows the C-V data for a typical sample when first subjected to an applied bias. The data includes the forming history of the sample under the external bias. At point (1) on the curve, the virgin sample is characterized by a high capacitance and dissipation factor. If the parallel plate approximation is used, the apparent relative dielectric constant at this point is approximately 320, suspiciously high to be associated with the bulk material. When the bias is increased at a steady rate to six volts (point (2)) and held there, the capacitance begins to drop immediately and continues to drop as a function of time and is asymptotic to the value at point (3). This final capacitance was reached in less than 10 minutes and the sample was held under the field for 15 minutes. The bias was then reduced and the capacitance remained constant, independent of bias above zero volts. As the bias is reversed the capacitance and dissipation factor increase rapidly as point (5) is approached. The characteristics between (5), (4), and (3) can be reproduced and are independent of time.

The capacitance of the Schottky barrier in the reverse direction is merely that of a reverse biased one-sided junction and may be expressed as
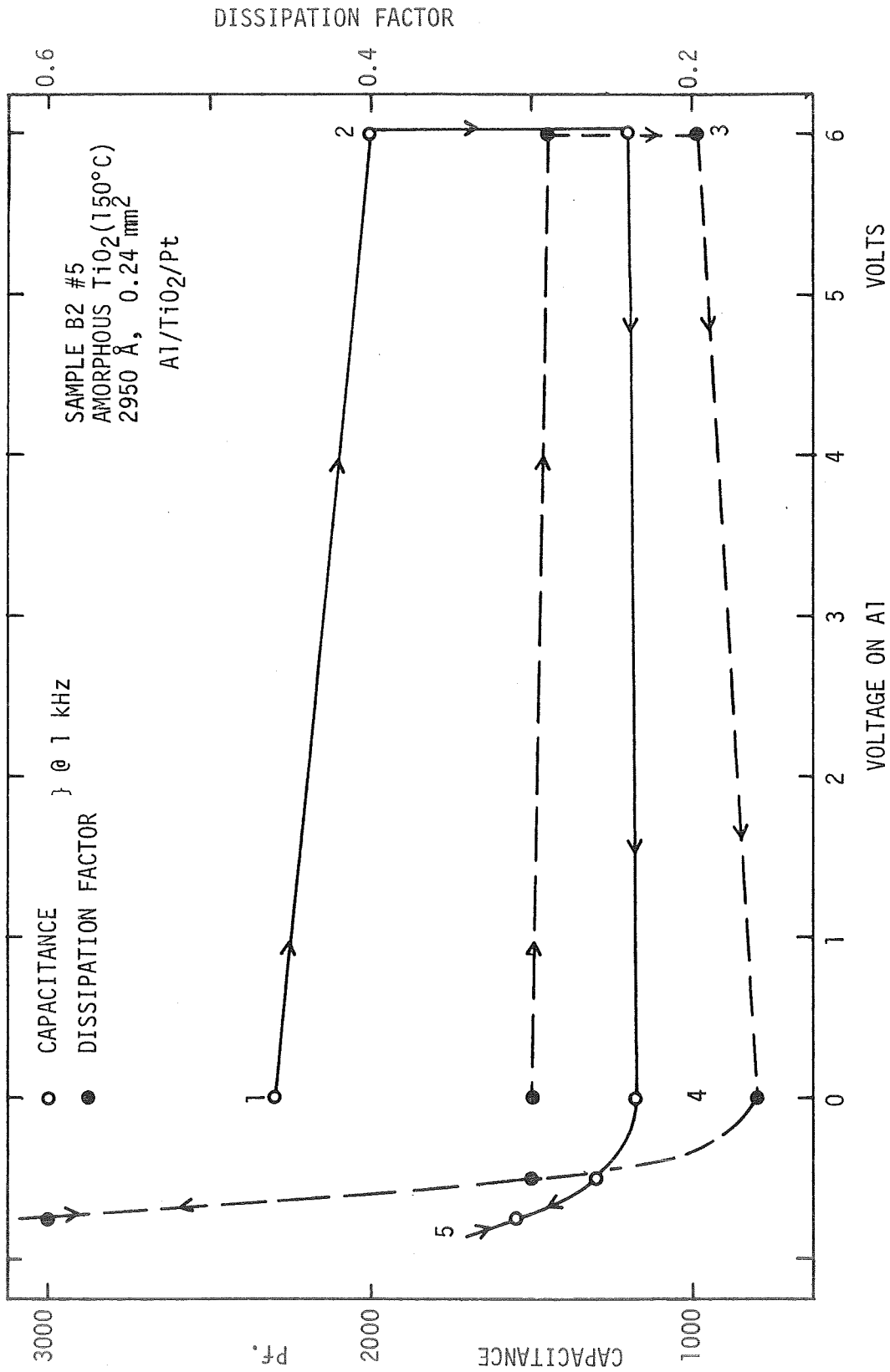
FIGURE 11. CAPACITANCE vs. VOLTAGE FOR AMORPHOUS TiO$_2$.

$$\frac{1}{C_d^2} = \frac{2(V_{bi} - V)}{qK\varepsilon_o N_D} \qquad [14]$$

i.e., the depletion capacitance, C_d, is expected to decrease as $V^{-1/2}$ as

long as the depletion region continues to grow. After the depletion re-

gion reaches the counterelectrode at V_d, the capacitance is independent of

bias and may be expressed as

$$C_d = \frac{K\varepsilon_o A}{d}, \; V > V_d \qquad [15]$$

If V_d is fairly low then the capacitance can be expected to be independent

of bias over most, if not all, of the reverse bias range. In this range

between points (3) and (4) in Fig. 11, Eq. [15] yields for the relative di-

electric constant K = 165. Feuersanger[38] reports a dielectric constant of

178 and a dissipation factor of over 0.1 for films grown from TPT at low

temperatures.

Ionic drift may take place during the forming process, but it is

difficult to believe that this could cause such a marked decrease in the

capacitance. By comparing the dielectric constant with that found in the

next section for some of the annealed material, it appears that some form

of field induced ordering may be taking place.

In the forward direction the capacitance is the sum of that as-

sociated with the finite width of the junction and the contribution from

the rearrangement of the minority carrier density known as the diffusion

capacitance. Sze[55] calculates this diffusion capacitance for a one-sided

junction to be

$$C_{dif} = \frac{q}{kT} \left\{ \frac{qL_n n_{po}}{2} \right\} e^{qV/kT} \qquad [16]$$

where L_n and n_{po} are properties of the material bulk.

Once again, any applied voltage V appears only in part across the junction, the rest appears across the bulk and cancels built-in voltages to assure that the junction is forward biased. Hence, the total forward capacitance may be written as

$$C = C_J + C_{dif} \qquad [17]$$

where, from Eq. [16]

$$C_{dif} \propto \exp \{\frac{q}{kT} (\frac{V - V_f}{h})\}, \; h \geq 1 \qquad [18]$$

Little capacitance data was collected in the forward direction to assure that the sample was not destroyed by excessively high currents. The data that is shown exhibits only a rapid increase in the forward direction, perhaps suggestive of the exponential dependence predicted by Eq. [18].

(2)   The 350°C Annealed Material

Unlike the sample in the previous section, those tested after a 350° 14-hour anneal, are of the MIS type based on 1 ohm cm. p type Si substrates. In Chapter III it was stated that TiO_2 subjected to such an anneal is generally in the pure anatase form, of moderate density and physical hardness and is in a state characterized by far higher ordering than the amorphous films considered in the previous section. It was not determined whether samples, after such an anneal, are completely anatase. It was determined that no higher crystalline forms are present in any substantial amounts. However, the presence of amorphous inclusions in the anatase lattice could not be detected and this possibility must always be considered. No estimation of the perfection of the polycrystals, the presence of impurities or any deviation from stoichiometry can be gathered from the data taken to this point.

Figs. 12 and 13 show the C-V and I-V characteristics, respectively, of typical samples that have been grown at 150°C and annealed at 350°C. A complete explanation of generalized C-V curves for MIS samples has been given by Terman[58], Grove[57], Nicollian and Goetzberger[59], and Sze[55]. No attempt to reproduce their analyses will be made here. Rather, only specific results from their work that has direct bearing on these experiments will be used.

Quite simply, standard C-V characteristics for an MIS sample are divided into three regions determined by the bias:

1. The accumulation region in which the surface of the Si is heavily populated by majority carriers and resemble a metal. In this case, the capacitance is not a function of bias and is determined by the characteristics of the insulator alone.

2. The depletion region in which the surface of the Si and part of the bulk near the surface is devoid of majority carriers. In this region the total capacitance is the total series capacitance of the insulator capacitor and the depletion region capacitance. This total capacitance continues to decrease as a function of bias until the inversion region begins.

3. The inversion region, in which the surface of the Si becomes populated by minority carriers and the depletion region ceases to grow as a function of bias. In this region the total capacitance remains constant as a function of bias.

The boundaries of these regions with bias are determined by numerous parameters of the MIS system, including the dielectric constant of the insulator, the work function difference between the metal and the

SAMPLE CV-7 #3
350°C 14 HOUR ANNEAL
ANATASE TiO2
1150 Å, 0.24 mm² AREA

1 OHM-CM P TYPE Si

Al/TiO2/Si

o   1kHz

□   100kHz

VOLTS

VOLTAGE ON Al

CAPACITANCE vs. VOLTAGE FOR ANATASE TiO2.

PICOFARADS

4000

2000
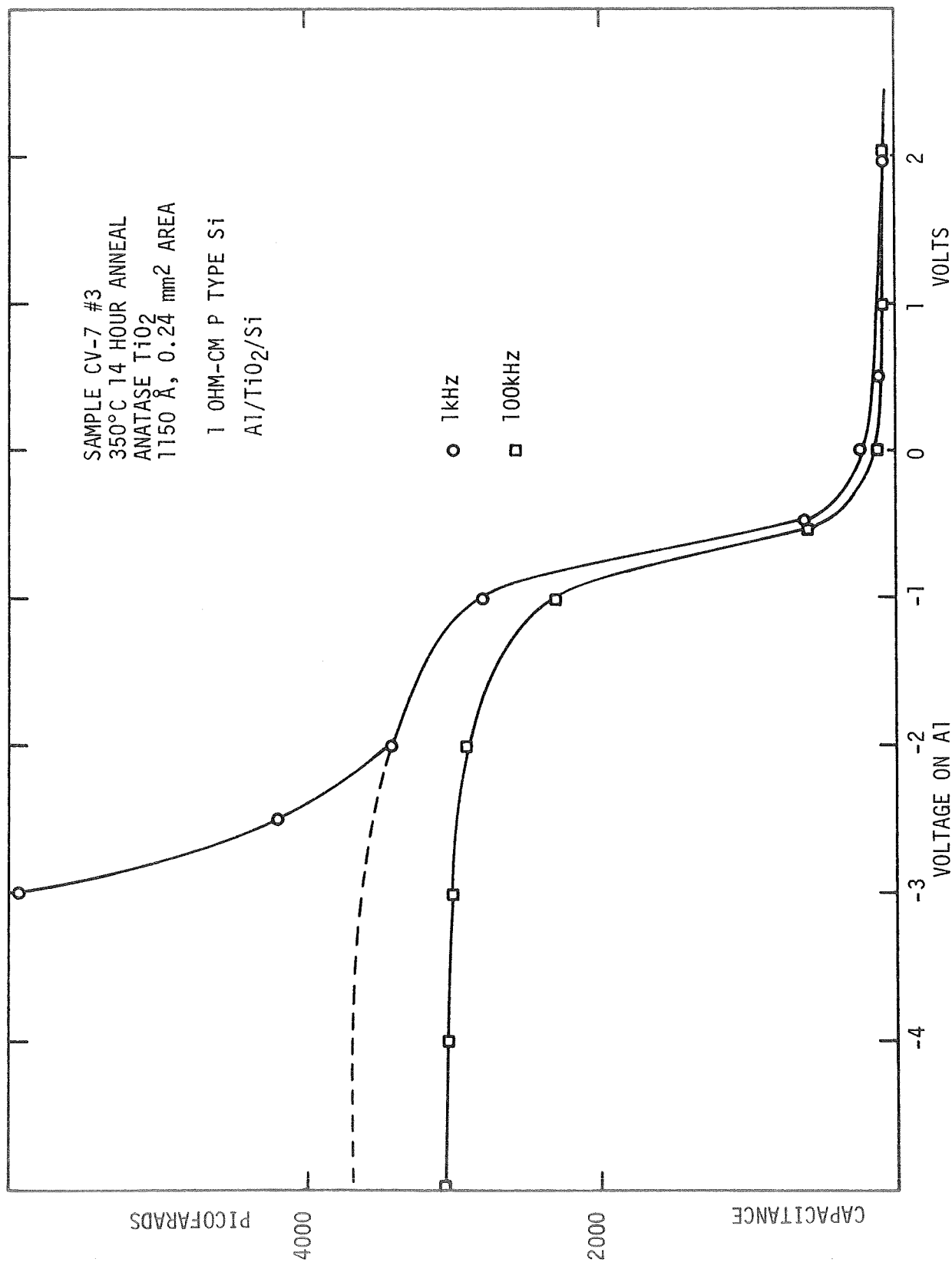
CAPACITANCE

FIGURE 12.   CAPACITANCE vs. VOLTAGE FOR ANATASE TiO2.

SAMPLE CV-7 #17
350°C, 14 HOUR ANNEAL
ANATASE TiO_2
1300 Å, 0.20 mm^2 AREA
ACCUMULATED
CAPACITANCE = 2300 pf.

Si 1 OHM-CM P TYPE
    $Al/TiO_2/Si$
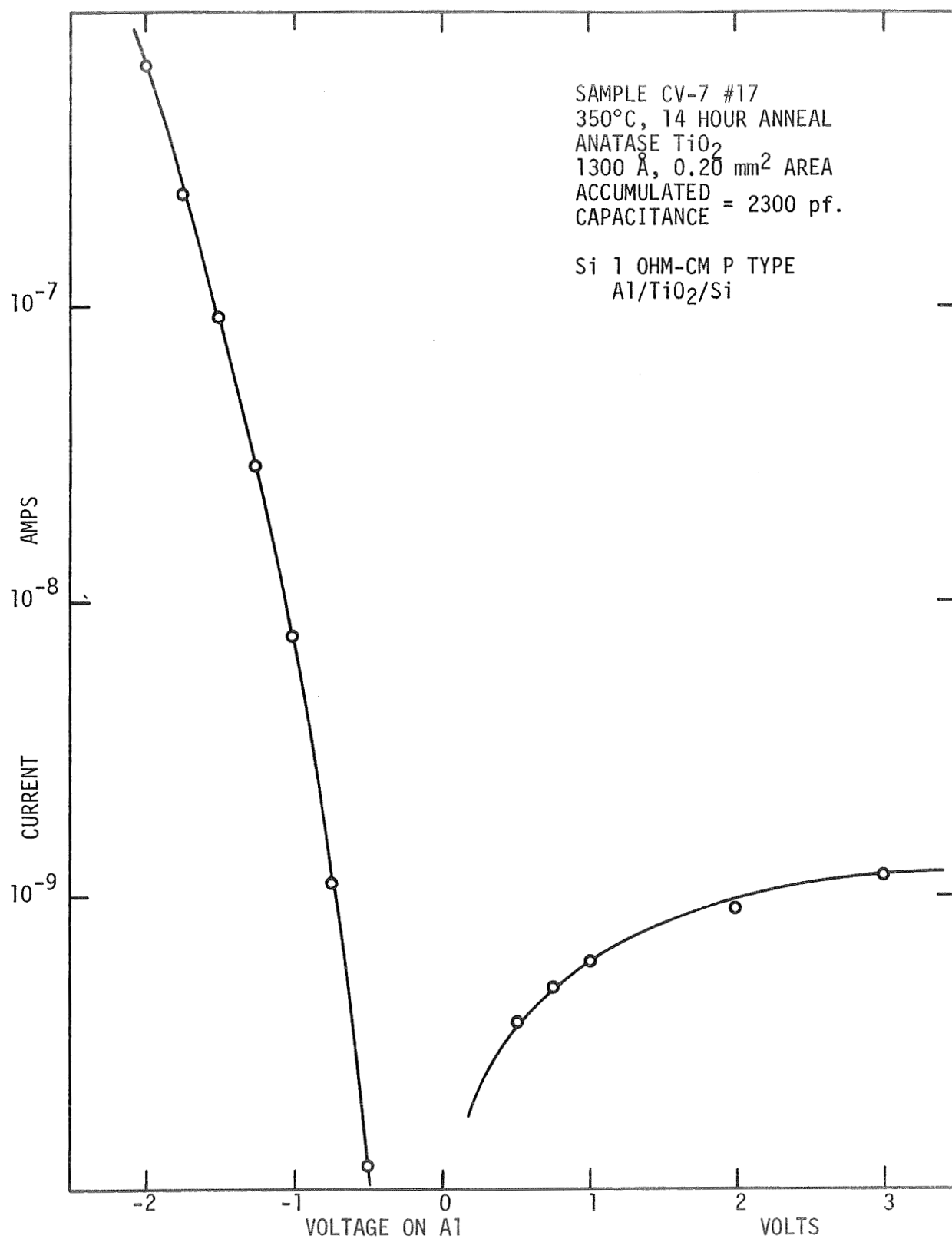
FIGURE 13.   CURRENT vs. VOLTAGE FOR ANATASE TiO_2.

semiconductor, the nature and number of surface states at the insulator-semiconductor interface, the doping density of the Si and other parameters of the Si bulk. An important quantity is the flatband voltage, V_{FB}, which defines the division between the depletion and accumulated region. This voltage can be determined from the C-V characteristic by identifying the capacitance at flatband. According to Sze[55] (Chapter 9, Eq. [26]) the total capacitance at flatband is

$$C_{FB} = \frac{K_i \epsilon_o}{d + (\frac{K_i}{K_s}) (\frac{kTK_s \epsilon_o}{p_{po}q^2})^{1/2}} \qquad [19]$$

where K_i = relative dielectric constant of TiO_2

K_s = relative dielectric constant of Si

d = thickness of TiO_2

$p_{po} \simeq N_A$ = equilibrium density of holes in the p type semiconductor.

By defining two quantities C_o and C_{SFB} as

$$C_o = \frac{K_i \epsilon_o}{d}, \quad C_{SFB} = q \{\frac{K_s \epsilon_o N_A}{kT}\}^{1/2} \qquad [20]$$

Eq. [19] may be re-written as

$$C_{FB} = \frac{C_o C_{SFB}}{C_o + C_{SFB}} \qquad [21]$$

C_o is the accumulation region capacitance of the structure determined by the properties of the insulator. C_{SFB} may be calculated for 1 Ω cm p type Si to be 0.3 $\mu f/cm^2$. From Fig. 12 at 100 kHz the value of C_o for this specific sample is 1.06 $\mu f/cm^2$ (2550 pf/2.4 x $10^{-3}cm^2$). Using Eq. [21] C_{FB} = 560 pf and, from the graph, V_{FB} = -0.5 volts.

The difference in the accumulation behavior in Fig. 12 as a function of frequency is not predicted by any of the C-V theories. The characteristic at 100 kHz is completely as expected while the large increase in the capacitance in the 1 kHz curve in the accumulation mode is without explanation in the MIS theory. This sharp increase in capacitance is quite similar to the forward biased junction capacitance of the MIM samples of the previous section. This effect can be explained in terms of the "semi-insulating" properties of the TiO_2 after the 350°C anneal. In the previous section the amorphous TiO_2 layer was most conveniently described as an n type semiconductor of a high bulk resistivity. If this description is also used for the anatase films, then it is possible to postulate a simple model to explain the phenomenon above. Characteristic of the high resistivity bulk is a relaxation time τ. Such relaxation times have traditionally been associated with loss mechanisms in insulating materials and have been described theoretically by von Hipple[3], Frolich[60] and observed in a number of materials by Hartwig[61] and other workers. In the case of the anatase TiO_2 if the period of the excitation signal is longer than or comparable to the relaxation time τ, then the electrons in the insulator are able to follow the signal and the impedance of the insulator appears low. The characteristics of the p-n junction at the TiO_2/Si interface dominates the characteristics. However, if the excitation frequency is high, the TiO_2 is unable to respond and appears as an insulator. In this case, the standard MIS characteristics are observed. In the case of the anatase TiO_2 this transition between semiconducting and insulating material occurs between 1 kHz and 100 kHz.

If this model is valid, the increase in capacitance in the forward bias configuration at 1 kHz is due to the diffusion capacitance of a forward biased p-n junction. Lindmeyer and Wrigley[62] show that this diffusion capacitance is proportional to the forward current of the junction and both increase exponentially with the junction bias. That is

$$C_{dif} \propto J_F \propto exp \left\{ \frac{q(V - V_F)}{nkT} \right\}$$ [22]

where V_F was the bias needed to guarantee that the junction is forward biased and n is a scaling factor as in Eq. [5]. As in Eq. [17]

$$C_{dif} = C_{total} - C_J$$

where C_J is the junction capacitance and, in this case, may be taken to be the normal capacitance of the MIS structure. This capacitance appears in Fig. 12 as the dotted line in the 1 kHz characteristic, drawn by scaling the 100 kHz curve by a factor of 1.2, a constant derived in later sections. V_F may be approximated by V_{FB} since both describe when the junction begins to be forward biased. Fig. 14 shows C_{dif} versus $V - V_{FB}$. The curve breaks slightly away from the straight line predicted by Eq. [22], as does the forward I-V characteristic in Fig. 13. However, Eq. [22] also predicts that both characteristics should have the same slopes at corresponding voltages. The value of q/nkT from Fig. 14 between $1.75 < V - V_{FB} < 2.25$ is 4.36/volt while the same slope from Fig. 13 in the same voltage range ($2.25 < V. < 2.75$) is 4.26/volt. This good agreement lends strength to the argument that for some purposes and, in this case, at a sufficiently low frequency ($\sim$ 1 kHz) the TiO_2 may be best described as an n type semiconductor with a high resistivity.
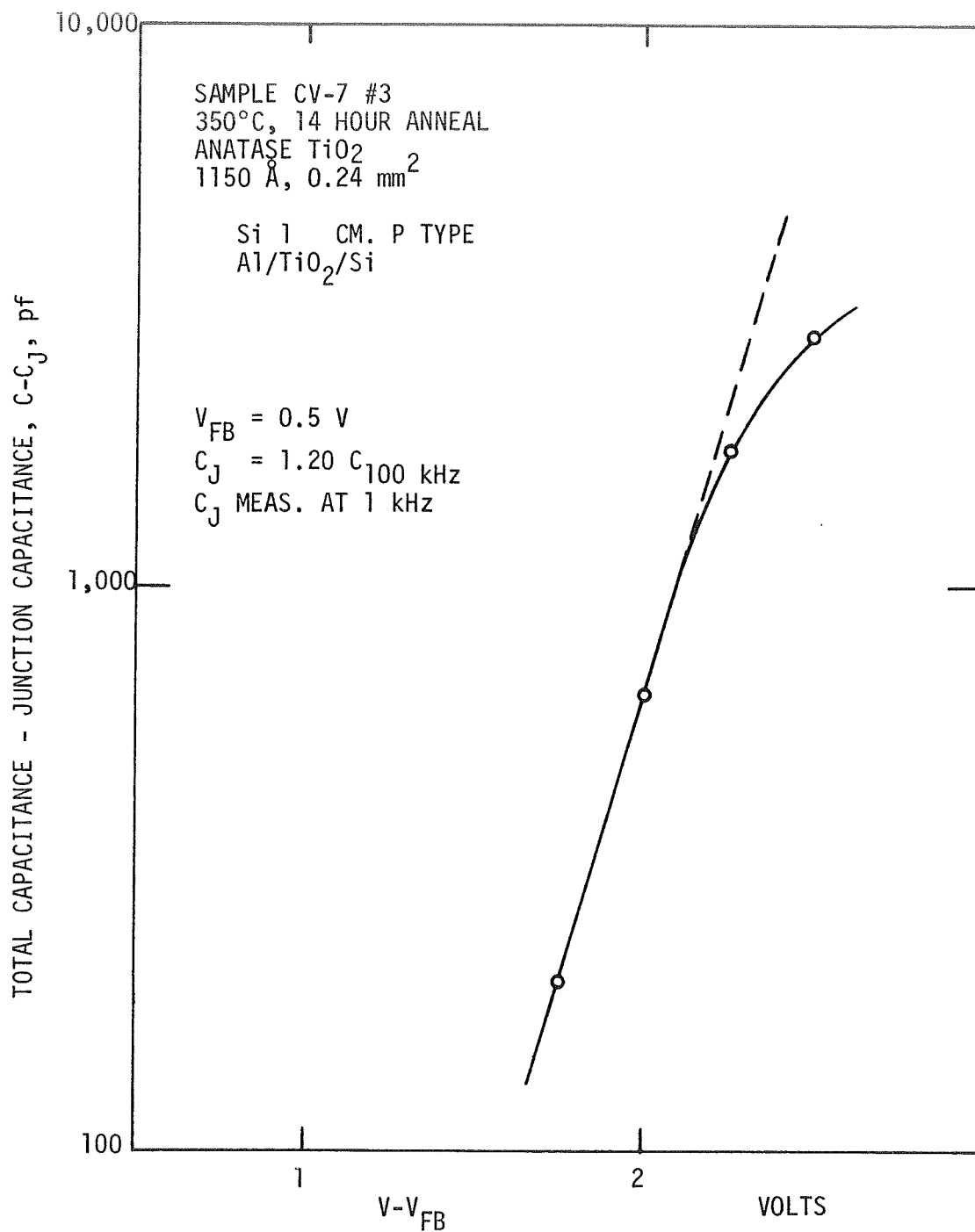
FIGURE 14. DIFFUSION CAPACITANCE vs. FORWARD BIAS FOR AN
ANATASE TiO_2 - SILICON JUNCTION.

The reverse characteristics of the C-V curves at both 1 kHz and 100 kHz are quite similar since both are controlled by the depletion layer in the Si. This is the case due to the low "doping" density of the TiO_2; very little bias is necessary to completely deplete the TiO_2 bulk and to cause it to function as an insulator. The reverse characteristic of the I-V data in Fig. 13 is suggestive of the saturation current in a back-biased diode. The saturation current in this case is approximately 10^{-9} amps.

The C-V curves may also be used to gauge the magnitude and sign of interface charge vs. surface state charge. Such charge existing at or in close proximity to the TiO_2/Si interface may be due to several sources. Among these are (a) a fixed surface charge, Q_{SO}, which is due to ionized atoms or impurities at the surface. Such a charge is relatively independent of bias, operating conditions or temperature and does not drift with the bias field; (b) electrons occupying fast surface states, Q_{FS}. Such states are in thermal equilibrium with the semiconductor and may be emptied and filled rapidly following an applied a.c. signal. The occupation of such states is a strong function of temperature and surface potential. The fixed surface charge exerts its influence by shifting the C-V curves as a function of bias. Ideally, with no surface charge or work function difference the flatband voltage falls at zero bias, i.e., the only band bending is accomplished when an external field is applied. However, the presence of such charges cause the flat band to be displaced from the origin. An additional displacement is caused by the work function difference between the metal electrode and the Si. For an Al electrode and p type Si this difference, ϕ_{ms}, is 4.2 - 5.25 volts, or - 1.05 volts. Then

$$Q_{SO} = (\phi_{ms} - V_{FB}) \, C_o/A \qquad\qquad [23]$$

and

$$N_{SO} = Q_{SO}/q$$

Because the charge in the fast surface states is a strong function of surface potential and hence bias, the C-V curves have a tendency to be distorted by this charge rather than to be displaced by it. This distortion takes the form of a deviation from the inverse square root dependence of the capacitance on the applied bias while the surface of the Si is depleted. Grove[57] states that if little distortion appears the fast surface state density is less than $5 \times 10^{10}/cm^2$.

Previously, with the aid of Eq. [21] the flatband voltage, V_{FB}, for the 100 kHz characteristic in Fig. 12 was shown to be -0.5 volts. From Eq. [23]

$$Q_{SO} = [-1.05 - (-0.5)] \times 1.06 \times 10^{-6} \ coul/cm^2$$
$$= -.585 \times 10^{-6} \ coul/cm^2$$

and $\qquad N_{SO} = 3.6 \times 10^{12}/cm^2.$

That is, there are 3.6×10^{12} negative charges per cm^2, at or near the TiO_2 /Si interface. The nature of these charges will be discussed in a later section.

From the accumulation region of the 100 kHz curve the relative dielectric constant of the TiO_2 may be calculated for that frequency. Using the parallel plate approximation, the relative dielectric constant is $K = 169$. Although this value is unexpectedly high for good insulating TiO_2, it is not unlike those values found by other workers for lossy films and is quite close to the value calculated for the amorphous film which was allowed to form under a bias in the previous section.

(3)   The 700°C Annealed Material

X-ray analysis in the previous chapter revealed that material an-
nealed at 700°C in air is a mixture of the anatase and rutile crystalline
forms. Long anneals tended to increase the rutile content, however, the
films remained a mixture of both forms for all practical purposes.

The C-V characteristics of an MIS sample of this type is shown
in Fig. 15. Some distortion of the curve is obviously present when com-
pared with the curves shown by Grove[57] (Fig. 9.19). Such distortion is due
to the presence of fast surface states. No calculation of this density or
distribution can be made from this data alone except that this effect is
noticable and hence the density is greater than $5 \times 10^{10}/cm^2$. A complete
discussion of the nature of these states is given by Many, Goldstein and
Grover[63]. From Eq. [19] and Eq. [21] the flat band voltage, V_{FB} is 0.0
volts. This corresponds to a surface charge density of $-6 \times 10^{12}/cm^2$
where the negative sign indicates that, once again, these are negative
charges residing near the surface.

From the accumulation region the dielectric constant at 1 kHz is
120, while at 100 kHz it is approximately 100. The average over a large
number of samples yields slightly different values for these numbers. At
1 kHz the average dielectric constant and dissipation factor is 116 and
.04, respectively, while at 100 kHz these values are 95 and .09. The ratio
of the relative dielectric constant at 1 kHz and 100 kHz is quite constant
from sample to sample and is approximately 1.2.

The I-V data for the 700°C samples has been included with this
same data for the 1000°C samples as it is all quite similar. The analysis
of this data is included in the next section.
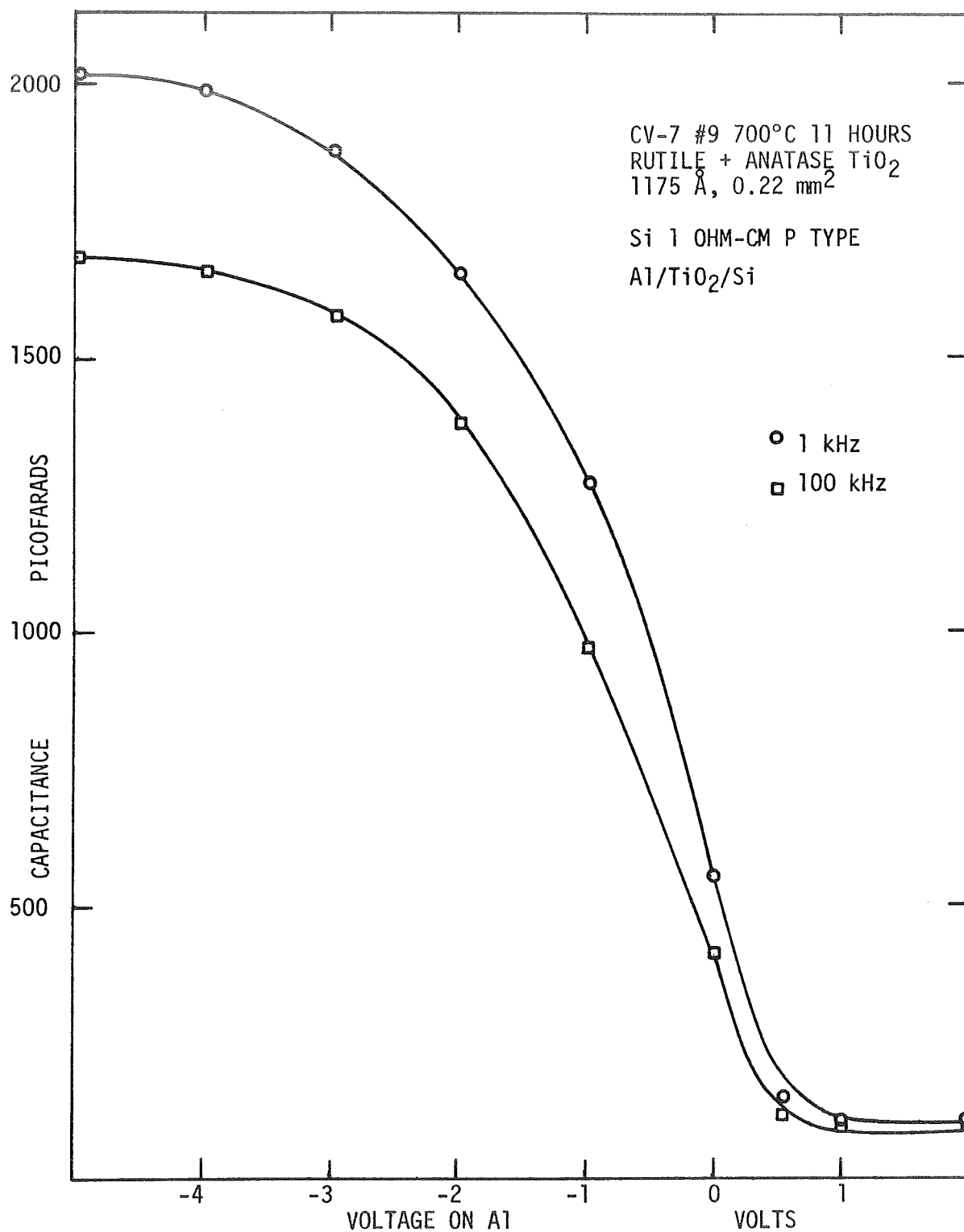
FIGURE 15. CAPACITANCE vs. VOLTAGE OF ANATASE+ RUTILE TiO_2.

(4)   The 1000°C Annealed Material

TiO$_2$ films annealed at 1000°C have been shown to be in the rutile crystalline form. However, no measure of the perfection of the individual polycrystals, their size, the nature of the grain boundaries, or any impurity inclusions could be measured. The conversion of thin amorphous films into the rutile form was shown to occur very rapidly at 1000°C (on the order of 1 min), but longer anneals may be necessary to give the film sufficient time in which to order itself and come into equilibrium.

After annealing for about an hour in air at 1000°C an increase in the thickness of the TiO$_2$ appears to have taken place along with a "dulling" of the interference color of the TiO$_2$/Si system. It is proposed that this is due to a growth of SiO$_2$ between the TiO$_2$ and Si. This SiO$_2$ layer makes the entire film look thicker since, in fact, it is and also dulls the interference colors by providing a diffusing rather than sharp interface between the TiO$_2$ and the Si. There is no reason to believe that this SiO$_2$ growth does not begin immediately or after some short delay time and this conclusion is born out in the electrical tests. The mechanism of this oxide growth beneath the TiO$_2$ is not clear, however, several possibilities exist.

(a) Oxygen or H$_2$O diffusing through the TiO$_2$ film reaches the Si surface and forms SiO$_2$. Further SiO$_2$ growth occurs in a standard fashion, except that the oxidizing agent must first diffuse through the TiO$_2$. Burger and Donovan[64] show that if the supply of oxidents is the limiting factor (limited by the diffusion through the TiO$_2$ and the existing SiO$_2$) then the oxide thickness should increase with the square root of the oxidation time. This type of process preserves the stoichiometry of the TiO$_2$ film.

(b) Diffusion at the interface could force some of the oxygen from

the TiO_2 into the Si causing SiO_2 growth. The situation at the

interface may, after a period of time, reach equilibrium and

the SiO_2 growth cease. This process may be governed by the re-

lative oxygen affinities or free energies of the TiO_2 and SiO_2.

In this case, the stoichiometry of the TiO_2 near the interface

may be seriously altered.

Whatever the growth mechanism of the SiO_2 may be, it will, undoubtedly, af-

fect the electrical properties of the resulting structure. The presence

of SiO_2 will greatly reduce the capacitance per unit area, alter the sur-

face state charge, and generally obfuscate the anneal data.

The C-V data for two MIS samples, one annealed for 5 minutes and

the other for 10 minutes, are shown in Fig. 16. Optical inspection of the

two samples showed some evidence of SiO_2 growth in the 10 minute sample by

virtue of the diffuse interference color while that of the 5 minute sample

remained sharp. The electrical data bears out this conclusion.

From Fig. 16 and other data on samples annealed at 1000°C for 5

minutes, in air, the average dielectric constant is 100 and the average dis-

sipation factor 0.04 at 1 kHz while at 100 kHz these values are 87.5 and

0.07, respectively. The C-V characteristic shows little or no distortion

suggesting that the density of fast surface states is low. The flatband

voltage is -0.2 volts corresponding to an interface charge density of -5.5

x 10^{12}/cm^2. Once again the sign of this charge is negative. It is as-

sumed that little SiO_2 is present beneath the TiO_2 film and that the rela-

tive dielectric constant of 100 at 1 kHz represents the value for a purely

rutile film. Rutile single crystals are reported[65] to have K_c = 170 and
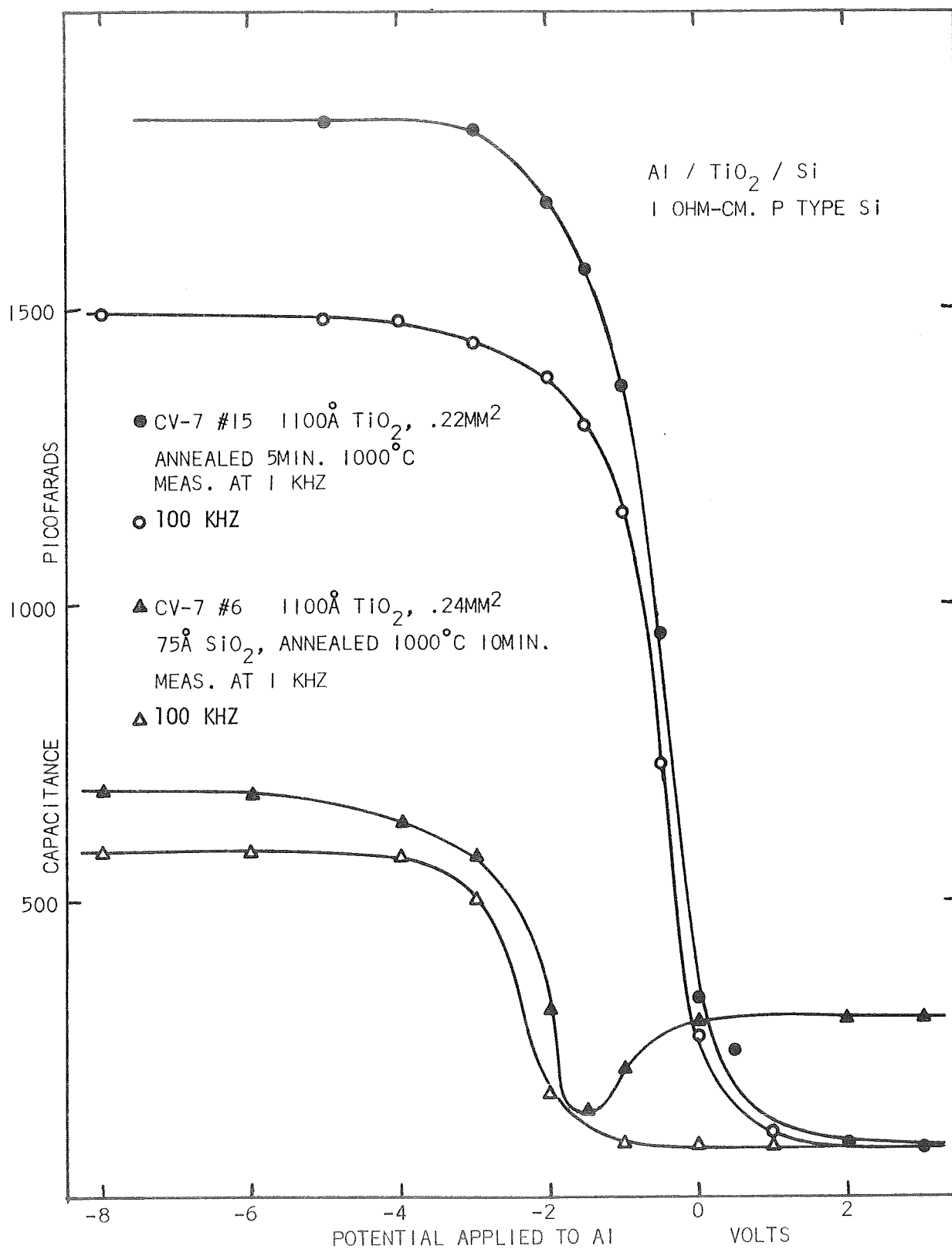
FIGURE 16. CAPACITANCE vs. VOLTAGE FOR RUTILE TiO_2.

and K_a = 90, while sputtered rutile polycrystalline films with a dielectric constant of 55 have been made by Lakshmanan, et al[26].

The curves for the material annealed for 10 minutes show a marked decrease in the capacitance at accumulation and a small inflection in the inversion capacitance at 1 kHz. This increase indicates that the inversion layer is able to follow the external field and the capacitance of the insulator, rather than the depletion layer, becomes dominant again. This effect is not usually seen at frequencies as high as 1 kHz, but can be caused by a non-equilibrium condition, such as light shining on the Si. This may have been the case here. The average value of the dielectric constant and dissipation factor for several of these samples at 1 kHz and 100 kHz are 40., 0.04 and 35., .05, respectively. This decrease in the dielectric constant may be explained in terms of an SiO_2 layer below the TiO_2. The total capacitance measured is the series capacitance of these two layers. If it is assumed that for the TiO_2 layer K = 100, while for the SiO_2 layer K = 3.9, then it is necessary to postulate the presence of only 75 Å of SiO_2 to account for the low capacitance. As further proof of the presence of the SiO_2 layer, it is interesting to observe the shifting of the curves away from the origin giving a flatband voltage of -2.0 volts. Corresponding to this number is a surface charge density of 1.7 x 10^{12} positive charges per cm^2. It is characteristic of the SiO_2/Si interface to trap positive charge, usually thought to be associated with Si^+ ions in the oxide. Densities of these charges between 10^{11}/cm^2 are typical, depending on the way the oxide is formed and the anneal history. Apparently, the charges in the TiO_2 and SiO_2 tend to cancel each other and a situation can be envisioned in which the net effect surface charge

density is zero. The nature of the negative surface charges in the TiO_2

is not understood since unpaired Ti ions, drawing a parallel with the

Si/SiO_2 system, would result in a positive charge. It is possible that

this charge arises from electrons held in uncharged electron traps near

the interface in the TiO_2. That is, the trap is uncharged before the

electron is captured and has a net negative charge only when an electron

is being held. These traps should be relatively deep to make their popu-

lation of bound electrons relatively insensitive to the external bias, etc.

The I-V data for the 700°C and 1000°C samples is displayed in

Fig. 17. Unlike the amorphous and anatase samples, the characteristics

in the forward direction (Al⁻) are far from straight lines and the cur-

rents increase much less rapidly with bias. Harbison[40] shows that the

electron transport through similar films of TiO_2 is governed by a Poole-

Frenkel law. This law may be written as

$$J_{PF} \propto \xi \exp\{\frac{-q\phi_B}{kT}\} \exp\{\frac{1}{kT}\sqrt{\frac{q^3\xi}{\pi K_o \epsilon_o}}\} \qquad [24]$$

where ξ = electric field across the insulator

= V/d where d is the insulator thickness

ϕ_β = barrier height or trapping depth for electrons

K_o = optical dielectric constant of insulator.

From Eq. [24]

$$J_{PF}/\xi \propto \exp\{m\xi^{1/2}\} \qquad [25]$$

where

$$m = \frac{q}{kT}\{\frac{q}{\pi K_o \epsilon_o}\}^{1/2} \qquad [26]$$

If K_o = (index of refraction)² = (2.5)² = 6.25 is used in Eq. [26], then

the value of m at T = 300°K is

○ CV-7,#14, 700°C, 11 HOURS
RUTILE AND ANATASE TiO_2
1150 Å, 0.23 mm^2

□ CV-7,#4, 1000°C, 5 MIN.
RUTILE TiO_2
1100 Å, 0.24 mm^2

△ CV-7,#14, 1000°C, 10 MIN.
RUTILE TiO_2 1150 Å
SiO_2 75 Å, 0.24 mm^2

1Ω CM Si P TYPE

Al/TiO_2/Si
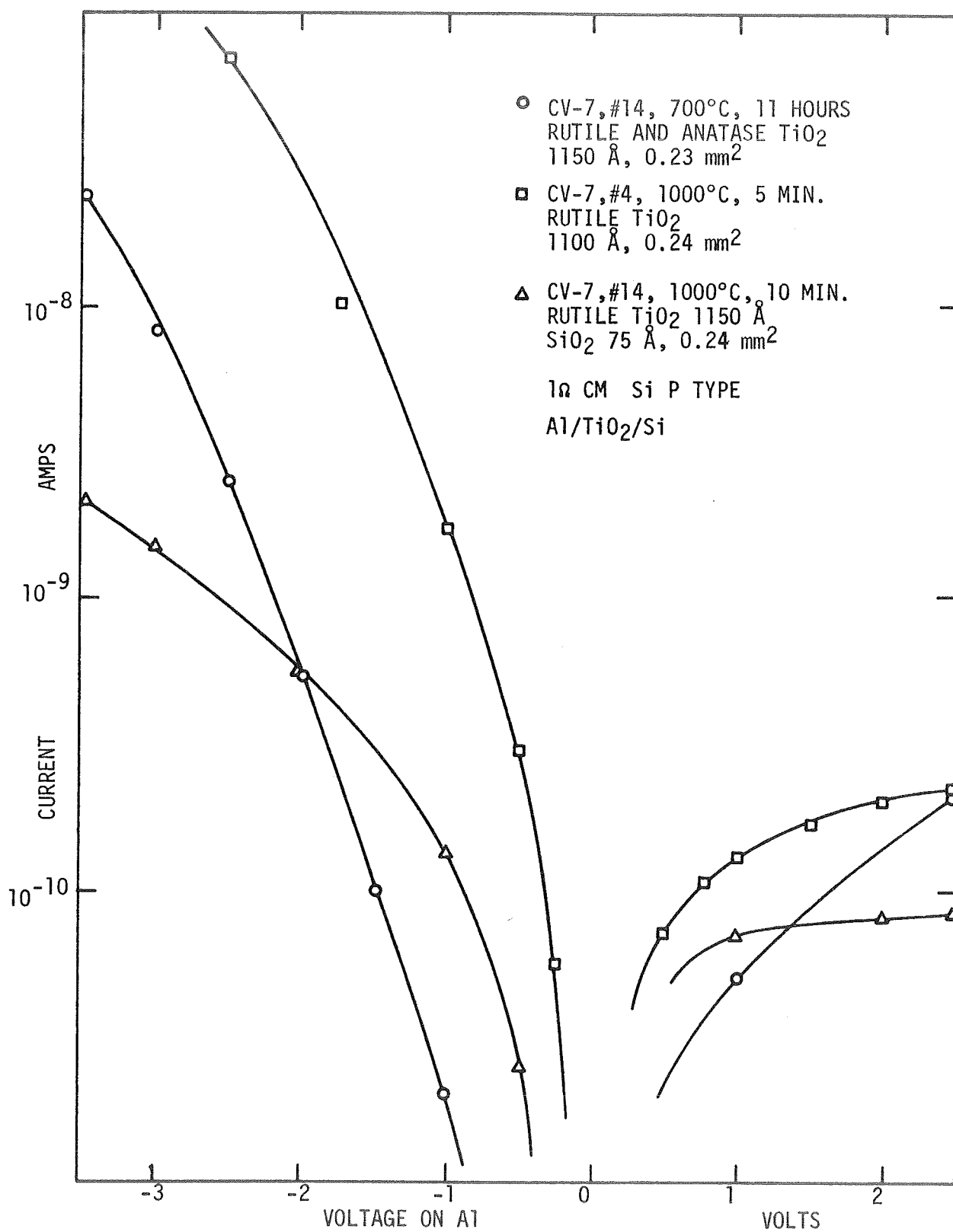
FIGURE 17.   CURRENT vs. VOLTAGE AS A FUNCTION OF ANNEAL.

$$m = 1.17 \times 10^{-3} \text{ (m/volt)}^{1/2}$$

A more generalized case of the Poole-Frenkel theory developed by Yeargan[66] shows that the slope may take on any value from the one above to 1/2 its value depending on the degree of compensation present in the insulator (i.e., rather than having donor states alone both donor and acceptor states in the insulator are considered). Hence, the restriction on the slope is

$$.58 \times 10^{-3} \le m \le 1.17 \times 10^{-3} \text{ (m/volts)}^{1/2}$$

Fig. 18 shows the I-V data plotted as $\ln(I/\xi)$ vs. $\xi^{1/2}$. Good straight lines approximations can be made to the data points and the slopes of the resulting lines are as follows

$$700^\circ C \quad m = 2.25 \times 10^{-3} \text{ (m/volt)}^{1/2}$$
$$1000^\circ C, \text{ 5 min. } m = 1.50 \times 10^{-3} \text{ (m/volt)}^{1/2}$$
$$1000^\circ C, \text{ 10 min. } m = .60 \times 10^{-3} \text{ (m/volt)}^{1/2}$$

It is evident that only the last value is inside the allowed values and since it is very near the lower value, it must be postulated that a high degree of compensation has taken place in the TiO_2/SiO_2 system. A similar type of conclusion was drawn about the corresponding C-V curves and the interface charge density. The first two values are well above the upper limit predicted by the Poole-Frenkel theory. This, however, has been the case in a number of other studies and a number of explanations have been given. Principal among them is the premise that spots exist in the insulator which are appreciably thinner than the average thickness, d, and it is these spots which control the I-V characteristics. This may easily be the case for the $700^\circ C$ and $1000^\circ C$, 5 minute samples.

The reverse (Al+) characteristics represent the saturation current in a back-biased field-induced junction in the Si substrate. This
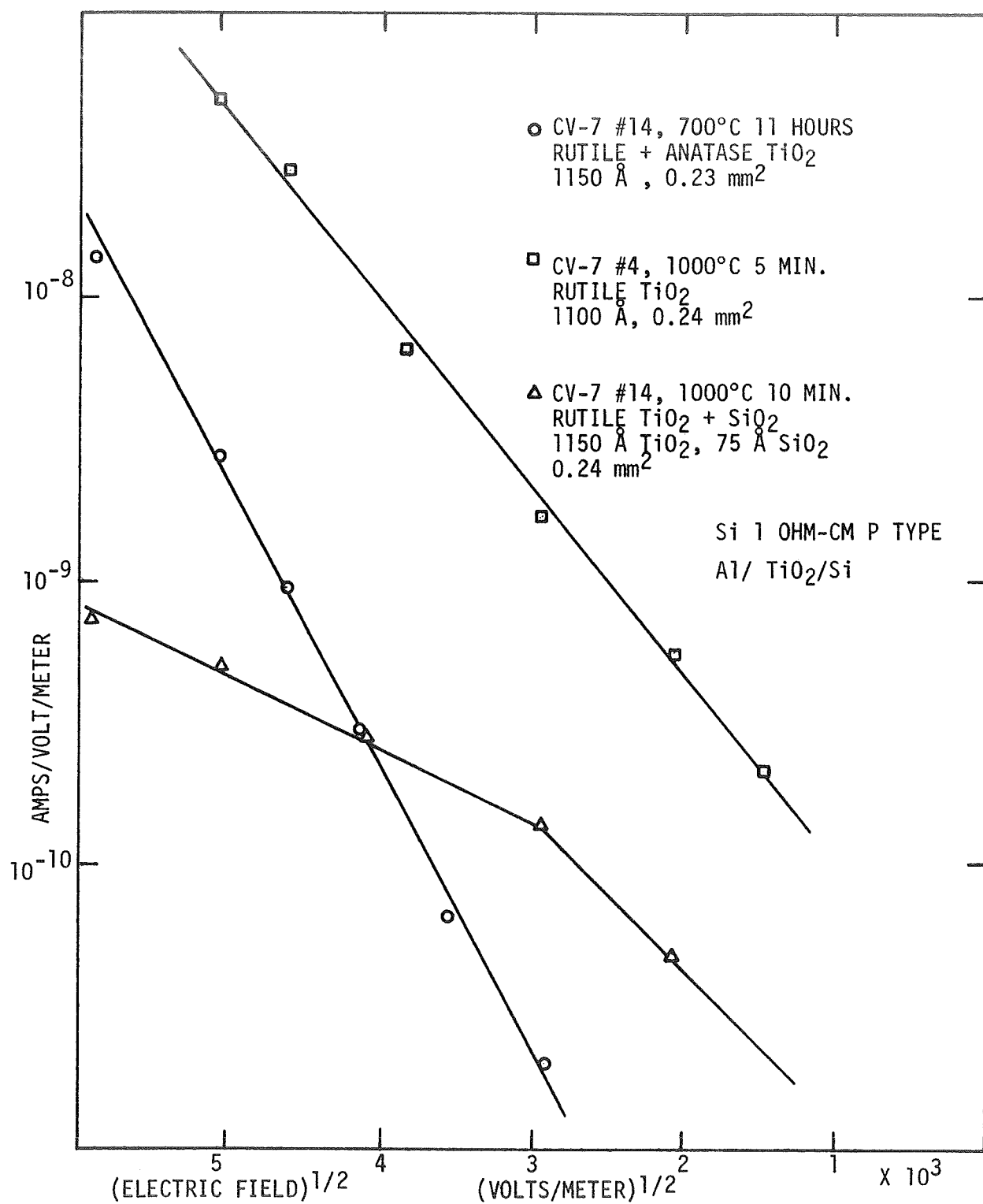
FIGURE 18. CURRENT/ELECTRIC FIELD vs. (ELECTRIC FIELD)$^{1/2}$ AS A FUNCTION OF ANNEAL

diode is created as the surface of the p type Si is inverted relative to
the depletion layer directly below it and the semiconductor bulk below
that. J.D. Trotter, of this laboratory, has suggested that the current
observed is the generation current from the depletion region and is pro-
portional to the volume of this region. Experiments showing the strong
dependence of this current on ambient light lend strength to this argument.

SUMMARY

A general summary of the electrical data for the films ranging
from amorphous to polycrystalline rutile to a multilayer structure with
SiO_2 present are contained in Table III. Several interesting trends are
evident and are discussed below.

(a) As the ordering in the crystal increases, that is, as it is con-
verted from the amorphous to the crystalline states, the dielec-
tric constant is reduced. This is to be expected as the lattice
binding becomes tighter and the polarizability is reduced. In
each particular film the ratio of the relative dielectric con-
stants at 1 kHz and 100 kHz is near 1.2. The dissipation factor
of the films at 100 kHz is higher than at 1 kHz, indicating the
presence of a relaxation mechanism at work.

(b) The resistivity data is titled "apparent" resistivity since, in
the case of the amorphous and anatase films, the I-V character-
istics are governed by the properties of the junction rather than
the bulk. In these cases approximate saturation currents in the
forward direction were used for the calculation assuming the cur-
rents are limited by the bulk resistivity of the film. It is
evident, however, that the resistivity is a strong function of

the anneal history of the material, increasing rapidly as the higher crystalline forms are reached. It is interesting to note that the resistivity of the films annealed at 1000°C for 5 minutes is about a factor of 10 lower than that of the 700°C, 11-hour sample. This may indicate that although after 5 minutes at 1000°C, the film is nominally rutile, the transition from the amorphous state to the rutile form occurred so quickly that a large amount of disorder (dangling bonds, high dislocation density) remains in the film adding to its conductivity by the creation of states in the forbidden band. Longer anneals produced a layer of SiO_2 beneath the TiO_2 and provided a longer period for the TiO_2 to order itself and achieve stoichiometry. Together, these two effects increased the resistivity sharply, but the specific capacitance was reduced due to the SiO_2 layer.

(c) The interface charge for the TiO_2/Si system is roughly constant and on the order of $-5 \times 10^{12}/cm^2$. As discussed previously, this negative charge may be due to electrons held in neutral traps or states near the interface. A compensating effect is observed with the growth of the SiO_2.

(d) The breakdown field increases as the material is annealed and seems to be given a boost by the growth of the SiO_2. These relatively low (compared with SiO_2 and Si_3N_4) breakdown fields are understandable in the light of the high dielectric constant. The products of the relative dielectric constant and the breakdown field for these three materials are

$$TiO_2 \ (1000°C, \ 5 \ min.) = 100 \ x \ 7 \ x \ 10^5 V/cm = 7 \ x \ 10^7 V/cm.$$

$$SiO_2 \qquad\qquad\qquad = 3.9 \ x \ 5 \ x \ 10^6 V/cm = 2 \ x \ 10^7 V/cm.$$

$$Si_3N_4 \qquad\qquad\qquad = 6 \ x \ 1 \ x \ 10^7 V/cm = 6 \ x \ 10^7 V/cm.$$

(e) In general, the amorphous material may be treated as an n type
semiconductor of a high resistivity with a donor level approxi-
mately 0.35 eV below the conduction band.

	AMORPHOUS FILM TiO$_2$, NO ANNEAL	ANATASE FILM, TiO$_2$, 14 HR., 350°C ANNEAL	ANATASE & RUTILE FILM, TiO$_2$, 11 HR., 700°C ANNEAL	RUTILE FILM, TiO$_2$, 5 MIN., 1000°C ANNEAL	RUTILE TiO$_2$+ 75 Å SiO$_2$, 10 MIN. 1000°C ANNEAL
REL.DIEL.CONST./DISS.FACTOR, 1kHz	——	——	116/.04	100/.04	40/.04
REL.DIEL.CONST./DISS.FACTOR, 100 kHz	——	169/.09	95/.04	87/.07	35/.05
APPARENT RESISTIVITY AT 2 × 10^5 V/cm	5×10^4 cm.	3×10^8 cm.	5×10^{11} cm.	5×10^{10} cm.	5×10^{11} cm.
INTERFACE CHARGE Q$_{so}$ with 1 Ω CM. p Si	——	−3.6×10^{12}/cm^2	−6×10^{12}/cm^2	−5.5×10^{12}/cm^2	+1.7×10^{12}/cm^2
OTHER PROPERTIES, COMMENTS	EXHIBITS STRONG FORMING TENDENCIES IN BIAS FIELD	SHOWS MIXED PROPERTIES - AT HIGH FREQUENCIES (~100 kHz) IT IS BEST DESCRIBED AS AN INSULATOR. AT LOW FREQ. AND D.C., IT ACTS AS AN n TYPE HIGH RES. SEMICONDUCTOR	GOOD INSULATOR. HIGH SPECIFIC CAPACITANCE AND GOOD BREAKDOWN STRENGTH	LOWERED RESIS. AND BREAKDOWN MAY BE DUE TO SHORT ANNEAL TIME, POORLY ORDERED FILM	TiO$_2$/SiO$_2$ COMPOUND STRUCTURE SHOWS SIGNS OF TRAPPED CHARGE COMPENSATION IN BOTH C-V AND I-V DATA

TABLE III - SUMMARY OF ELECTRICAL DATA

CHAPTER V.

OTHER INTERESTING ASPECTS OF A TiO_2 TECHNOLOGY

INTRODUCTION

Up to this point, several basic properties of thin film TiO_2 have been studied and the basis for a TiO_2 thin film technology has been established. The work presented in the first four chapters has led to the following conclusions:

(a) A successful process for deposition of TiO_2 thin films from an organometallic source at a low temperature on a variety of substrates has been developed. The resulting film is amorphous.

(b) These amorphous films may be converted to polycrystalline films in the anatase, anatase and rutile, or pure rutile phases by annealing in the air at temperatures between 300°C and 1000°C.

(c) The amorphous film is easily etched in a weak solution of HF and, for this reason, is most suitable to standard thin film pattern definition techniques. The lower crystalline forms are moderately difficult to etch while the pure rutile form is fairly impervious to chemical attack.

(d) The amorphous film is best characterized as a high resistivity n type semiconductor. The anatase film shows mixed properties — at D.C. and low frequencies it can be described as a semiconductor while at higher frequencies it appears to be an insulator. The mixed phase and rutile films exhibit the characteristics of a high dielectric constant insulator of moderate loss tangent and breakdown voltage.

(e)   The interface charge in the TiO_2/Si system is such as to accumulate the surface of p type Si. This leads to the possibility of several interesting MIS types of devices.

Additional experiments were performed to see if a hybrid or integrated circuit technology employing TiO_2 films offered any decided advantages or unique properties other than those mentioned or inferred above. Several recent trends in the state-of-the-art provided suggestions for these experiments.

Continued emphasis on the dimensional reduction of integrated circuit components has lead to work with photoresist exposed by an electron beam. The use of light for patterning a standard photoresist limits the narrowest line width to 2μ while typical line widths greater than 10μ are usually found to be employed. Patterning the same resists with a focused electron beam has led to lines as narrow as 0.25μ because of the greater resolution of a beam of electrons than a beam of light.

Some attempts have been made to eliminate the need for photoresist completely by bombarding the material to be etched with an electron beam directly. In the case of SiO_2 the beam induces sufficient damage to cause a greatly enhanced susceptibility to etches and hence, the etching of SiO_2 can be accomplished without the use of photoresists.

Insulators other than SiO_2 have been tested for possible use with Si as a surface passivation material or as a diffusion mask. Multilayer structures using other metal oxides and nitrides are being tested to reduce the effect of drifting ionic contaminants in MIS structures.

It was decided that, owing to the high etchability of the amorphous TiO_2 compared with the crystalline forms and the relative ease of

conversion of the amorphous form into a polycrystalline film, experiments would be undertaken to test the results of direct irradiation of amorphous films by electron beams. Other selective energy delivery schemes, such as u.v. photons, would also be considered.

Rutile TiO_2 has a specific gravity that is greater than that of SiO_2 by a factor of 2. By taking into account the relative atomic weights of Ti and Si, it is evident that the packing density of the two oxides is approximately equal. It is not unreasonable to expect that both films would present similar high impedance paths to diffusing impurities. Tests performed to see if this is the case are discussed.

EFFECT OF KILOVOLT ELECTRONS ON ORGANIC AND INORGANIC FILMS

(1) Exposure of Organic Photoresists

The gain in component density is impressive when electron beams expose the photoresists. Thornley and Sun[67] showed that electrons in the 10 to 20 kV range could expose negative resists so that they were able to protect underlying SiO_2 against etchants. They also found that a threshold electron flux exists, below which no hardening of the photoresist occurs and above which varying degrees of protection are afforded. A dependence of this optimum exposure flux on the incident energy of the bombarding electrons was demonstrated by Matta[68].

Broyde[69] attempts to define the minimum threshold flux in terms of the energy of the incident beam and the gel point for two standard organic photoresists, Kodak KPR and KTFR. He defines two different flux levels as the threshold flux at which the film first begins to gel and the minimum usable flux as that dosage at which adequate protection is afforded an underlying layer during etching. The threshold flux principally depends

on the incident energy of the beam and is only slightly dependent on the

initial thickness of the film, while the minimum useable flux is a func-

tion of both electron energy and initial thickness of the film. He ob-

serves that the threshold flux for 6000 Å of KTFR for 10, 15 and 20 keV

irradiation is 0.7, 0.9, and 1.6μ coul/cm^2, while the minimum useable

flux for these same energies is 1.5, 8.0 and 16.0μ coul/cm^2, respectively.

The penetration depth of electrons in KTFR (specific gravity 0.9) is 6500

Å for 5 keV electrons, 2.3μ for 10 keV electrons, 4.8μ at 15 keV and 8.3μ

at 20 keV.

(2)   Exposure of Inorganic Films

O'Keefe and Handy[70] have established that the susceptibility of

thermal SiO_2 to chemical etches is enhanced by approximately a factor of

three when the SiO_2 film is irradiated with high energy electrons. Reso-

lution with this process is quite high and openings in SiO_2 0.6 x 5μ have

been obtained. The increased etch rate is due to the electron-induced dam-

age in the SiO_2. Dislocations are formed and bonds are broken in the ma-

terial which increases its potential for chemical attack. Hill[71] has ob-

served just the opposite effect in evaporated films of Al_2O_3 and anodized

films of Al_2O_3 and Ta_2O_5. The etch rate of a 7000 Å film of evaporated

Al_2O_3 was reduced from 500 Å/min to 320 Å min after a total dose of 2 coul

/cm^2 by 15 keV electrons. Dosages above 2 coul/cm^2 did not further reduce

the etch rate. Doses below 0.5 coul/cm^2 appeared to have no effect on the

etch rate.

Shiojiri, et al[72, 73] observed the effects of high energy elec-

tron beams on thin films of metal oxides and Se. He reported that, in

general, amorphous films of these oxides could be converted into

crystalline forms if sufficient energy could be supplied by the electron beam. Amorphous films of evaporated Al_2O_3, tin oxide, lead oxide and iron oxide were always crystallized by electron irradiation into very fine poly-crystalline grains usually less than 1000 Å in size. Exceptions to this trend were evaporated amorphous films of TiO_2 and Se metal. These two tended to crystallize into large grains, some more than 10μ in size. Often the tension due to volume reduction during crystallization caused marked wrinkling of the amorphous film near the crystal inducing grain boundaries and dislocations to form. Small angle twist boundaries and twinning crystals were formed in TiO_2 during the crystallization. The metal oxide films required intense electron beams on the order of 100 ma/cm^2 before crystallization occurred, although when sufficient beam current was supplied, the films were observed to crystalize immediately. Se films required much lower intensity beams ($\sim$ 5μa/cm^2), but for a duration of several hundred seconds.

In a very recent paper, Shiojiri[34] continued his work on evaporated TiO_2 films. Unsupported films (evaporated onto rock salt, then floated off) of amorphous TiO_2 were either heated to 300-500°C by a near-by heat source or bombarded by electrons. In both cases a single anatase crystal appeared and grew as long as energy was supplied. Larger crystals became composed of many grains, each growing mostly along the axis of the tetragonal structure.

Cecil and Silvertsen[74] bombarded a large single crystal of rutile TiO_2 with a very high power electron beam with incident energies over 100 keV. A large amount of damage was done in the crystal along the path of the beam. Measurable volumes of oxygen were released during this

process and, corresponding to this loss of oxygen, a decrease in resistivity from 10^{12} Ω-cm to less than 1 Ω-cm was observed.

(3)   Effect of Kilovolt Electrons on Amorphous TiO_2

Several experiments were performed to discover the effect of high energy electrons on amorphous films of TiO_2 grown as per Chapter III. These experiments may be broken down into several groups in response to a number of questions.

(a) Does irradiation with high energy electrons produce any visible result in the amorphous film? Is the etch rate affected by the bombardment?

(b) What crystalline form or forms is produced by irradiation?

(c) Is there some value roughly equivalent to the threshold level observed in organic films? What effect does continued irradiation have on the films after a threshold value is reached?

Two types of electron bombardment equipment were used to perform the various experiments. In the first, an electron gun was removed from a standard CRT and was mounted in either a standard vacuum system equipped with an oil diffusion pump and a LN_2 cold trap capable of 1×10^{-6} torr or a completely dry Varian system pumped by VacSorb, VacIon and titanium sub-limination pumps capable of 10^{-11} torr. In the case of both vacuum systems an external power supply and control, provided an accelerating potential of from 0.8 kV to 1.5 kV along with intensity, focusing and deflecting potentials to the electron gun. Typical operating conditions for the e-gun are as follows: accelerating potential 1.5 keV, electron irradiation current $\sim$ .05 ma, beam focus $\sim$ 1 mm. diameter.

Experiments to determine more quantitative information, such as a threshold flux, etc., were performed using the e-beam in a Phillips Model AMR3 Electron Microprobe. This equipment permitted the beam to sweep out a line of predetermined length or over a raster of known area. Accelerating potentials between 10 kV and 30 kV were used and beam currents between 0.025 μa and 0.15 μa are available depending on the accelerating potential used. Beam spot diameters on the order of 5 μ are typical, however, beam diameters on the order of 2 μ have been obtained with the equipment.

Initial experiments involved the bombardment of amorphous TiO_2 films, 1000 Å thick, on polished Si conducting substrates. A major concern with the experiment conducted in the oil pumped vacuum system is that any change in the TiO_2 etch rate or apparent thickness may, in fact, be due to the growth of a polymer film on the TiO_2 film. This polymer film has been described previously[75] and results from the electron induced polymerization of the diffusion pump oil (D.C. 704) at the surface of the substrate. Such a polymer film could afford underlying layers of TiO_2 protection from chemical attack and give the appearance of an etch resistant TiO_2 film. Hill[71], also concerned with this problem, surrounded his samples with a LN_2 cold finger to trap oil molecules. In the equipment set-up described above, this procedure proved extremely impractical. Instead, the substrates were heated in the oil-pumped system to 150°C to reduce the residence time of any oil molecules on the surface of the TiO_2. Experiments with glass slides and bare Si substrates showed that heating to 150°C virtually eliminated the polymer growth after a 90 minute radiation time. Identical

substrates bombarded under the same conditions, except that no heat was supplied, showed the presence of 200 to 400 Å of the polymer film after 90 minutes.

This heating proved to have a second effect besides driving away oil molecules. By raising the film temperature to its growth temperature, and hence closer to the amorphous to anatase transition, the bombarding electrons are more efficatious in supplying the energy for change. This is discussed in more detail below.

An amorphous TiO_2 film, 1000 Å thick on polished Si, was bombarded for 15 minutes with 1.5 keV electrons at an average beam current of .035 ma. Spot diameter was approximately 1 mm giving a current density of 4.5 ma/cm^2 and a power density of 6.75 watts/cm^2. The sample was held at 130°C during the entire irradiation. Inspection of the sample after the bombardment showed that the irradiated area could be seen easily, and gauging from the changes in the interference color, this area had become slightly thinner. The entire wafer was placed in an etch known to attack only the amorphous material at a reasonable rate (0.5% HF in H_2O) and the 1000 Å of amorphous material was removed completely in 1.5 minutes. During this time only 200 Å maximum appeared to be removed from the irradiated area. Hence, the etch rate had been reduced by a factor of 5 or more after a total electron dosage of approximately 4 coul/cm^2. This dosage value may be as much as a factor of 5 too large owing to any error introduced by approximating the area of the electron spot which had an irregular shape and an assumption that all the electrons leaving the electron gun reach the substrate, 5 cm away.

To insure that the increase in etch resistance was indeed a result of the electron bombardment, and not due to the growth of a polymer or some effect of the substrate heating, a second experiment was conducted in the Varian oil-free vacuum system. An amorphous 800 Å TiO_2 film was subjected to an electron beam from a new and completely clean e-gun. No substrate heating was provided and the experiment was conducted in the 10^{-7} torr range. The 1.5 keV beam current average was .035 ma while the spot diameter was approximately 2 mm. The bombardment was allowed to proceed for 45 minutes to overcome any effect of removing the substrate heater. Inspection after the completion of this period resolved, once again, that the irradiated area appeared slightly thinner. Ellipsometer data was taken on this spot and the surrounding unexposed amorphous material. Confirming the findings of Chapter III, the unexposed material had an index of refraction 2.0 and a thickness of approximately 750 Å while the exposed area had an index of 2.18 and a thickness of 660 Å. By comparing these values with Fig. 3, Chapter III, it is apparent that the material has been, at best, only partially converted into the anatase form. As with the sample above, the exposed material proved to be less affected by the etch during the period it took to completely remove the amorphous material, the etch rate being reduced by about a factor of 2. The total integrated flux during this experiment was approximately 3 $coul/cm^2$. Once again, this is a maximum value.

It is evidently the case that the 1.5 keV electrons are penetrating the full 1000 Å of the samples and causing the material to become uniformly etch resistant. If this were not the case, the etch could undercut the exposed area and cause it to float off of the substrate. A similar effect was observed by Broyde[69] for standard photoresists.

A third experiment was conducted to confirm the hypothesis that the e-beam was providing sufficient energy to convert the material from the amorphous form to a crystalline form. A layer of 3000 Å of TiO_2 was deposited on a polished Al wafer. The Al substrate was chosen for two reasons, (i) the substrate should be a conductor to help diffuse any built-up charge in the insulator during irradiation and (ii) any x-ray peaks from the substrate should be as far removed as possible from the expected peaks from the crystalline (anatase) TiO_2. A 24 mm^2 area (a 1 mm diameter dot was used to sweep out the area) was irradiated for 3 hours with 1.5 keV electrons. The beam current was .15 ma and the sample was held at 170°C during the exposure period. The total integrated flux was 6.75 $coul/cm^2$. X-ray analysis of the unexposed area yielded peaks associated only with the substrate Al. No crystallization occurred in the unexposed area due to the "heat bias" of 170°C during the irradiation period. However, analysis of the area exposed to the e-beam produced strong evidence for the presence of the anatase material. The 100% and 30% lines could be clearly seen above the background noise while the presence of the weaker lines was only questionable. No indication of the degree of crystallization has been found, but it is known that some portion of the amorphous film was converted to the anatase, polycrystalline form.

In general, the conversion to a material at least partially anatase and far more etch resistant than the amorphous form occurs for total integrated fluxes greater than approximately 2 $coul/cm^2$ with beam power densities between 1 and 10 $watt/cm^2$ and substrate temperatures on the order of 150°C. It is interesting that the value of the total electron dose to produce a significant change in the etch rate of the TiO_2 is the same

as that found by Hill[71] for irradiation of Al_2O_3 and Ta_2O_5 with much higher

electron energies (> 10 keV).

In order to get higher accelerating potentials and high power den-

sities further experiments were carried out in the Phillips Microprobe.

With this instrument, beam diameters under 10 μ could easily be obtained

and the beam could be swept over various lines and rasters. Amorphous TiO_2

films 2700 $\overset{\circ}{A}$ thick on Si substrates were used for all of the experiments.

Once the desired exposure was reached the sample was etched in the 0.5% HF

solution until all of the unexposed amorphous film was completely removed

and only the exposed pattern remained. Usually, the etch time was on the

order of 40 to 50 seconds. A standard exposure consisted of allowing the

beam to scan over a single line 300 μ in length and from 3 to 10 μ wide un-

til a predetermined dosage, determined by the beam current density and ex-

posure time, was reached. The beam was then deflected to a new area and

another line with a different dosage was drawn. Groups of from 5 to 10

lines (usually 10) were drawn for a given accelerating potential, each line

corresponding to a different total integrated electron flux. Once the back-

ground was etched away the lines were examined under a microscope to de-

termine the degree to which they survived the etch. Of some interest is

the fact that the areas remaining after the etch were very nearly the same

thickness, showing very little change from the original 2700 $\overset{\circ}{A}$. Either the

line was completely removed, leaving very few traces or, if it remained,

its thickness was not diminished by the etch. This is not to say that

those lines which remained were not affected by the etch. On the contrary,

some had rough edges and were characterized by breaks and tears. The ver-

tical portion defining the edge of the line was, at times, not vertical at

all, but had a shallow slope. These problems and defects decreased as the dosage increased and the films could be easily graded by eye with a microscope. Two values of the total dosage could be defined as:

(a) The threshold dosage below which little trace of the line remained after the etch. Above this value the TiO_2 lines remained on the Si and continued to improve in quality with increasing dosage.

(b) Minimum useful dosage below which the exposed areas, while remaining on the Si are characterized by etched areas, rough edges, line-width irregularities and poor edge resolution and definition. Above this value the lines are uniform, unbroken, and possess smooth, well defined edges.

Experiments were first performed to determine the optimum method for exposing the line patterns, i.e., should the entire electron dosage be delivered to the line in one slow pass, or should the exposure be built up by sweeping over the same line repeatedly? A series of lines were drawn with the 15 keV beam at a power density of 2.8×10^3 watts/cm^2 at a rate of 120μ/min., 600μ/min., 350μ/15 sec., 350μ/3 sec., and $350μ/2 \times 10^{-3}$ sec., until each line had a total dosage of 1.0 coul/cm^2. The lines resulting from the two slowest scans were quite poor after the etching, characterized by a large number of breaks and no line width uniformity whatsoever. Lines produced at 350 /15 sec. and 350 /3 sec. were much improved and had good line width uniformity and edge definition. However, occasional breaks and networks of cracks bisected the lines. However, at the fastest sweep speed no such problems were encountered. The beam seemed to be slightly less efficient at the higher speeds in that the overall development of the lines

seemed to lag slightly behind those formed at the slower speeds, but no cracking was observed and it was felt that the lower efficiency was worth the more perfect film. A sweep speed of $350\mu/2 \times 10^{-3}$ sec. was adopted for the rest of the experiments.

Table IV summarizes the results of a series of exposures with beams from 10 to 30 keV and power densities from 0.8×10^3 watts/cm^2 to 7.2×10^3 watts/cm^2. A range of exposures has been given wherever possible to reflect the experimental error and the uncertainty in the somewhat subjective judgments involved. Despite the uncertainty, it is evident that both the threshold and minimum useful flux are functions of either the electron energy or the beam power density or both. The effect of the electron energy on the efficiency can be tested by constructing a simple model based on known properties of electron absorption in materials.

	Threshold Dosage	Minimum Useful Dosage
10kV $J = .08$ a/cm^2 $P/A = 0.8 \times 10^3 \Omega/$cm^2	$.06 - .09$ coul/cm^2	1.5 coul/cm^2
15kV $J = .185$ a/cm^2 $P/A = 2.8 \times 10^3 \Omega/$cm^2	$.09$ coul/cm^2	$.9 - 1.8$ coul/cm^2
20 kV $J = .25$ a/cm^2 $P/A = 5 \times 10^3 \Omega/$cm^2	$.06 - .09$ coul/cm^2	$1.2 - 2.1$ coul/cm^2
25 kV $J = .24$ a/cm^2 $P/A = 6 \times 10^3 \Omega/$cm^2	$.12$ coul/cm^2	$1.8 - 2.7$ coul/cm^2
30 kV $J = .24$ a/cm^2 $P/A = 7.2 \times 10^3 \Omega/$cm^2	$.15$ coul/cm^2	$2.1 - 3.0$ coul/cm^2

TABLE IV.

Bethe[76] has proposed a simple model for the transfer of energy from a beam of electrons to an absorbing medium via inelastic collisions. It is assumed in this model that the electrons follow a straight path into the material until the first collision after which they diffuse randomly. This model predicts the penetration depth or range, R, for an electron with energy E to be

$$R = \frac{I_P^2}{8\pi e^4 NZ} \left[Ei\left(2 \ln \frac{2E}{I_P}\right) \right] \qquad [27]$$

where NZ is the number of electrons per cm^3 in the absorber and I_P is the ionization potential or energy needed to produce an ion pair in the absorber. This number is not known for the TiO_2 film, but by comparison with values for other inorganic or organic materials, it is most likely less than 100 eV. Ei indicates the exponential integral which may be evaluated[77] as

$$Ei(x) \simeq \frac{e^x}{x} \left(1 + \frac{1}{x} + \frac{2}{x^2}\right) \qquad [28]$$

where $x = 2 \ln \left(\frac{2E}{I_P}\right)$. But $\frac{2E}{I_P}$ is quite large since E is between 10^4 and 3×10^4 eV. Hence, for a first approximation, it can be assumed that $x >> 1$. In this case Eq. [28] can be rewritten as

$$Ei(x) \simeq \frac{e^x}{x} \qquad [29]$$

The ratio of the penetration depths of two electrons with incident energies E_1 and E_2 may be written using Eqs. [27] and [29]

$$\frac{R_1}{R_2} = \frac{Ei(x_1)}{Ei(x_2)} = \frac{x_2}{x_1} e^{x_1 - x_2} \qquad [30]$$

but

$$x_1 = 2 \ln \left(\frac{2E_1}{I_P}\right) = 2 \left[\ln 2E_1 - \ln I_P\right]$$

$$x_2 = 2 \ln \left(\frac{2E_2}{I_P}\right) = 2 \left[\ln 2E_2 - \ln I_P\right]$$

and

$$x_1 - x_2 = \ln \left(\frac{E_1}{E_2}\right)^2 \qquad [31]$$

Further

$$\frac{x_2}{x_1} = \frac{\ln}{\ln} \frac{2E_1 - \ln I_P}{2E_1 - \ln I_P}$$

may be approximated since $2E \gg I_P$ as

$$\frac{x_2}{x_1} = \frac{\ln 2E_2}{\ln 2E_1} \qquad [32]$$

combining Eqs. [30], [31], and [32]

$$\frac{R_1}{R_2} \simeq \frac{\ln 2E_2}{\ln 2E_1} \left(\frac{E_1}{E_2}\right)^2 \qquad [33]$$

This approximation is quite good when compared against the values calculated by Broyde[69].

Charlesby[78] has determined an empirical relation between the fraction of the energy transferred by an electron as a function of the penetration/penetration range ratio. If the electron passes completely through the absorbing layer, which is the case with 2700 Å of TiO_2 and 10-30 keV electrons, then the penetration is the film thickness, d, and the penetration range is found from Eq [27]. Because several parameters in Eq. [27] are not known, it is not possible to calculate this range for TiO_2, but comparison with calculated values for other materials leads to the conclusion that the penetration range $\gg$ d. In the range of d/penetration range $\ll$ 1, Charlesby's curve predicts a linear relation with the fraction of energy transferred with a slope of 1. That is

$$\text{Fraction transferred} = d/\text{penetration range}$$

The fraction of the energy transferred at energy E_1 is d/R_1 and the fraction at energy E_2 is d/R_2. The total energy transferred per electron, E_T/e^-, is then

$$\frac{E_T}{e^-} = (\text{fraction transferred}) \times (\text{energy of the electron})$$

or

$$\frac{E_{T1}}{e^-} = E_1 \, d/R_1 \quad \text{and} \quad \frac{E_{T2}}{e^-} = E_2 \, d/R_2 \qquad [34]$$

The ratio of the energy transferred per electron for electron energies E_1 and E_2 is

$$\frac{E_{T1}/e^-}{E_{T2}/e^-} = \frac{E_1}{E_2} \frac{R_2}{R_1}$$

Combining this with Eq. [33]

$$\frac{E_{T1}/e^-}{E_{T2}/e^-} \simeq \frac{E_1}{E_2} \frac{\ln 2E_1}{\ln 2E_2} (\frac{E_2}{E_1})^2 \qquad [35]$$

$$= \frac{E_2}{E_1} \frac{\ln 2E_1}{\ln 2E_2}$$

Eq. [35] predicts that the energy transferred per electron decreases in a roughly linear fashion as the electron energy is increased.

The total energy transferred to the film by the electron beam is the product of the total energy per electron and the electron dosage. That is

$$E_{T1} = \frac{E_{T1}}{e^-} \cdot D_1 \quad \text{and} \quad E_{T2} = \frac{E_{T2}}{e^-} \cdot D_2 \qquad [36]$$

It is now assumed that the same total energy must be transferred to the film to achieve the same results, e.g., reach the minimum useful dosage point. The limitations of this assumption will be discussed below.

That is,

$$E_{T1} = E_{T2}$$

Then from Eq. [35] and Eq. [36]

$$\frac{D_1}{D_2} = E_{T2}/e^- \Big/ E_{T1}/e^- = \frac{E_1}{E_2} \frac{\ln 2E_2}{\ln 2E_1} \qquad [37]$$

By using average values from Table IV (D_1 = 4.5 coul/cm^2, E_1 = 15 x 10^3 eV; D_2 = 8.5 coul/cm^2, E_2 = 30 x 10^3 eV), the right hand side of Eq. [37] is 0.535 while the left hand side is 0.53. It is felt that the agreement between these two values is due, in part, to the similar current densities of the two beams, especially in light of the assumption leading to Eq. [37]. This assumption stated that, to achieve a given degree of conversion of a film from the amorphous to crystalline form, the same total energy must be imparted to the film irregardless of the rate of energy delivery. For a given energy beam this then implies that there should exist no dependence of the conversion process on the beam current density, but only on the total integrated flux.

A more complex model, considering the energy transfer process from a microscopic view, includes a current density dependence. This model acknowledges the need for the atoms and molecules in a microscopic neighborhood in the film to be excited simultaneously to permit the migration of, and to overcome any potential barriers between, the various species which constitute the crystalline form. This simultaneous excitation of the various TiO_2 molecules in a given volume implies a current density dependence. Large electron dosages at very low electron arrival rates produce little conversion to the crystalline form because of the low probability of the simultaneous arrival of a sufficient number of electrons. Very high

current densities may also prove inefficient by virtue of the fact that so much energy is available at any given time that some disordering or even damage may occur. The crystallization process may also involve a characteristic ordering time. Pumping the material with energy at a rate higher than it can be used also leads to an inefficient process. A far more complex mathematical model would have to be fashioned to accurately predict the relative efficiencies of two beams differing in both energy and current density.

The line width and resolution of the electron-beam-produced patterns are functions of the focus and definition of the electron beam, the total integrated flux and the properties of the amorphous TiO_2 itself. In general, electron beam diameters less than 2 μ could not be obtained with the e-gun in the microprobe. Exposure to doses less than the minimum usable flux produced lines with non-uniform widths and beveled edges. However, with the beam focused as small as possible, and after exposures greater than the minimum useable flux, lines 3 μ wide could regularly be produced after etching. These lines have edge definitions (i.e., the transition from the full thickness of the film to the bare substrate) of 0.5 μ or less. In these cases, it is felt that the limiting factor is the diameter and electron distribution in the bombarding beam. In certain rare cases, a line would be observed to have slightly scalloped edges and rather poor edge definition. These scallops are highly regular occurring with a period of approximately 5 μ and were first thought to be due to a deflecting or chopping signal or noise being impressed on the beam sweep voltages. However, in the light of the recent work by Shiojiri, et al[72] in which he observed preferential crystal growth in amorphous TiO_2 films

during an anneal, it is possible that the points extending out from the line defined by the beam sweep are crystallites of anatase TiO_2. According to Chalmers[79], crystallization of a thin film from an amorphous phase will generally not proceed along a smooth interface, but owing to the instability of such a configuration an indented crystal growth front will be formed. This is due to the fact that in Chalmer's model, a crystal will grow more slowly in the direction characterized by the larger thermal conductivity. Heat generated at the crystal-amorphous interface during crystallization will be conducted away by areas of high thermal conductivity retarding further growth while areas of low conductivity will retain the heat and the process of crystallization will be enhanced in those areas. The ratio of thermal conductivities along the "a" axis to that along the "c" axis for anatase TiO_2 is 1.8 leading to the speculation that such an indented boundary (the line edge in this case) could be due to this effect. If this is the case, such a phenomenon may provide a lower limit on the dimensions of pattern formed by electron beams in amorphous TiO_2.

The etch resistance of the TiO_2 films brought about by the electron beam bombardment is, then, undoubtedly brought about by the conversion of some or all of the film from the amorphous form to a crystalline phase. The threshold and minimum useful dosages are evidently associated with conversion to the anatase form. An experiment was designed and performed to ascertain if continued bombardment would supply sufficient energy to the film to allow it to continue ordering itself and, ultimately, reach the rutile phase. Once again, the electron gun in the Phillips microprobe was used as the supply of electrons, but rather than sweeping the beam over a line, it was not deflected and allowed to strike a single spot

approximately 10 μ in diameter. During this process, the bombarded area was observed through the microprobe optical system and any changes in the film interference color could be detected. Such a change in interference color reflected a combined change in the thickness and index of refraction of the film at that point. Figures 3, 4 and 5 in Chapter III correlate this change in the index of refraction and thickness with the anneal temperature and the crystalline phase of the film. By observing the interference color of the film during bombardment and assuming a constant index of refraction, the apparent thickness of the film may be correlated with the bombardment parameters such as time, dosage, beam energy and power. If a model is assumed yielding a functional relation between the thickness and index of refraction as in Chapter III, then the apparent thickness can be converted into the true thickness and this in turn can be correlated with the irradiation parameters.

Rather than using the thickness, either apparent or true, as a parameter a normalized ratio was devised. This ratio is simply

$$r = (d_i - d)/(d_i - d_f) \qquad [38]$$

where d_i and d_f are the initial and final thicknesses of the film while d is the thickness at any given moment. This ratio can be "scaled" to the conversion process of amorphous films to rutile by properly choosing d_i and d_f. This was done by taking an identical sample of the TiO_2 on Si used with the electron bombardment and heating it at 1000°C for 5 minutes, a process known to yield the rutile form. The quantities d_i and d_f were measured from this control sample. The value of d is obtained from the bombarded film. Hence, the value of r is determined by the degree of conversion to the rutile form achieved by the electron beam. A value of r = 0 indicates that the material is essentially amorphous while a value of r = 1

implies that the rutile form has been reached. An apparent value of r

corresponding to the apparent thickness and based on the initial index of

refraction of the film can also be defined as

$$r_a = \frac{d_i - d_a}{d_i - d_{fa}}$$ [39]

This quantity is displayed as a function of irradiation time for 10, 15, 20

and 30 keV electron beams in Fig. 19. The curves immediately suggest sev-

eral interesting conclusions.

(a)   Given a sufficient length of time, the value of r_a reaches and

slightly exceeds unity indicating that the rutile form has been

reached. During the exposure to the beam the interference colors

changed as a function of time, remaining clear and sharp until

long times were reached. At this point, the color fringe became

dull and appeared rather gray. A detailed examination revealed

the presence of small cracks and other surface damage appearing

during this period. It may be the case that at very high dosages

sufficient damage has occurred to allow the film to collapse some-

what accounting for the values of $r_a > 1$.

(b)   The interference color change occurred so rapidly during the ini-

tial phase of the bombardment with the 20 and 30 keV beam that no

data below r = 0.5 could be obtained in these cases. The mater-

ial was converted most rapidly by the highest energy, highest

power density beam; least rapidly by the lowest energy, lowest

power density beam.

(c)   The curves are all reminiscent of rate-type of phenomena charac-

terized by steep slopes initially becoming asympototic to a final

value.

$$r_a = \frac{d_i - d_a(t)}{d_i - d_{fa}}$$

d_i = 2600 Å AMORPHOUS TiO$_2$

		P/A= .35 w/cm^2
10 kV	J= .035 a/cm^2	
15 kV	= .113	= 1.7
20 kV	= .159	= 3.2
30 kV	= .238	= 7.1
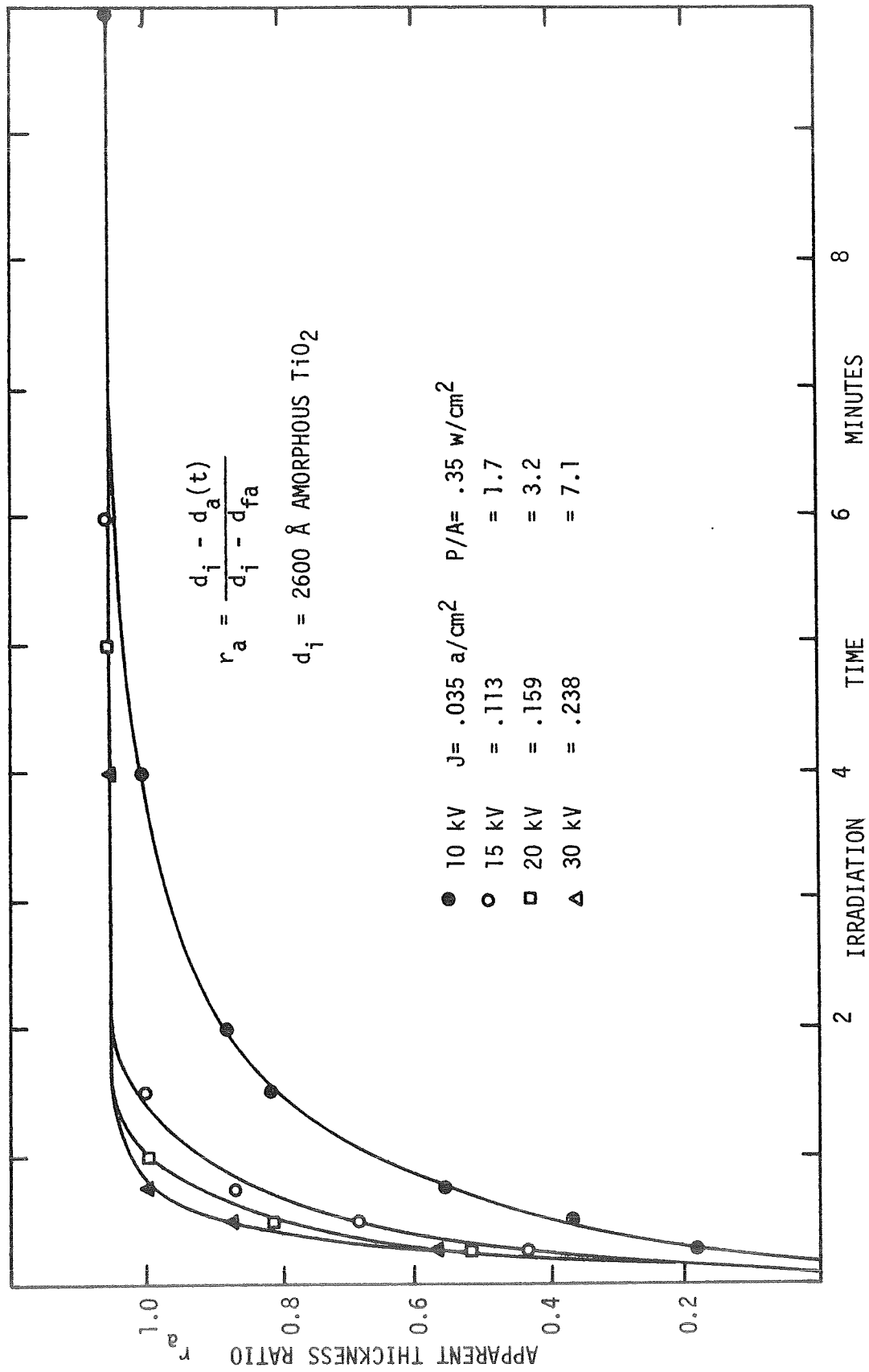
APPARENT THICKNESS RATIO vs. ELECTRON IRRADIATION TIME.
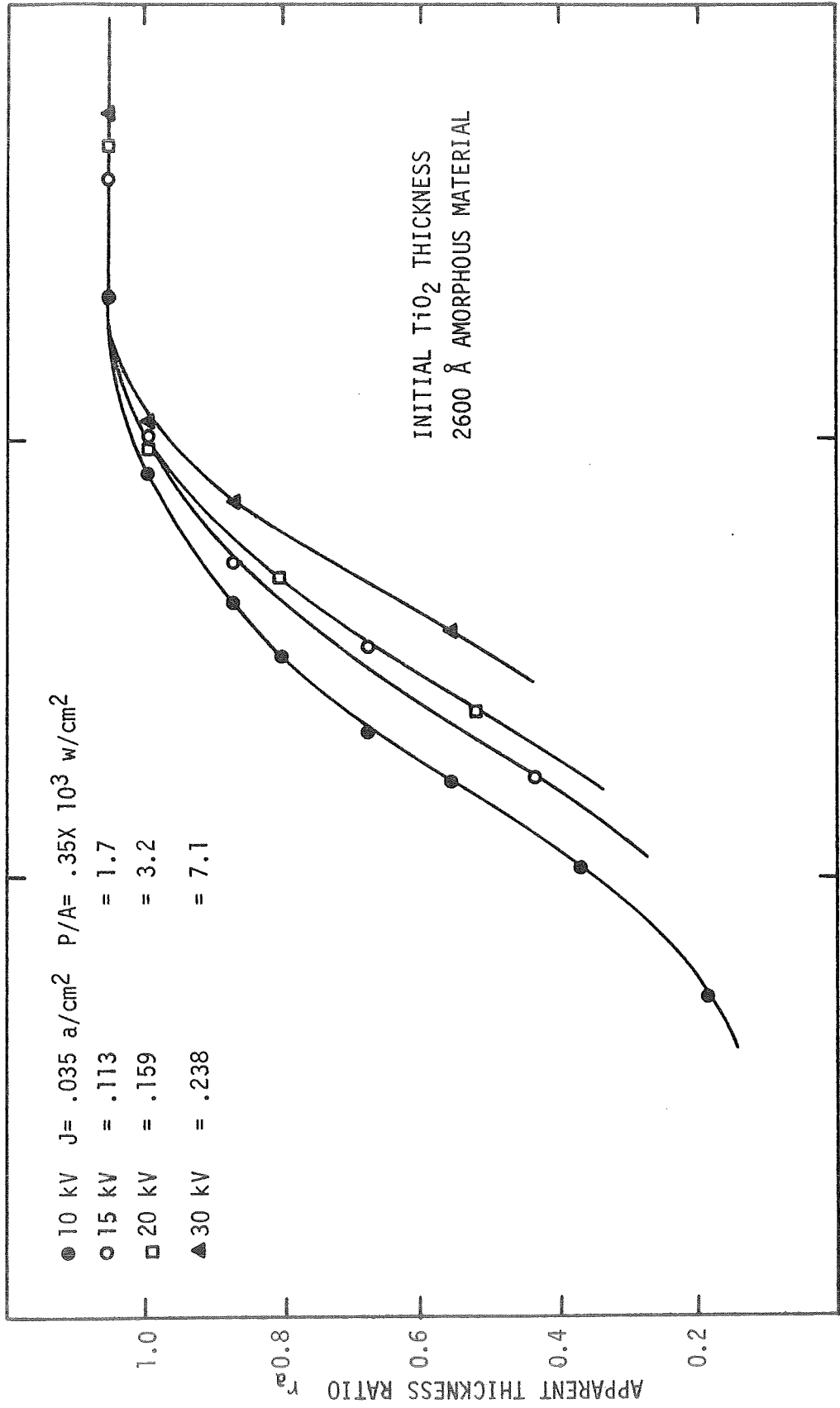
FIGURE 19.

FIGURE 20.   APPARENT THICKNESS RATIO vs. TOTAL INTEGRATED ELECTRON FLUX.

This same data has been plotted in Figure 20 as a function of total electron dosage on a semi-log plot. This plot was not used to suggest a model but only to expand the data in the lower dosage regions. The order of the curves has been reversed from Figure 19, that is, the low energy, low power density electron beam provided the most efficient conversion of the material while the high energy beam was the least efficient. This effect was considered earlier in this chapter where the difference in efficiences was ascribed by a qualitative model, to the variation in energy and current density of the beam. The beam current densities vary appreciably from curve to curve in the figure increasing by almost a factor of 10 from the 10 keV to the 30 keV beam. Eq. [37] predicts that, if the current density were constant for all cases then the ratio of dosages at any given r_a should be 1:1.44:1.87:2.7. For r_a = 0.6 the curves in the figure are in the ratio 1:1.55:1.81:2.35, indicating either the error in the experiment or a dependence on the current density.

Rough extrapolations of the curves to the r_a = 0 intercept yields values between approximately 0.2 and 0.8 coul/cm^2. Comparing these values with those of Table IV, it can be seen that the intercept values lie between those listed for threshold and minimum useable fluxes. From this comparison it would appear that very little conversion need take place to afford some degree of etch resistance while the minimum useful values represent more substantial conversion.

Figure 21 displays data similar to that in Figure 20, except that in the case of the 15, 20 and 30 keV beams, the current densities have been reduced in order to observe any effect on the conversion efficiencies. The current densities now vary less than a factor of 2. Little difference is
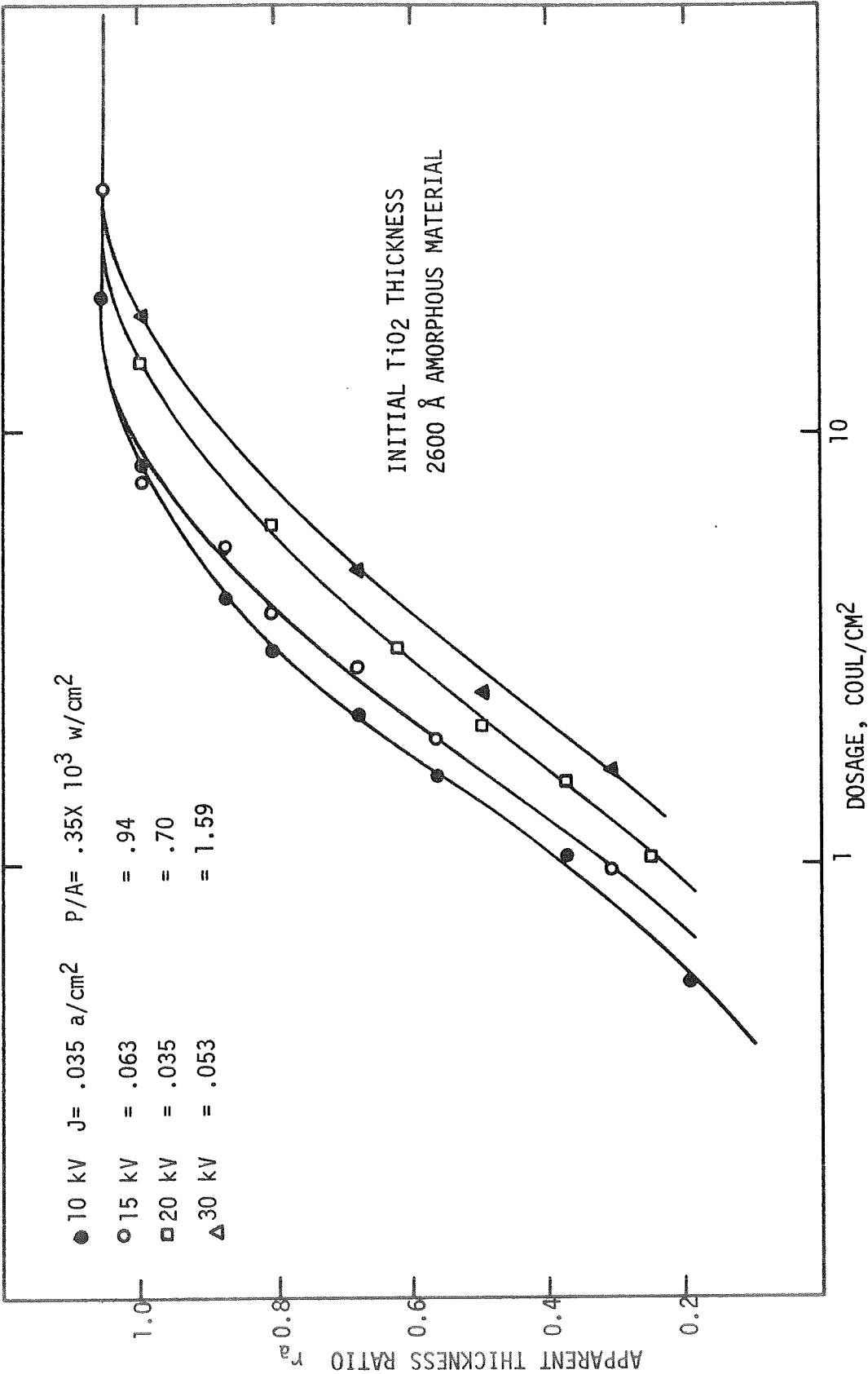
FIGURE 21. APPARENT THICKNESS RATIO vs. TOTAL INTEGRATED ELECTRON FLUX AT LOW CURRENT DENSITIES

exhibited by the curves in the two figures, except for a tendency for the low current density beams to be less efficient between the values $r_a \simeq 0.9$ and above. Otherwise, the current density seems to play a minor role in determining the energy transferred to the film or, if it is a factor, it is roughly constant over the range of current densities utilized. The ratio of the dosages at $r_a = 0.6$ is 1:1.24:1.68:2.18.

If a model is assumed relating in some way the thickness and index of refraction, then the apparent thickness may be converted to the true thickness and the apparent ratio, r_a, may be converted to the actual ratio, r. Such a model was proposed in Chapter III in which the functional relationship between changes in the thickness and index of refraction is given as

$$\frac{n_2}{n_1} = (\frac{d_1}{d_2})^{1/2} \tag{40}$$

It is then true that

$$d = d_a (\frac{n_o}{n})$$

where d is the actual thickness, d_a is the apparent thickness at any given moment, n is the index of refraction of the film at that same moment and n_o is the index to which the d_a was originally scaled. If these substitutions are made in Eq. [39] then the actual ratio may be written in terms of the apparent ratio

$$r = r_a \{\frac{2 - r_a (1 - d_{fa}/d_i)}{(1 + d_{fa}/d_i)}\} \tag{41}$$

where d_{fa} and d_i are the same as in Eq. [38]. The data from Figure 20 is redisplayed in Figure 22 as a function of r rather than r_a. Only a very slight change has occurred due to the transformation and the relative positions of the curves remains unaltered.
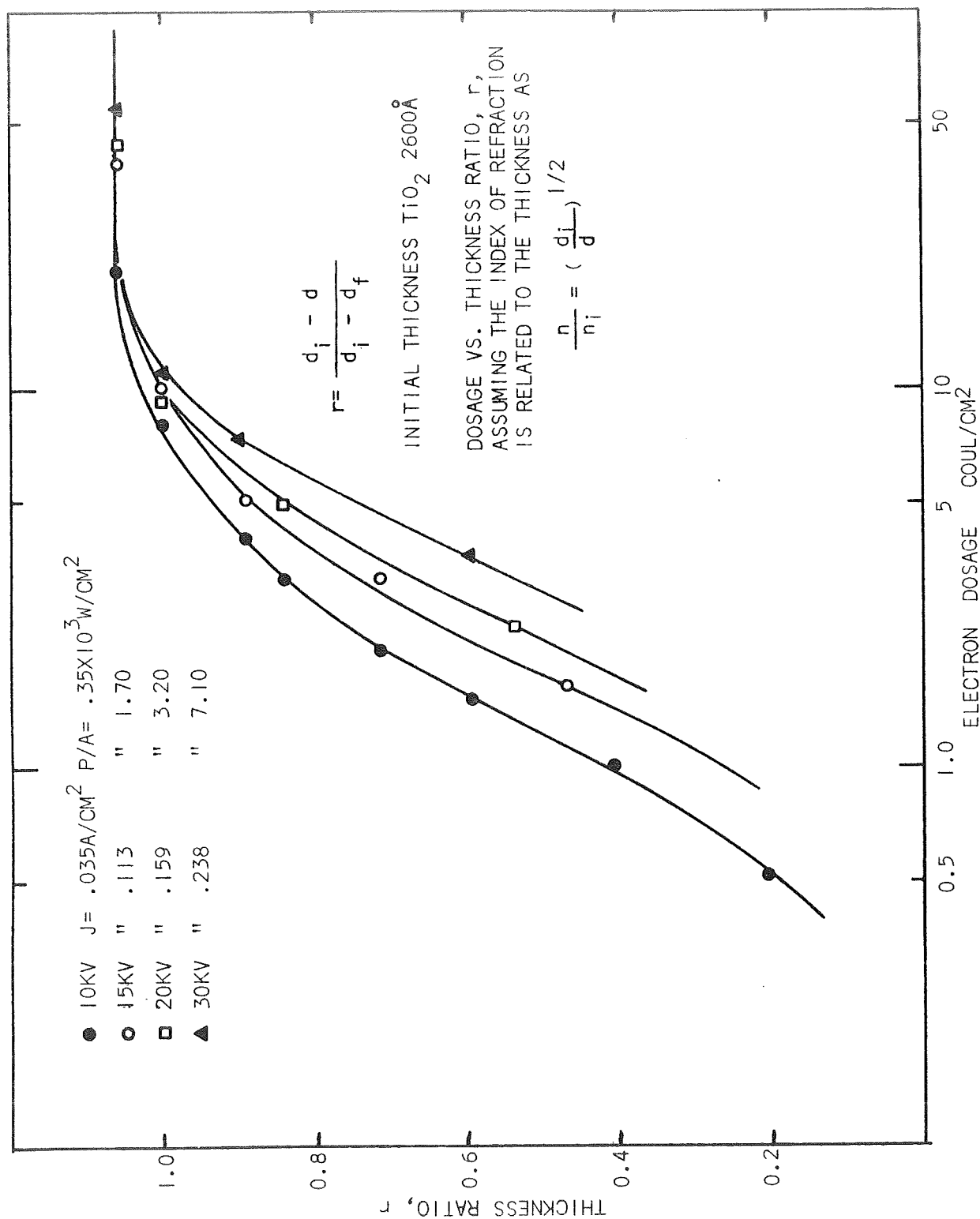
FIGURE 22. ACTUAL THICKNESS RATIO vs. TOTAL INTEGRATED ELECTRON FLUX.

Several models were considered in an attempt to mathematize the conversion process of the amorphous films to the rutile form. The applicability of two possible models are discussed below.

(a) In Chapter III amorphous material was converted to rutile by merely heating it by conduction or convection to the neighbor- of 1000°C for a short period of time. For the case of electron-beam-induced conversion it would not be unreasonable to expect that the electron beam was merely heating the absorbing material to a temperature high enough to allow the rutile phase to form, supposedly in the neighborhood of 1000°C. This same principle is used for electron beam vacuum evaporation of numerous mater-ials. An expression could be derived correlating the tempera-ture of the bombarded area with irradiation time or dosage in-volving the specific heat, thermal conductivity and some geo-metrical factors. The fact remains, however, that the rutile phase was reached without elevating the temperature substantial-ly, at least on a macroscopic scale since the samples were not observed to glow and showed no signs of approaching temperatures associated with the rutile transition.

(b) Faced with the fact that if a temperature rise need be postu-lated, then it must occur on a microscopic atomic scale rather than a macroscopic one. Rather than considering an electron in-duced temperature increase, it would be more appropriate to model an electron induced ordering in the film, where the amorphous film is in a state of complete disorder and the rutile film is completely ordered. Such a model is quite general in that this

process of ordering in the crystal may be visualized as taking

place by a number of different energy transferring sequences,

all, however, resulting in the continued ordering of the film.

In order to remain as general as possible to allow for various

interpretations, the second model will be pursued. We assume the material

is made up of ordered and disordered neighborhoods. The number of neigh-

borhoods in an ordered rutile state is $\overline{N}_O$, while the number in a disor-

dered state is $\overline{N}_D$. The sum of $\overline{N}_O$ and $\overline{N}_D$ is N, the total number of neigh-

borhoods, each containing a fixed number of molecules, which are either

ordered or disordered.

Let

$$\frac{\overline{N}_O}{N} = N_O; \quad \frac{\overline{N}_D}{N} = N_D; \quad N_O + N_D = 1 \qquad [42]$$

It is then assumed that a basic rate process governs the transitions into

and out of the ordered state. That is

$$\frac{dN_O}{dt} = A'N_D + B'N_O \qquad [43]$$

where A' is the transition probability into, and B' the transition probabil-

ity out of the ordered state. Since the crystallization process is known

to be exothermic it can be assumed that very few transitions out of the

ordered state will occur and B' $\sim$ 0. Rewriting Eq. [43]

$$\frac{dN_O}{dt} = A' (1 - N_O) \qquad [44]$$

but

$$\frac{dN_O}{dt} = \frac{dN_O}{dD} \frac{dD}{dt} \qquad [45]$$

where D is the dosage of electrons and dD/dt is the current density and is

a constant.

$$\frac{dN_o}{dD} = A(1 - N_o) \qquad [46]$$

The solution to this equation, assuming some threshold dosage, D_o, exists is

$$N_o = 1 - e^{-A(D - D_o)} \qquad [47]$$

In order to correlate this solution with the experimental curves, it will be assumed that the quantities r and N_o represent the same thing and are interchangeable. That they should have some functional relationship is obvious, that they are identical is open to some question. Both quantities have a value of zero, when the material is amorphous and a value of unity when the rutile form is reached.

$$r = 1 - e^{-A(D - D_o)} \qquad [48]$$

Figure 23 shows a plot of the 10 keV data presented previously, except graphed as a function of 1 - r to facilitate comparison with Eq.[48]. This experimental data is a straight line initially at low dosage but tends to break away at higher values. A plot of Eq. [48] is also included using the parameters D_o = .19 and A = .65. Obviously, the simple model in Eq. [48] is not able to account for somewhat of a conversion slowdown or increased inefficiency at higher dosage levels. This may be due to several factors.

(1) The film becomes thinner as the ordering proceeds and it reaches its thinnest point in the rutile form. Less of the incident energy is transferred to the film as a result and the process appears to be less efficient as the irradiation continues.

(2) As the conversion process nears completion, unordered molecules are prevented from joining with other unordered groups to form a crystallite by interposing volumes of rutile material.
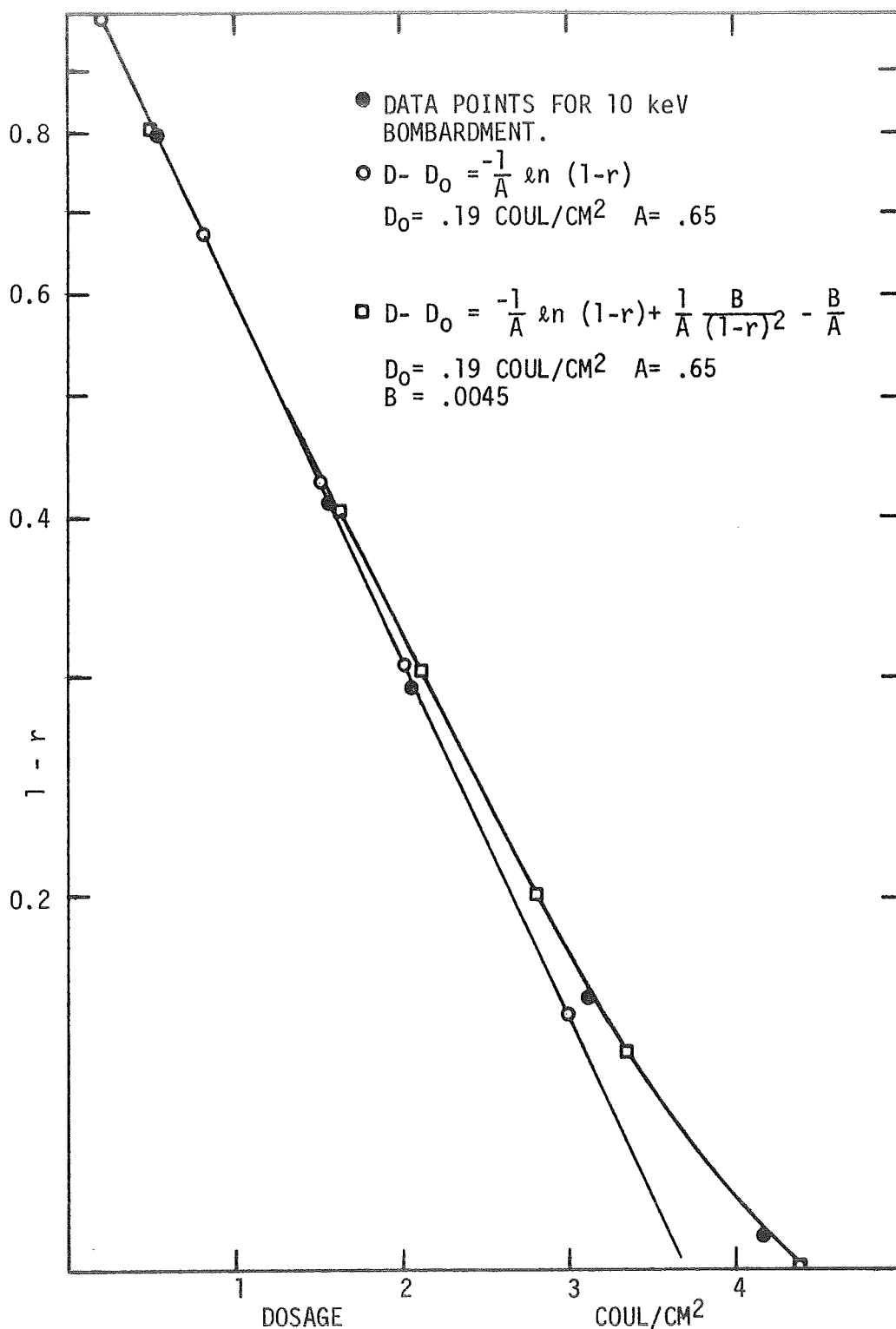
FIGURE 23.   THICKNESS RATIO vs. TOTAL INTEGRATED ELECTRON
FLUX FOR PROPOSED MODELS AND EXPERIMENTAL DATA.

A number of variations or corrections to the model above have been used to afford some compensation at high dosages. These additions to the model were suggested by the two factors above and consist of altering the slope, A, by linear and exponential functions of r. Very few that were derived starting from any physical effects, such as the variation in energy absorbed as a function of thickness, produced a significant correction. However, an empirical relationship was found which provides fairly good agreement with the experimental data over the region of interest. The differential equation for this empirical formula is

$$\frac{dN_o}{dt} = \frac{dr}{dt} = A''(1 - r) \qquad [49]$$

where, rather than being a constant, A'' is

$$A'' = A' \left(\frac{1}{1 + \frac{B}{1-r}}\right) \qquad [50]$$

Using the relations $\frac{dr}{dt} = \frac{dr}{dD} \frac{dD}{dt}$, and $A = A' \frac{dD}{dt}$, the solution to Eq. [48] is

$$D - D_o = -\frac{1}{A} \{\ln(1 - r) - \frac{B}{(1 - r)^2} + B\} \qquad [51]$$

This equation is plotted in Figure 23 using $D_o = .19$ coul/cm^2, $A = .65$ and $B = .0045$. The significance of this particular functional relationship of the slope A'' on r is not understood in terms of the arguments (1) and (2), above.

Generally, however, the simple model proposed initially and expressed in Eq. [48] seems to be quite valid for describing the conversion phenomena observed.

OTHER CONVERSION TECHNIQUES

Besides supplying amorphous films with sufficient energy to order themselves with an electron beam two other energy delivery techniques

were attempted to ascertain their feasibility. Little other than fairly informal qualitative experiments were performed, yet some interesting observations were made.

(1)   Direct Photon Absorption

Thin TiO_2 films on Si, identical to those used for the electron beam exposure experiments, were subjected to a focused beam from a 100 mw C.W. HeNe laser. From Figure 6, Chapter III, it is evident that the TiO_2 films are quite transparent to photons in the visible range and absorb very little of the photon energy supplied by the .6328 μ HeNe beam. Exposure to the focused beam (approximately 0.1 mm diameter) for 15 minutes provided a fair degree of protection from the standard 0.5% HF etch which readily attacked the unexposed background. No protection was afforded by exposure to the unfocused beam.

In order to take advantage of the strong absorption in the u.v. region, light from a 100 watt mercury vapor lamp was employed to supply the conversion energy. Little focusing could be accomplished and power densities between 0.1 and 1 watt/cm^2 were thought to be available at a distance of 5.0 cm from the lamp. The light was allowed to strike only selected areas of an amorphous TiO_2 film by using a standard I.C. photomask with clear and opaque areas. Standard procedure included placing the substrate coated with the amorphous film and covered with the mask approximately 5 cm from the lamp and allowing the exposure to continue from 10 to 15 minutes. Heating of the mask and substrate was retarded by using a heat sink. However, after approximately 15 minutes the opaque areas of the mask became quite hot and a "contact printing" process, described below, assumed a competing and then a dominant role, destroying the resolution of the photon

converted areas. Once the exposure has been completed the material is sub-
jected to the standard 0.5% HF etch to remove the unexposed material which
was found to be removed at rates from 2 to 5 times faster than the con-
verted areas. Patterns with line widths of 50 µ could easily be defined in
3000 $\overset{\circ}{A}$ of TiO_2 with this process.

While the experiments performed served to make only the major
parameters apparent in even a qualitative way, it was clear that the compe-
tition between conversion by direct photon absorption and conductive heat-
ing from the mask or substrate makes the power density and spectral output
of the lamp, the heat sink arrangements for the mask and lamp, and the ex-
posure time all important parameters. If the exposure is allowed to con-
tinue to the point that conversion by photons has occurred below the clear
areas of the mask and conversion by conduction or convection has occurred
below the opaque areas, then the entire film will have developed some etch
resistance and no distinct pattern will be defined by the process. Hence,
either the direct photon process or the "contact printing" process must be
enhanced. The first has been described above, the second below.

(2)   Pattern Definition by "Contact Printing"

Several variations of this process were attempted. In the first,
a standard photomask used for IC production was placed directly on the sur-
face of a TiO_2 coated Si wafer, the opaque emulsion side of the mask in con-
tact with the TiO_2 surface. Light from a flood lamp was allowed to pass
through the mask to the emulsion side. The black opaque areas of the emul-
sion absorb the photon energy and become hot, transferring the heat directly
to the contacting TiO_2. The clear areas of the mask allow the photons to
pass through directly into the TiO_2 where some conversion, depending on the

spectral output of the lamp and exposure time is experienced. If the Hg lamp is used, long exposures (20 to 30 min.) were necessary to make the contact process dominate. Subsequent etching removed the film below the clear areas of the mask while the film heated by contacting the opaque area remained. Excellent pattern definition was achieved by this method with no noticeable misregistration at the edges or corners due to heat flow laterally in the film and line widths on the order of 50 μ were again observed. This process is, however, rather destructive to standard Kodak glass-emulsion photomasks.

This same technique was used with a thin stainless steel evaporation mask with a pattern of lines and holes in it. The mask was heated by an infrared lamp, the solid portions of the mask absorbing the photon energy and conducting it as heat to the amorphous TiO_2 film while the open portion of the mask allowed the light to pass directly into the film where little effect was seen. Once again, etching produced a sharp image of the pattern of the contacting mask in the unetched TiO_2.

The methods of directly transferring a pattern into a TiO_2 film could, after some refining, provide an excellent and quick way of producing high resolution TiO_2 patterns for hybrid or integrated circuits completely circumventing the need for the numerous steps associated with the application, exposure and removal of standard photoresists.

TiO_2 AS A DIFFUSION MASK

Because of the ease with which patterns can be defined in the TiO_2 film either by a directed electron beam, direct photon absorption, or through a contact printing process, the films were considered for a number of applications in hybrid or integrated circuit technology. In Chapter III

the possibility of using TiO_2 films as an etch mask were discussed. The electrical measurements of Chapter IV showed the film had a number of exploitable properties depending upon the anneal history. In this section TiO_2 will be considered as a diffusion mask, protecting a Si wafer from a phosphorous dopant.

Three samples were placed in a phosphorous oxycholoride and oxygen atmosphere at 1000°C - a bare p type 1 Ω-cm Si wafer, a 1 Ω-cm p type Si wafer covered with 2000 Å of SiO_2 thermally grown in an O_2 atmosphere and a similar wafer covered with 2000 Å of rutile TiO_2. The backside of all three wafers was protected by 8000 Å of SiO_2 during the diffusion. At given intervals, small chips were broken off of each sample and removed from the diffusion oven. The surface and backside oxides were stripped with 48% HF and an ohmic contact was made to the backside of each chip. A pressure contact was brought down on the front surface of each chip and the I-V characteristics displayed on a curve tracer. Those chips which were not subjected to the phosphorous diffusion showed completely ohmic characteristics and were used as the control samples. Where the phosphorous eventually diffused through the SiO_2 and TiO_2 a surface diode was formed in the Si and this change was immediately visible in the I-V characteristics. The reverse resistance (measured at 5 volts) of these samples as a function of time is shown in Figure 24. It is evident that some junction characteristics are becoming visible between 20 and 30 minutes. The time at which 2000 Å of SiO_2 failed under identical conditions was found by Sah, et al.[80] to be approximately 24 minutes. From the graph it can be seen that the TiO_2 continues to serve as a mask perhaps for as much as 5 minutes longer, a 20% improvement over the SiO_2.
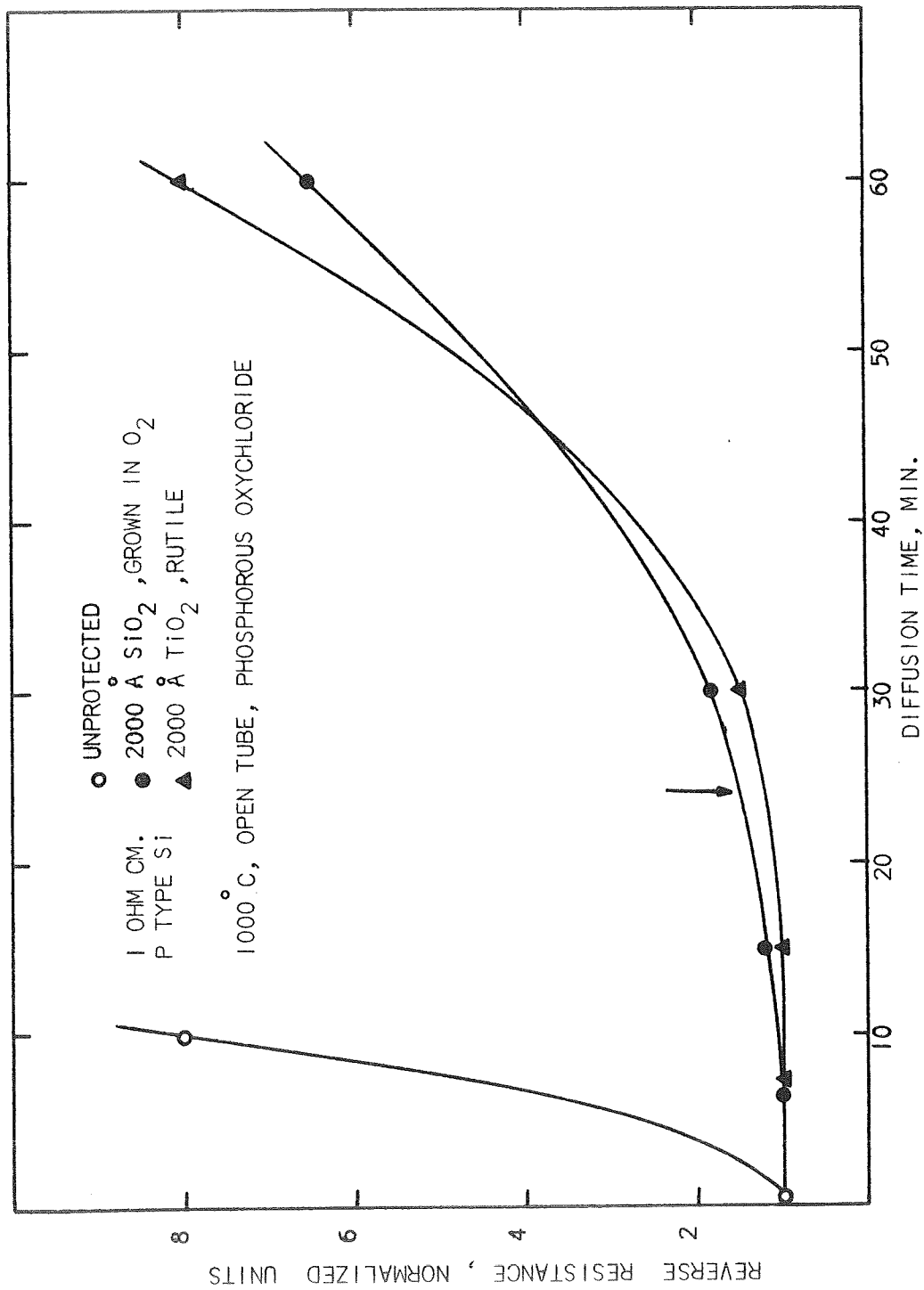
FIGURE 24. COMPARISON OF TiO₂ AND SiO₂ AS DIFFUSION MASKS ON SILICON.

It is not unreasonable to expect that TiO_2 and an equal thickness of SiO_2 would retard the diffusion of an impurity at approximately equal rates since the atomic packing density is similar for both materials. However, this may only partially affect the diffusion rate since the TiO_2 film is polycrystalline and, hence, most diffusion may take place at the grain boundaries as compared to the amorphous SiO_2.

SUMMARY

Amorphous films of TiO_2 can be given enough energy to permit crystallization to various degrees by an electron beam. Very little conversion to the anatase from the amorphous form is necessary to provide good etch resistance to 0.5% HF. By sweeping the e-beam over the area to be exposed repeatedly, patterns with line widths of approximately 3μ and edge resolution of less than 0.5μ are possible. Continued exposure to the electron beam will continue to convert the TiO_2 into higher crystalline forms until the rutile phase is reached. A simple rate ordering process describes, in a general fashion, the crystallization process and fits the experimental data reasonably well. Other methods of conversion and pattern definition were tried, including laser beam writing, u.v. photon exposure, and contact printing. While the laser beam technique was fairly unsuccessful, the contact printing, that is selective conversion at points of contact with a hot "embossed" press and the direct conversion utilizing energy supplied by a u.v. source proved to be quite successful. Because of its easy definition or patterning on the surface of a Si wafer, it was considered as a diffusion mask against phosphorous diffusion at $1000°C$. In this role, it showed itself to be more effective than thermally grown SiO_2.

CHAPTER VI.

SUMMARY AND CONCLUSIONS

SUMMARY

Thin films of TiO_2 have been produced by anodization, thermal oxidation, reactive sputtering, vacuum evaporation, pyrolysis of liquid sources, and a number of chemical vapor deposition schemes. Deposition temperatures from room temperature to over 1000°C have been used with reactive and inert atmospheres. The characteristics of these films were reviewed fairly thoroughly in Chapter I and comparisons between the material in thin film and bulk forms were made. This review made evident the wide range of values for material parameters, such as resistivity, index of refraction, dielectric constant, loss tangent and a number of others and, while it was clear that the crystalline state of the films was a strong controlling factor, no one deposition process proved sufficiently versatile to allow a rather extensive correlation to be made.

Hence, it was the object of this research to develop a process for producing and testing thin films of TiO_2 with enough versatility to help elucidate the correlation between the crystalline state of the material and a number of basic measurable parameters and to advance the state of the hybrid and integrated circuit art by making available to it TiO_2 films with a spectrum of useful and unique properties.

The film growth technique, covered in detail in Chapter II, is a typical chemical vapor deposition utilizing a tetraisopropyl titanate source and a hydrolyzing reaction at the deposition substrate heated to 150°C. The water for the reaction is supplied by the water vapor in the surrounding air and can be augmented by an extra water vapor source.

Typical deposition parameters are as follows: (i) substrate temperature 150°C; (ii) He carrier flow rate 1 l/min.; (iii) TPT source temperature 75°C. Using these values, about 10 minutes is required to cover a 1-1/4" Si substrate with 1500 Å of TiO_2. Because of the simple vapor delivery system and the low deposition temperature, it is possible to manually control the thickness of the film over a large area to within ± 100 Å by watching the interference colors of the growing film. While the deposition parameters did not prove to be critical, films which suffered incomplete reaction (milky looking, soft film) or premature reaction (films with white powdery inclusions) were made by allowing the parameters to range to extreme values.

Samples were ordinarily grown on three different substrates, polished fused quartz discs, soft glass microscope slides and polished single crystal Si wafers to facilitate the particular study undertaken. X-ray diffraction data was taken for all of the thin film samples and compared with a powder sample control. The films on Si and soft glass were found to be amorphous in the "as grown" condition and were converted to anatase polycrystalline films near 350°C and to the rutile form near 1000°C. At intermediate temperatures between 350° and 1000°C anatase and rutile polycrystal coexist in the film. The films on fused quartz are also initially amorphous and are converted to anatase at 350°C, but remain in this state as the temperature is elevated, evidently due to a favorable surface condition between the TiO_2 and the fused quartz. During the transition from the amorphous to the rutile crystalline form, the film undergoes a thickness change to 63% of its original thickness yet the surface remains smooth and the stresses involved are not sufficient to cause ruptures to form.

As the material changes from amorphous to anatase to rutile, the density increases markedly and is accompanied by a subsequent increase in the index of refraction from 2.0 to 2.5. The major change occurred at the 350°C amorphous to anatase transition. The anatase and rutile material has a strong absorption edge at 0.32 microns corresponding to an energy of 4.0 eV. A 2500 Å film on a quartz substrate reduced the amount of ultraviolet transmitted by the substrate alone at 0.32 by 87%.

TiO_2 grown at elevated temperatures (> 300°C) has been reported by a number of authors to be quite etch resistant and, for those films heated to 1000°C, fairly impervious to chemical attack. Because of this, its use in multilayer hybrid or integrated circuits is limited. It was reported in Chapter III, however, that the amorphous films are etched quite readily and uniformly in dilute HF (0.5%) at the rate of 50 Å/sec. The higher crystalline forms are attacked only slowly by hot H_2SO_4 and the pure rutile films are removed at the rate of approximately 1000 Å/hour in a 150°C solution of it.

It has been demonstrated in previous work in the literature that TiO_2 is best referred to as a semiconductor rather than an insulator because of the extremely wide range of resistivities brought about by slight deviations from stoichiometry, especially loss of oxygen. Material with resistivities from 10^{14} Ω-cm to 1 Ω-cm has been reported and, in one case, a loss of 1 ppm of O_2 from the rutile form accounted for a decrease of 10^4 in the resistivity.

The results of the electrical tests on the films used in this research were displayed in Chapter IV and present a rather consistent picture, the characteristics changing monotonically as the film is converted from the amorphous to the crystalline forms.

The amorphous films show poor insulating properties and are best described as n type semiconductors of a high resistivity in the 10^4 - 10^5 Ω-cm range. MIM samples yielded Schottky barrier characteristics for both I-V and C-V data. In the case of the latter, a strong forming tendency was noted causing the capacitance and the dissipation factor to decrease asymptotically with time in the reverse bias direction.

Anatase films on Si display a mixture of properties. At 100 kHz, the C-V characteristics are those of a typical MIS device with a dielectric constant of 169, while at 1 kHz they can be explained only in terms of a Schottky junction. The difference in performance as a function of frequency is evidently due to a relaxation mechanism occurring between 1 kHz and 100 kHz. The D.C. I-V characteristics are also those of a Schottky barrier junction. The resistivity of the TiO_2 is on the order of 10^8 Ω-cm. It is quite possible that the conversion to the anatase has not been completed at the 350°C anneal temperature and that the semiconducting properties are explained by the presence of minute inclusions of amorphous material.

Those films annealed at 700°C, i.e., mixtures of anatase and rutile material, display quite conventional insulating properties at all frequencies between 1 kHz and 100 kHz. The dielectric constant/dissipation factor at these frequencies are 116/.04 and 95/.09, respectively. The breakdown field for these films is on the order of 8×10^5 V/cm., while the resistivity is 5×10^{11} Ω-cm.

Films of rutile TiO_2 on Si were produced by anneals of 5 and 10 minutes at 1000°C in air. Once again, the samples are good insulators and display conventional C-V and Poole-Frenkel type I-V characteristics. The samples heated for 5 minutes have a dielectric constant/dissipation factor

of 100/.04 and 87/.07 at 1 kHz and 100 kHz, respectively. The breakdown field for these devices is approximately 7×10^5 V/cm. Those annealed for 10 minutes grew slightly thicker by virtue of 75 Å of SiO_2 growth beneath the TiO_2. The effective dielectric constant and dissipation factor of these multiple layer samples at 1 and 100 kHz is 40/.04 and 35/.05, respectively.

The surface charge densities for the anatase, mixed and rutile film, is on the order of 10^{12} negative changes per cm^2, while that same charge for the TiO_2/SiO_2 structure is 10^{12} positive charges per cm^2. It appears that the TiO_2 and SiO_2 induce charges of different sign to the surface of the substrate Si and the combination of the two insulators produce a compensating effect. No identification could be made of these negative charge sites in the TiO_2 near the surface. The possibilities include uncharged trapping sites which become negatively charged when occupied by an electron or ionized impurities, such as oxygen, trapped at the interface.

In general, the electrical resistivity changes approximately seven orders of magnitude as the material is converted from the amorphous to the rutile form. At the low end of this scale, the material most resembles a high resistivity semiconductor while at the upper end, it is an adequate insulator of quite a high dielectric constant. The characteristics change rather smoothly over the anneal range as do the majority of other measurable parameters.

It was observed that a focused beam of kilovolt electrons could supply sufficient energy to convert the amorphous material into one of the crystalline forms and, in doing so, render that spot resistant to a chemical etch which readily attacks the unconverted material. This

electron-induced conversion in 3000 Å films appears to have a threshold of approximately 0.1 coul/cm^2 to obtain well defined patterns after the etch removes the unexposed material. The electron efficiencies of the beams decrease as the energy of the beams increase. This effect is predicted by a simple Bethe'-Charlesby model and is confirmed by the experimental data. Poor results were obtained if the entire electron dosage was imparted to an area at one time in that cracks and tears often formed. Excellent results were achieved by repeatedly scanning the area to be exposed until the desired dosage was reached. The resolution of lines "written" in such a fashion is approximately the width of the beam itself. Line widths under 10µ can easily be obtained with a lower resolution limit determined by the equipment limitations and the crystal grain size of the converted material. Lines 3µ wide were made fairly easily with sharp delineation between the etched and unetched materials occurring in less than 0.5µ. These values are all dependent on the beam width and the distribution of the electrons in the beam itself.

During the electron irradiation the interference color of the film continued to change corresponding to the thickness and index of refraction at any given moment. It was found that this change continued until the rutile form was reached. Small subsequent changes are attributed to electron-induced damage to the film. The conversion rate is a function of electron energy, total integrated flux and the current density of the beam. A simple model was derived to predict the basic exponential dependence of the conversion process on the electron dosage for a given electron energy and beam current. Dosages between 25 and 30 coul/cm^2 were required for complete conversion of 2700 Å of amorphous film into the rutile by

electron beams ranging in energy from 10 to 30 keV. Typical current densities on the order of 0.1 a/cm^2 were employed.

Other experiments were attempted in which the energy to order the lattice was supplied in a number of different ways. Exposure to a focused beam from a 100 mw HeNe laser provided some, but very little, conversion etch resistance. Ultraviolet photons from a mercury arc source were absorbed by the film and, unlike the visible laser light, provided sufficient conversion to establish good etch resistance. Typical exposure times of 10 minutes at power densities of approximately 0.1 watt/cm^2 were required.

Energy was successfully transferred to the film selectively by contacting it with a heated embossed pattern. The possibility for producing truly "printed" capacitors for hybrid circuits was demonstrated.

To enhance its usefulness in a Si based technology, films of TiO_2 were tested to determine their ability to protect a Si surface from a phosphorous dopant. By checking the surface of a p type wafer for the presence of a diode, it was determined that a 2000 $\overset{o}{A}$ film of TiO_2 protected the underlying Si for 30 minutes at 1000°C before enough phosphorous accumulated to form a diode. A similar layer of SiO_2 fails to protect after 24 minutes. It is felt that the superiority of the TiO_2 is not necessarily due to a characteristically lower diffusion constant. Rather, the migration of the phosphorous in the polycrystalline TiO_2 is most likely governed by conditions at the grain boundaries.

CONCLUSIONS

A list of the conclusions which can be drawn from this work follows below. Included in the conclusions are statements describing the significance of this work in terms of present or future technologies.

(1) The low deposition temperature and simplicity of the chemical vapor deposition process makes TiO_2 an attractive choice for any number of optical or electronic applications. The thickness of the film can be controlled to within $\pm$ 100 Å over a fairly large area.

(2) The result of the 150°C deposition in an amorphous film which can be easily etched (50 Å/sec) in a chemical bath (0.5% HF) which is normally not corrosive to other integrated or hybrid materials, such as Si, SiO_2, Si_3N_4, Al, Ta, Ta_2O_5, etc. The anatase, mixed and rutile forms, are progressively more resistant and will stand attacks by most standard etchants and react only weakly to hot H_2SO_4. Rutile material is fairly impervious to attack and can be removed from the surface of Si only by undercutting it by attacking the thin SiO_2 sublayer with 48% HF. Because of this chemical inactivity, it is easy to visualize the rutile TiO_2 as a protective coating or as an etch mask.

(3) The crystalline state of the material is controlled by the after-deposition anneal. The index of refraction and density are both functions of the crystalline phase. Because of the high index of refraction in all forms (2.0-2.5), it is ideal for optical surface coatings for lenses, mirrors and other components to aid optical impedance matching.

(4) The strong absorption peak at 0.32μ (87% absorption by 2500 Å at 0.32μ) allows a unique photomask to be made with a TiO_2 layer on quartz since visible wavelengths pass easily through the mask to allow for accurate alignment.

(5)   The electrical characteristics, especially the bulk resistivity,
are strong functions of the stoichiometry and the crystalline
phase of the film. These properties range from a high resistiv-
ity n type semiconductor to a high dielectric constant insula-
tor. In the lower resistivity range (10^4 Ω-cm) devices, such as
thin film resistors, Schottky diodes and others, are suggested.
Some evidence was gathered that the resistivity of the film can
be drastically altered by doping the TiO_2 with impurities during
the anneal process. If this proves to be the case, the useful-
ness of TiO_2 as a semiconducting material will be greatly en-
hanced. Analysis of the Schottky barrier diodes constructed re-
vealed a Fermi level in the TiO_2 approximately 0.35 eV below the
conduction band edge. The addition of impurities could be cal-
culated to add to or compensate for these donor states and thus
greatly adjust the resistivity. The high resistivity ($10^{11}\Omega$-cm)
high dielectric constant (100) films lend themselves to high
value, low area capacitors with moderate dissipation factors in
addition to varicaps, surface varactors and IGFET's. Because of
the compensating effect the TiO_2/SiO_2 combination has on the sur-
face charge, these varicaps, surface varactors and IGFET's can
be fabricated with dynamic regions at or near zero bias.

(6)   The electrical characteristics of the rutile thin films appear
to be quite stable with time. Applied electrical stresses in the
range of half the breakdown field strength resulted in a leakage
current which was observed to be independent of time after a
short stabilization period. There are no indications that under

these fields the films undergo a process of oxygen loss (a process thought to be observed with bulk crystals) and hence a decrease on bulk resistivity. At or near the breakdown field strength the current does increase with time, slowly at first and then at an increasing rate. This is consistent with standard breakdown phenomena associated with localized heating and induced damage in the insulator.

(7) Conversion to an etch resistant crystalline form can be accomplished by electron bombardment with 10 to 30 keV beams. Threshold levels of 0.1 coul/cm^2 and minimum useful doses of 2.0 coul/cm^2 were observed for 2700 Å TiO_2 films while complete conversion to the rutile form took place at higher (25-32 coul/cm^2) dosage levels. Excellent pattern definition and 3μ line widths have been obtained with this method, the lower limit being determined by the electron beam diameter in these experiments. Edge definition in the neighborhood of 0.3μ was common. The simplicity of this process for obtaining a desired pattern in a TiO_2 film lends itself to computer controlled electron beam techniques already developed. A number of microsized devices can be made by this process and are not hindered by the problems associated with normal photolithographic techniques. The land area of a microcapacitor, the gate region of an IGFET or the conducting area of a thin film resistor can be defined with the electron beam in the amorphous material, the unexposed material removed with the HF etch, and then the remaining material treated or annealed to obtain the desired electrical characteristics.

Computer generated master photomasks can be produced by exposing a TiO_2 film on quartz with a computer-directed beam to convert the proper areas. After the etch the remaining areas are opaque to the u.v. while the open areas allow the exposure of underlying photoresists.

(8) The strong absorption of u.v. photons by the amorphous films also provides a means by which energy may selectively be delivered to the film. Exposure to light from a mercury floodlamp with an energy density between 0.1 and 1 $watt/cm^2$ for 10 minutes provided sufficient conversion to provide good etch resistance and excellent pattern definition.

(9) Several plans to allow "contact" printing of TiO_2 films with some desired pattern were discussed. This method may ultimately allow capacitor land areas and high value resistors to be printed directly into a TiO_2 layer in a hybrid circuit without the usual intermediate steps associated with standard photomasking techniques.

(10) 2000 Å of TiO_2 protected a p type Si surface from phosphorous impurities at 1000°C for 30 minutes. This diffusion masking capability along with the properties mentioned above, that is the ability to define microsize windows in TiO_2 films with a programmed e-beam, makes these films quite a valuable addition to the Si IC technology for executing micron sized diffused areas.

REFERENCES

1. Haas, G., "Preparation, Properties and Optical Applications of Thin Films of TiO_2," Vacuum, 2, 331, 1952.

2. Haas, G., A.P. Bradford, "Optical Properties and Oxidation of Evaporated Ti Films," J. Optical Society of America, 47, 125, 1957.

3. von Hippel, A.R., Dielectric Materials and Applications, Technical Press, MIT, Wiley, 1954.

4. Parker, R.A., "Static Dielectric Constant of Rutile (TiO_2), 1.6 - 1060°K," Phys. Rev., 124, 1719, 1961.

5. Hollander, L.E., P.L. Castro, "Anisotropic Conduction in Non-stoichiometric Rutile," Phys. Rev., 119, 1882, 1960.

6. Hollander, L.E., P.L. Castro, "Dielectric Properties of Single-Crystal Nonstoichiometric Rutile (TiO_2)," J. Appl. Phys., 33, 3421, 1962.

7. van Raalte, J.A., "Conduction Phenomena in Rutile Single Crystals," AD 610 101.

8. Kunin, V. Ya., Yu. N. Sedunov, A.N. Tsikin, "Changes in the Conductivity Type in Rutile Ceramics and Rutile Single Crystals During Electric Aging," Soviet Physics - Solid State, 5, 2028, 1964.

9. Acket, G.A. and J. Volger, "On Electrical Conduction in Reduced Rutile," Physics 30, 1667, 1964.

10. Davis, G., W.W. Grannemann, "Point Contact Diodes Utilizing Single Crystal Reduced Rutile TiO_2," J. Appl. Phys., 34, 228, 1963.

11. English, F., B. Gossick, "TiO_2 Rectifying Barriers," Solid State Electronics, 7, 193, 1964.

12. Cardon, F., "Polarization and Space-Charge-Limited Currents in Rutile TiO_2," Physics, 27, 841, 1961.

13. Cross, L.E., C.F. Groner, "Dielectric Measurements on Flux-Grown Crystals of Rutile (TiO_2) without Contacting Electrodes," J. Appl. Phys., 40, (1), 126, 1968.

14. Bergman, J.G., G.D. Boyd, A, Ashkin, S.K. Kurtz, "New Nonlinear Optical Materials: Metal Oxides with Nonbonded Electrons," J. Appl. Phys., 40, (7) 2860, 1969.

15. Young, L, Anodic Oxide Films, New York, Academic Press, 1961.

16. Sasaki, Y., "p-i-n Junction in the Anodic Oxide Film of Tantalum," J. Phys. Chem. Solids, 13, 177, 1960.

17. Vromen, B.H., J. Klerer, "Properties and Performance of Ta_2O_5 Thin Film Capacitors," IEEE Trans. on Parts, Materials and Packaging PMP1, 194, 1965.

18. Gerstenberg, D., "Properties of Anodic Films Formed on Reactively Sputtered Ta," J. Electrochem. Soc., 113, 542, 1966.

19. Huber, F., "Thin Film Titanium Oxide Diodes," Solid State Electronics, 5, 410, 1962.

20. Huber, F., "Thin Films of Titanium and Titanium Oxide for Microminiaturization," IEEE, Component Parts CP-11, (2), 38, 1964.

21. Huber, F., A. Rottersman, "Graded P-N Junctions in Thin Anodic Oxide Films of Titanium," J. Appl. Phys., 33, 3385, 1962.

22. Magill, P.J., "Comment on Proposed Barriers in Thin Film TiO_2 Diodes," Solid State Electronics, 6, 531, 1963.

23. Huber, F., "Microminiaturized Thin Film Diode Matrices," IEEE, Component Parts CP 10 (1) 10, 1963.

24. Hogiwara, H., A. Yamashita, "Characteristics of Titanium Electrolytic Capacitors," Proc. IEEE 51, 1320, 1963.

25. Kover, F., M.J. Musselin, "A Comparative Study of Anodic Oxide Films on Titanium, Niobium and Tantalum," Thin Solid Films, 2, 211, 1968.

26. Lakshmanan, T.K., C.A. Wysocki, W.J. Slegesky, "Sputtered Titanium Oxide Films for Microcircuit Application," IEEE Component Parts, CP-11 (2), 14, 1964.

27. Wasa, K., S. Hayakawa, "Reactively Sputtered Titanium Resistors, Capacitors and Rectifiers for Microcircuits," Microelectronics and Reliability, 6, 213, 1967.

28. Lakshmanan, T.K., "Chemical Formation of Microcircuit Elements," AD 613 563, March, 1965.

29. Davidse, P.D., L.I. Maissel, "Dielectric Thin Films through R.F. Sputtering," J. Appl. Physics, 37, 574, 1966.

30. Gruner, E.H., D.H. Whitemore, "Non-ohmic Behavior in Near-stoichiometric Rutile (TiO_2)," J. Appl. Phys., 32, 1320, 1961.

31. Komolova, T.I., D.N. Nasledov, "Investigation of the Steady State Volt-Ampere Characteristics of Rectifiers in Semiconducting TiO_2," Soviet Physics – Solid State, 3, 2469, 1962.

32. Maserjian, J., C.A. Mead, "Conduction through TiO_2 Thin Film with Large Ionic Space Charge," J. Phys. Chem. Solids, 28, 1971, 1967.

33. Johansen, I.T., "Electrical Conductivity in Evaporated Silicon Oxide Films," J. Appl. Phys., 37, 499, 1966.

34. Shiojiri, J., H. Morikawa, E. Suito, "Crystal Growth from Amorphous Phase in Thin Films, " Japanese J. Appl. Phys., 8 (9), 1077, 1969, (Sept.).

35. Powell, C.F., J.H. Oxley, J.M. Blocher, Vapor Deposition, John Wiley, New York, 1966.

36. Buck, R.H., "The Vapor Phase Deposition of Metals and Their Compounds: Applications in Electronics," Microelectronics and Reliability, 6, 231, 1967.

37. Tyzor Organic Titanates, E.I. du Point de Nemours and Co., Technical Bulletin.

38. Feuersanger, A.E., "Titanium Dioxide Dielectric Films Prepared by Vapor Reaction," Proc. IEEE 52, (12), 1463, 1964.

39. Shiojiri, M., H. Morikawa, E. Suito, "Crystal Growth from Amorphous Phase in Thin Films," Japanese J. Appl. Phys. 8, (9), 1077, 1969 (Sept)

40. Harbison, D.R., "Thin Film Titanium Dixoide by Chemical Vapor Deposition," Doctoral Dissertation, Univ. of Texas at Austin, Jan., 1969. NASA Report, "Research on Digital Transducer Principles," Vol. X, Jan., 1969.

41. Peterson, D.R., J. Black, W. Brand, D. Dulaney, "Non Vacuum Deposition Technique for Use in Fabrication Thin Film Circuits," AD 462 743 (April 1965).

42. Yokozawa, M., H. Iwasa, "Vapor Deposition of TiO_2," Japanese J. Appl. Phys., 7, 96, 1968.

43. Gannon, R.E., R.C. Folweiler, T. Vasilos, "Pyrolytic Synthesis of Titanium Diboride," J. Am. Ceramic Soc., 46 (10), 496, 1963.

44. Sterling, H.F., R.C.G. Swann, "Chemical Vapor Deposition Promoted by R.F. Discharge," Solid State Electronics, 8, 653, 1965.

45. Peterson, D., "Evaluation of Vapor Plated Oxide Films for Capacitor Dielectrics," IEEE Component Parts, CP 10 (3), 119, 1963.

46. Krylova, T.N., G.O. Bagdyk'yants, "Study of the Optical Properties and Structure of Titanium Dioxide Films," Optics and Spectroscopy, 9, 339, 1960.

47. Mitchell, J.J., "Preparation and Dielectric Properties of a Multicomponent Metallic Oxide Film," AD 416 330.

48. Sakurai, Watanabe, Rev. Elec. Comm. Lab, 11, 178, 1963.

49. Burger, R.M., R.P. Donavan, Fundamentals of Silicon Integrated Device Technology, Vol. 1, Prentice Hall, Inc., Englewood Cliffs, N.J., 1967.

50. Barksdale, J., Titanium. Its Occurrence, Chemistry and Technology, Ronald Press, New York, 1949.

51. Maserjian, J., "Conduction Through Thin TiO_2 Films," JPL Tech. Report for NASA, #32-976.

52. Dorin, V.A., A. Ya. Patrokova, "Investigation of the Electrical Properties of the TiO_2-x Contact with an Intermediate Insulator Layer," Soviet Physics - Solid State, 5, 1506, 1964.

53. Shockley, W., Electrons and Holes in Semiconductors, Van Nostrand, Princeton, N.J., 1950.

54. Henisch, H.K., Rectifying Semiconductor Contacts, Clarendon Press, Oxford, 1957.

55. Sze, S.M., Physics of Semiconductor Devices, John Wiley & Sons, N.Y., 1969.

56. Crowell, C.R., J.C. Sorace, S.M. Sze, "Tungsten-Semiconductor Schottky Barrier Diodes," Trans. Met. Soc. AIME, 233, 478, 1965

57. Grove, A.S., Physics and Technology of Semiconductor Devices, John Wiley & Sons, N.Y., 1967.

58. Terman, L.M., "An Investigation of Surface States at Silicon/Silicon Dioxide Interface Employing Metal-Oxide-Silicon Diodes," Solid State Electronics, 5, 285, 1962.

59. Nicollian, E.H., A. Goetzberger, "The Si-SiO$_2$ Interface-Electrical Properties as Determined by the MIS Conductance Technique," Bell Syst. Tech. J., 46, 1055, 1967.

60. Froehlich, H., Theory of Dielectrics, Clarendon Press, Oxford, 1958.

61. Hartwig, W.H., D. Grissom, "Dielectric Dissipation in NaCl and KCl Below 4.2°K," J. Appl. Phys., 37, 4784, 1966.

62. Lindmayer, J., C.Y. Wrigley, Fundamentals of Semiconduction Devices, Van Nostrand, Princeton, 1966.

63. Many, A, Y. Goldstein, N.B. Grover, Semiconductor Surfaces, North Holland Pub. Co., Amsterdam, 1965.

64. Burger, R.M., R.P. Donavan, Fundamentals of Silicon Integrated Device Technology, Vol. 1, Prentice Hall, Inc., Englewood Cliffs, 1967.

65. Handbook of Chemistry and Physics, 46th edition, Chemical Rubber Publishing Co., 1966.

66. Yeargan, J.R., H.L. Taylor, "Conduction Mechanisms of Pyrolytic Silicon Nitride Films," J. Electrochem. Soc., 115, 273, 1968. NASA Report "Research on Digital Transducer Principles," Vol. IV, 1967.

67. Thornley, R.F.M., T. Sun, "Electron Beam Exposure of Photoresists," J. Electrochem. Soc., 112, 1151, 1965.

68. Matta, R.K., Electrochem. Technol., 5, 382, 1967.

69. Broyde, B., "Exposure of Photoresists: Electron Beam Exposure of Negative Photoresists," J. Electrochem. Soc., 116, (9), 1241, 1969.

70. O'Keeffe, T.W., R.M. Handy, Solid State Electronics, 11, 261, 1968.

71. Hill, B.H., "Effect of Kilovolt Electrons on the Etch Rate of Al_2O_3 and Ta_2O_5," J. Electrochem. Soc., 115, (5), 668, 1969.

72. Shirojiri, M., H. Morikawa, E. Suito, Electron Microscopy, 1966, Vol. 1, p. 467, Maruzen, Tokyo, 1966.

73. Shiojiri, M., "Crystallization of Amorphous Selenium Films Prepared by Vacuum Evaporation," Japanese J. Appl. Phys., 6, (2), 163, 1967.

74. Cecil, O.B., D.R. Silvertsen, "Preferential Changes in Electronic Materials," Technical Report AFAL - RF 65, AD - 479914, 1965.

75. Fitzgibbons, E.T., "Current Mechanisms in Thin Polymer Films," Master's Thesis, Univ. of Texas at Austin, 1967. NASA Report "Research on Digital Transducer Principles," Vol. III, 1967.

76. Bethe, H.A., J. Ashkin, Experimental Nuclear Physics, Vol. II, p. 253, John Wiley & Sons, New York, 1953.

77. Mathews, J., R.L. Walker, Mathematical Methods of Physics, p. 72, Benjamin, New York, 1965.

78. Charlesby, A., Atomic Radiation and Polymers, p. 32, Pergamon Press, New York, 1960.

79. Chalmers, Principles of Solidification, p. 91, John Wiley & Sons, New York, 1964.

80. Sah, C.T., H. Sello, D.A. Tremere, "Diffusion of Phosphorous in Silicon Oxide Films," J. Phys. Chem. Solids, II, 288, 1959

81. Wells, A.F., Structural Inorganic Chemistry, p. 126, Clarendon Press, Oxford, 1962.

82. Evans, R.C., Introduction to Crystal Chemistry, Cambridge Press, 1966.

DEPARTMENT OF DEFENSE

Asst Director (Research) (1)
Office of Director of Defense Res. and Eng
Pentagon, Rm 3C128
Washington, D. C. 20301

Technical Library (1)
DDR&E
Room 3C-122, The Pentagon
Washington, D. C. 20301

Director for Materials Sciences (1)
Advanced Research Projects Agency
Room 3D179, Pentagon
Washington, D. C. 20301

Chief, R & D Division (340) (1)
Defense Communications Agency
Washington, D. C. 20305

Defense Documentation Center (50)
Attn: DDC-TCA
Cameron Station
Alexandria, Virginia 22314

Dr. Alvin D. Schnitzler (1)
Institute for Defense Analyses
Science and Technology Division
400 Army-Navy Drive
Arlington, Virginia 22202

Central Intelligence Agency (1)
Attn: CRS/ADD/Publications
Washington, D. C. 20505

M. A. Rothenberg (STEPD-SC (S)) (1)
Scientific Director
Deseret Test Center
Bldg 100, Soldiers' Circle
Fort Douglas, Utah 84113

DEPARTMENT OF THE AIR FORCE

Hq USAF (AFRDDD) (1)
The Pentagon
Washington, D. C. 20330

Hq USAF (AFRDDG) (1)
The Pentagon
Washington, D. C. 20330

Hq USAF (AFRDSD) (1)
The Pentagon
Washington, D. C. 20330
Attn: LTC C. M. Waespy

Colonel E. P. Gaines, Jr (1)
ACDA/FO
1901 Pennsylvania Avenue N. W.
Washington, D. C. 20451

LTC H. W. Jackson (SREE) (5)
Deputy Dir. of Elec. & Solid State Sciences
Air Force Office of Scientific Research
1400 Wilson Boulevard
Arlington, Virginia 22209

Mr. I. R. Mirman (1)
Hq AFSC (SGGP)
Andrews Air Force Base
Washington, D. C. 20331

Rome Air Development Center (1)
Attn: Documents Library (EMTLD)
Griffiss Air Force Base, New York 13440

Mr. H. E. Webb, Jr. (EMBIS) (1)
Rome Air Development Center
Griffiss Air Force Base, New York 13440

Dr. L. M. Hollingsworth (1)
AFCRL (CRN)
L. G. Hanscom Field
Bedford, Massachusetts 01730

Hq ESD (ESTI) (2)
L. G. Hanscom Field
Bedford, Massachusetts 01730

Professor R. E. Fontana, Head (1)
Dept of Electrical Engineering
Air Force Institute of Technology
Wright-Patterson AFB, Ohio 45433

Director (1)
Air Force Avionics Laboratory
Wright-Patterson AFB, Ohio 45433

AFAL (AVTA/R. D. Larson) (1)
Wright-Patterson AFB, Ohio 45433

Director of Faculty Research (1)
Department of the Air Force
U. S. Air Force Academy
Colorado 80840

Academy Library (DFSLB) (1)
USAF Academy, Colorado 80840

Director of Aerospace Mechanics Sciences (1)
Frank J. Seiler Research Laboratory (OAR)
USAF Academy, Colorado 80840

Major Richard J. Gowen (1)
Tenure Associate Professor
Dept. of Electrical Engineering
USAF Academy, Colorado 80840

Director, USAF PROJECT RAND (1)
Via: Air Force Liaison Office
The RAND Corporation
Attn: Library D
1700 Main Street
Santa Monica, California 90406

AFAL (AVT) Dr. H. V. Noble, Chief
Electronics Technology Division
Air Force Avionics Laboratory
Wright-Patterson AFB, Ohio 45433

Hq SAMSO (SMTAE/Lt Belate) (1)
AF Unit Post Office
Los Angeles, California 90045

AUL3T-9663 (1)
Maxwell AFB, Alabama 36112

AFETR Technical Library (1)
(ETV, MU-135)
Patrick AFB, Florida 32925

ADTC (ADBPS-12) (1)
Eglin AFB, Florida 32542

Mr. B. R. Locke (1)
Technical Advisor, Requirements
USAF Security Service
Kelly Air Force Base, Texas 78241

Hq AMD (AMR) (1)
Brooks AFB, Texas 78235

USAFSAM (SMKOR) (1)
Brooks AFB, Texas 78235

Commanding General (2)
Attn: STEWS-RE-L, Technical Library
White Sands Missile Range, New Mexico 88002

Hq AEDC (AETS) (1)
Arnold AFB, Tennessee 37389

European Office of Aerospace Research (1)
Technical Information Office
Box 14
FPO New York 09510

Electromagnetic Compatibility Analysis Center (1)
(ECAC) Attn: ACOAT
North Severn
Annapolis, Maryland 21402

VELA Seismological Center (1)
300 North Washington Street
Alexandria, Virginia 22314

Capt. C. E. Baum (1)
AFWL (WLRE)
Kirtland AFB, New Mexico 87117

DEPARTMENT OF THE ARMY

Director
Physical & Engineering Sciences Division (1)
3045 Columbia Pike
Arlington, Virginia 22204

Commanding General (1)
U. S. Army Security Agency
Attn: IARD-T
Arlington Hall Station
Arlington, Virginia 22212

Commanding General (1)
U. S. Army Materiel Command
Attn: AMCRD-TP
Washington, D. C. 20315

Director (1)
Advanced Materiel Concepts Agency
Washington, D. C. 20315

Commanding General (1)
USACDC Institute of Land Combat
Attn: Technical Library, Rm 636
2461 Eisenhower Avenue
Alexandria, Virginia 22314

Commanding Officer (1)
Harry Diamond Laboratories
Attn: Dr. Berthold Altman (AMXDO-TI)
Connecticut Ave and Van Ness Street N.W.
Washington, D. C. 20438

Commanding Officer (AMXRD-BAT) (1)
U. S. Army Ballistics Research Laboratory
Aberdeen Proving Ground
Aberdeen, Maryland 21005

Technical Director (1)
U. S. Army Land Warfare Laboratory
Aberdeen Proving Ground
Aberdeen, Maryland 21005

U. S. Army Munitions Command (1)
Attn: Science & Technology Information
Branch, Bldg 59
Picatinny Arsenal, SMUPA-RT-S
Dover, New Jersey 07801

U. S. Army Mobility Equipment Research (1)
and Development Center
Attn: Technical Documents Center, Bldg 315
Fort Belvoir, Virginia 22060

Commanding Officer (1)
U. S. Army Engineer Topographic Laboratories
Attn: STINFO Center
Fort Belvoir, Virginia 22060

Dr. Herman Robl (1)
Deputy Chief Scientist
U. S. Army Research Office (Durham)
Box CM, Duke Station
Durham, North Carolina 27706

Richard O. Ulsch (CRDARD-IP) (1)
U. S. Army Research Office (Durham)
Box CM, Duke Station
Durham, North Carolina 27706

Technical Director (SMUFA-A2000-107-1)
Frankford Arsenal (1)
Philadelphia, Pennsylvania 19137

Redstone Scientific Information Center (1)
Attn: Chief, Document Section
U. S. Army Missile Command
Redstone Arsenal, Alabama 35809

Commanding General (1)
U. S. Army Missile Command
Attn: AMSMI-RR
Redstone Arsenal, Alabama 35809

Commanding General (1)
U. S. Army Strategic Communications Command
Attn: SCC-CG-SAE
Fort Huachuca, Arizona 85613

Commanding Officer (1)
Army Materials and Mechanics Research Center
Attn: Dr. H. Priest
Watertown Arsenal
Watertown, Massachusetts 02171

Commandant (1)
U. S. Army Air Defense School
Attn: Missile Science Division, C & S Dept.
P. O. Box 9390
Fort Bliss, Texas 79916

Commandant (1)
U. S. Army Command and General Staff College
Attn: Acquisitions, Lib Div
Fort Leavenworth, Kansas 66027

Mr. Norman J. Field, AMSEL-RD-S (1)
Chief, Science and Technology Division
Research and Development Directorate
U. S. Army Electronics Command
Fort Monmouth, New Jersey 07703

Mr. Robert O. Parker, AMSEL-RD-S (1)
Executive Secretary, TAC-JSEP
U. S. Army Electronics Command
Fort Monmouth, New Jersey 07703

Commanding General (1)
U. S. Army Electronics Command
Fort Monmouth, New Jersey 07703
Attn: AMSEL-SC, DL, GG-DD, XL-D,
XL-DT, BL-FM-P, CT-D, CT-R, CT-S,
CT-L (Dr. W. S. McAfee), CT-O, CT-I
CT-A, NL-D (Dr. H. Bennett), NL-A,
NL-C, NL-P, NL-P-2, NL-R, NL-S,
KL-D, KL-I, KL-E, KL-S, KL-SM, KL-T,
VL-D, VL-F, WL-D

Director (NV-D) (1)
Night Vision Laboratory, USAECOM
Fort Belvoir, Virginia 22060

Commanding Officer (1)
Atmospheric Sciences Laboratory
U. S. Army Electronics Command
White Sands Missile Range, New Mexico 88002

* The Joint Services Technical Advisory Committee has established this list for the
regular distribution of reports on the electronics research program of the University of Texas
at Austin. Additional addresses may be included on their written request to:

Mr. Robert O. Parker (AMSEL-RD-S)

U. S. Army Electronics Command

Fort Monmouth, New Jersey 07703

An appropriate endorsement by a Department of Defense sponsor is required except on requests
from a Federal Agency.

Commanding Officer (AMSEL-BL-WS-R) (1)
Atmospheric Sciences Laboratory
U. S. Army Electronics Command
White Sands Missile Range, New Mexico 88002

Chief (1)
Missile Electronics Warfare Tech. Area (AMSEL-WL-M)
Electronics Warfare Laboratory, USAECOM
White Sands Missile Range, New Mexico 88002

Project Manager NAVCOM (1)
Attn: AMCPM-NS-TM, Bldg 439 (H. H. Bahr)
Fort Monmouth, New Jersey 07703

DEPARTMENT OF THE NAVY

Director, Electronics Programs (3)
Attn: Code 427
Office of Naval Research
800 North Quincy Street
Arlington, Virginia 22217

Commander (1)
Naval Security Group Command
Naval Security Group Headquarters
Attn: Technical Library (G43)
3801 Nebraska Avenue, N.W.
Washington, D. C. 20390

Director
Naval Research Laboratory
Washington, D. C. 20390
Attn: Code 2027 (6)
       Dr. W. C. Hall, Code 7000 (1)
       Mr. A. Brodzinsky, Supt. Electronics
       Div (1)

Code 8050 (1)
Maury Center Library
Naval Research Laboratory
Washington, D. C. 20390

Dr. G. M. R. Winkler (1)
Director, Time Service Division
U. S. Naval Observatory
Washington, D. C. 20390

Naval Air Systems Command (2)
AIR 03
Washington, D. C. 20360

Naval Ship Systems Command (1)
Ship 031
Washington, D. C. 20360

Naval Ship Systems Command (1)
Ship 035
Washington, D. C. 20360

U. S. Naval Weapons Laboratory (1)
Dahlgren, Virginia 22448

Naval Electronic Systems Command (2)
ELEX 03, Rm 2534 Main Navy Bldg.
Department of the Navy
Washington, D. C. 20360

Commander (2)
U. S. Naval Ordnance Laboratory
Attn: Librarian
White Oak, Maryland 20910

Director (1)
Office of Naval Research
Boston Branch
495 Summer Street
Boston, Massachusetts 02210

Commander (ADL) (1)
Naval Air Development Center
Attn: NADC Library
Johnsville, Warminster, Pennsylvania 18974

Commander (Code 753) (1)
Naval Weapons Center
Attn: Technical Library
China Lake, California 93555

Commanding Officer (1)
Naval Weapons Center
Corona Laboratories
Attn: Library
Corona, California 91720

Commanding Officer (56322) (1)
Naval Missile Center
Point Mugu, California 93041

W. A. Eberspacher, Associate Head (1)
Systems Integration Division, Code 5340A
U. S. Naval Missile Center
Point Mugu, California 93041

Commander (2)
Naval Electronics Laboratory Center
Attn: Library
San Diego, California 92152

Deputy Director and Chief Scientist (1)
Office of Naval Research Branch Office
1030 East Green Street
Pasadena, California 91101

Library (Code 2124) (1)
Technical Report Section
Naval Postgraduate School
Monterey, California 93940

Glen A. Myers (Code 52 Mv) (1)
Assoc. Professor of Electrical Engineering
Naval Postgraduate School
Monterey, California 93940

Commanding Officer (Code 2064) (1)
Navy Underwater Sound Laboratory
Fort Trumbull
New London, Connecticut 06320

Commanding Officer (1)
Naval Avionics Facility
Indianapolis, Indiana 46241

Director (2)
Naval Research Laboratory
Attn: Library, Code 2029 (ONRL)
Washington, D. C. 20390

Director (1)
Office of Naval Research Branch Office
219 South Dearborn Street
Chicago, Illinois 60604

OTHER GOVERNMENT AGENCIES

Dr. H. Harrison Code RRE (1)
Chief, Electrophysics Branch
National Aeronautics and Space Administration
Washington, D. C. 20546

NASA Lewis Research Center (1)
Attn: Library
21000 Brookpark Road
Cleveland, Ohio 44135

Los Alamos Scientific Laboratory
Attn: Reports Library
P. O. Box 1663
Los Alamos, New Mexico 87544

Mr. M. Zane Thornton, Chief
Network Engineering, Communications
and Operations Branch
Lister Hill National Center for
Biomedical Communications
8600 Rockville Pike
Bethesda, Maryland 20014

U. S. Post Office Department (1)
Library - Room 6012
12th & Pennsylvania Ave. N. W.
Washington, D. C. 20260

Dr. J. Ryland Mundie (HRBB) (1)
Chief, Neurophysiology Branch
Biodynamics & Bionics Division
6570th Aerospace Medical Research Labs.
Wright-Patterson AFB, Ohio 45433

NON-GOVERNMENT AGENCIES

Director (1)
Research Laboratory of Electronics
Massachusetts Institute of Technology
Cambridge, Massachusetts 02139

Mr. Jerome Fox, Research Coordinator (1)
Polytechnic Institute of Brooklyn
333 Jay Street
Brooklyn, New York 11201

Director (1)
Columbia Radiation Laboratory
Columbia University
538 West 120th Street
New York, New York 10027

Director (1)
Coordinated Science Laboratory
University of Illinois
Urbana, Illinois 61801

Director (1)
Stanford Electronics Laboratories
Stanford University
Stanford, California 94305

Director (1)
Microwave Physics Laboratory
Stanford University
Stanford, California 94305

Director (1)
Electronics Research Laboratory
University of California
Berkeley, California 94720

Director (1)
Electronics Sciences Laboratory
University of Southern California
Los Angeles, California 90007

Director (1)
Electronics Research Center
The University of Texas at Austin
Austin, Texas 78712

Division of Engineering and Applied
    Physics (1)
210 Pierce Hall
Harvard University
Cambridge, Massachusetts 02138

Dr. G. J. Murphy (1)
The Technological Institute
Northwestern University
Evanston, Illinois 60201

Dr. John C. Hancock, Head (1)
School of Electrical Engineering
Purdue University
Lafayette, Indiana 47907

Dept. of Electrical Engineering (1)
Texas Technological College
Lubbock, Texas 79409

Aerospace Corporation (1)
P. O. Box 95085
Los Angeles, California 90045
Attn: Library Acquisitions Group

Airborne Instruments Laboratory (1)
Deerpark, New York 11729

The University of Arizona (1)
Dept. of Electrical Engineering
Tucson, Arizona 85721

Chairman, Electrical Engineering (1)
Arizona State University
Tempe, Arizona 85281

Engineering & Mathematical
    Sciences Library (1)
University of California at
    Los Angeles
405 Hilgred Avenue
Los Angeles, California 90024

Sciences - Engineering Library (1)
University of California
Santa Barbara, California 93106

Professor Nicholas George (1)
California Institute of Technology
Pasadena, California 91109

Aeronautics Library (1)
Graduate Aeronautical Laboratories
California Institute of Technology
1201 E. California Blvd.
Pasadena, California 91109

Hunt Library (1)
Carnegie-Mellon University
Schenley Park
Pittsburgh, Pennsylvania 15213

Dr. A. G. Jordon (1)
Head of Dept. of Electrical Engineering
Carnegie-Mellon University
Pittsburgh, Pennsylvania 15213

Case Institute of Technology (1)
Engineering Division
University Circle
Cleveland, Ohio 44106

Hollander Associates (1)
P. O. Box 2276
Fullerton, California 92633
Attn: Librarian

Dr. Sheldon J. Welles (1)
Electronic Properties Information Center
Mail Station E-175
Hughes Aircraft Company
Culver City, California 90230

Illinois Institute of Technology (1)
Department of Electrical Engineering
Chicago, Illinois 60616

Government Documents Dept. (1)
University of Iowa Libraries
Iowa City, Iowa 52240

New York University (1)
Engineering Library
Bronx, New York 10453

Utah State University (1)
Dept. of Electrical Engineering
Logan, Utah 84321

Professor James A. Codzow (1)
Dept. of Electrical Engineering
State University of New York at Buffalo
Buffalo, New York 14214

Dept. of Electrical Engineering (1)
Clippinger Laboratory
Ohio University
Athens, Ohio 45701

Raytheon Company (1)
Research Division Library
28 Seyon Street
Waltham, Massachusetts 02154

Dept. of Electrical Engineering (1)
Rice University
Houston, Texas 77001

Dr. Leo Young (1)
Stanford Research Institute
Menlo Park, California 94025

The Johns Hopkins University (1)
Applied Physics Laboratory
Attn: Document Librarian
8621 Georgia Avenue
Silver Spring, Maryland 20910

Lehigh University (1)
Department of Electrical Engineering
Bethlehem, Pennsylvania 18015

Lenkurt Electric Co., Inc. (1)
1105 County Road
San Carlos, California 94070
Attn: Mr. E. K. Peterson

Lincoln Laboratory (1)
Massachusetts Institute of Technology
P. O. Box 73
Lexington, Massachusetts 02173

Miss R. Joyce Harmon (1)
Project MAC, Room 810
545 Main Street
Cambridge, Massachusetts 02139

Professor R. H. Rediker (1)
Electrical Engineering, Professor
Mass. Institute of Technology
Building 13-3050
Cambridge, Massachusetts 02139

Professor Joseph E. Rowe (1)
Chairman, Dept. of Electrical Engineering
The University of Michigan
Ann Arbor, Michigan 48104

Sylvania Electronic Systems (1)
Applied Research Laboratory
Attn: Documents Librarian
40 Sylvan Road
Waltham, Massachusetts 02154

Syracuse University (1)
Dept. of Electrical Engineering
Syracuse, New York 13210
Attn: Dr. W. R. LePage, Chairman

Dr. F. R. Charvat (1)
Union Carbide Corporation
Materials Systems Division
Crystal Products Department
8888 Balboa Avenue
P. O. Box 23017
San Diego, California 92123

Research Laboratories for the
    Engineering Sciences (1)
School of Engineering and Applied
    Science
University of Virginia
Charlottesville, Virginia 22903

Yale University (1)
Engineering Department
New Haven, Connecticut 06520

DOCUMENT CONTROL DATA - R&D

(Security classification of title, body of abstract and indexing annotation must be entered when the overall report is classified)

1. ORIGINATING ACTIVITY *(Corporate author)*	2a. REPORT SECURITY CLASSIFICATION
The University of Texas at Austin Electronics Research Center Austin, Texas 78712	UNCLASSIFIED
	2b. GROUP

3. REPORT TITLE

VAPOR DEPOSITED TITANIUM DIOXIDE THIN FILMS: SOME PROPERTIES AS A FUNCTION OF CRYSTALLINE PHASE

4. DESCRIPTIVE NOTES *(Type of report and inclusive dates)*

Scientific   Interim

5. AUTHOR(S) *(Last name, first name, initial)*

E. T. Fitzgibbons
W. H. Hartwig

6. REPORT DATE	7a. TOTAL NO. OF PAGES	7b. NO. OF REFS
15 April 1970	152	82

8a. CONTRACT OR GRANT NO. AFOSR 69-1792	9a. ORIGINATOR'S REPORT NUMBER(S)
b. PROJECT NO. 4751	JSEP, Technical Report No. 86
c. 61102F	9b. OTHER REPORT NO(S) *(Any other numbers that may be assigned this report)*
d. 681305	AFOSR-70-

10. AVAILABILITY/LIMITATION NOTICES

1. This document has been approved for public release and sale; its distribution is unlimited.

11. SUPPLEMENTARY NOTES	12. SPONSORING MILITARY ACTIVITY JSEP through
TECH, OTHER	AF Office of Scientific Research (SREE) 1400 Wilson Boulevard Arlington, Virginia 22209 and NASA

13. ABSTRACT

Thin films of TiO_2 are grown in a low temperature (150° C) vapor deposition process by hydrolyzing tetraisopropyl titanate at the substrate. These films can be made uniform over a 1-1/4" substrate to within 100 Å and are found to be amorphous in the "as grown" condition. Films in the amorphous state have an index of refraction of 2.0 and can be etched easily (50 Å/sec) in 0.5% HF. Annealing in air at 350° C converts the film to the anatase tetragonal crystalline form and at 700° C to a mixture of anatase and rutile. Both forms are quite etch resistant, but the anatase can be etched by HF and warm H_2SO_4. At 1000° C, the film is completely rutile with an index of refraction of 2.5. This form is extremely etch resistant even in 120° C H_2SO_4 (1000 Å/hour). The conversion from amorphous to rutile is accompanied by a thickness decrease of 36%.

Electrically, the amorphous material was found to be semiconducting and subject to forming in an electric field. The anatase form showed a mixture of properties depending on the frequency used. The mixed and rutile forms both are insulators with dielectric constants/dissipation factors of 116/.04 and 100/.04, respectively, at 1 kHz. The breakdown filed for the rutile form is 7×10^5 V/cm. Surface state density of the rutile films on Si is 3×10^{12} negative states per cm^2. Combinations of TiO_2 and SiO_2 were made in which the sign and density of the surface states could be varied. Conversion from the amorphous to the crystalline forms could be accomplished selectively in the film by using an electron beam. Lines 2 microns wide were "written" in 3000 Å of amorphous material. An electron dosage of 0.2 coul/cm^2 with 15 keV electrons was needed to produce sharp lines which remained unetched while the unexposed material was etched away. Similar conversion can be accomplished by exposure to u.v. photons, allowing standard IC and hybrid circuit patterns to be defined in the TiO_2 films without the use of standard photolithographic techniques. Rutile films were tested as a diffusion mask against phosphorous at 1000° C. It was shown that, in that particular case, TiO_2 is a more effective mask than an equal thickness of SiO_2.

DD FORM 1473 1 JAN 64

| 14. | | LINK A | | LINK B | | LINK C | |
KEY WORDS		ROLE	WT	ROLE	WT	ROLE	WT
DIELECTRIC FILMS							
METAL OXIDE FILMS							
THIN FILMS							
TITANIUM DIOXIDE							
VAPOR DEPOSITE							

INSTRUCTIONS

1. ORIGINATING ACTIVITY: Enter the name and address of the contractor, subcontractor, grantee, Department of Defense activity or other organization *(corporate author)* issuing the report.

2a. REPORT SECURITY CLASSIFICATION: Enter the overall security classification of the report. Indicate whether "Restricted Data" is included. Marking is to be in accordance with appropriate security regulations.

2b. GROUP: Automatic downgrading is specified in DoD Directive 5200.10 and Armed Forces Industrial Manual. Enter the group number. Also, when applicable, show that optional markings have been used for Group 3 and Group 4 as authorized.

3. REPORT TITLE: Enter the complete report title in all capital letters. Titles in all cases should be unclassified. If a meaningful title cannot be selected without classification, show title classification in all capitals in parenthesis immediately following the title.

4. DESCRIPTIVE NOTES: If appropriate, enter the type of report, e.g., interim, progress, summary, annual, or final. Give the inclusive dates when a specific reporting period is covered.

5. AUTHOR(S): Enter the name(s) of author(s) as shown on or in the report. Enter last name, first name, middle initial. If military, show rank and branch of service. The name of the principal author is an absolute minimum requirement.

6. REPORT DATE: Enter the date of the report as day, month, year; or month, year. If more than one date appears on the report, use date of publication.

7a. TOTAL NUMBER OF PAGES: The total page count should follow normal pagination procedures, i.e., enter the number of pages containing information.

7b. NUMBER OF REFERENCES: Enter the total number of references cited in the report.

8a. CONTRACT OR GRANT NUMBER: If appropriate, enter the applicable number of the contract or grant under which the report was written.

8b, 8c, & 8d. PROJECT NUMBER: Enter the appropriate military department identification, such as project number, subproject number, system numbers, task number, etc.

9a. ORIGINATOR'S REPORT NUMBER(S): Enter the official report number by which the document will be identified and controlled by the originating activity. This number must be unique to this report.

9b. OTHER REPORT NUMBER(S): If the report has been assigned any other report numbers *(either by the originator or by the sponsor)*, also enter this number(s).

10. AVAILABILITY/LIMITATION NOTICES: Enter any limitations on further dissemination of the report, other than those imposed by security classification, using standard statements such as:

(1) "Qualified requesters may obtain copies of this report from DDC."

(2) "Foreign announcement and dissemination of this report by DDC is not authorized."

(3) "U. S. Government agencies may obtain copies of this report directly from DDC. Other qualified DDC users shall request through

_____ ."

(4) "U. S. military agencies may obtain copies of this report directly from DDC. Other qualified users shall request through

_____ ."

(5) "All distribution of this report is controlled. Qualified DDC users shall request through

_____ ."

If the report has been furnished to the Office of Technical Services, Department of Commerce, for sale to the public, indicate this fact and enter the price, if known.

11. SUPPLEMENTARY NOTES: Use for additional explanatory notes.

12. SPONSORING MILITARY ACTIVITY: Enter the name of the departmental project office or laboratory sponsoring *(paying for)* the research and development. Include address.

13. ABSTRACT: Enter an abstract giving a brief and factual summary of the document indicative of the report, even though it may also appear elsewhere in the body of the technical report. If additional space is required, a continuation sheet shall be attached.

It is highly desirable that the abstract of classified reports be unclassified. Each paragraph of the abstract shall end with an indication of the military security classification of the information in the paragraph, represented as *(TS)*, *(S)*, *(C)*, or *(U)*.

There is no limitation on the length of the abstract. However, the suggested length is from 150 to 225 words.

14. KEY WORDS: Key words are technically meaningful terms or short phrases that characterize a report and may be used as index entries for cataloging the report. Key words must be selected so that no security classification is required. Identifiers, such as equipment model designation, trade name, military project code name, geographic location, may be used as key words but will be followed by an indication of technical context. The assignment of links, rules, and weights is optional.